Expanding the toolbox for lanthanide-doped upconversion nanocrystals

Yiming Wu[1,5], Melgious Jin Yan Ang[1,2,5], Mingzi Sun[4], Bolong Huang*[4] and Xiaogang Liu*[1,2,3]

[1] Department of Chemistry, Faculty of Science, National University of Singapore, Singapore 117543, Singapore
[2] NUS Graduate School for Integrative Sciences and Engineering (NGS), 28 Medical Drive, Singapore 117456, Singapore
[3] Center for Functional Materials, National University of Singapore Suzhou Research Institute, Suzhou, Jiangsu 215123, People's republic of China
[4] Department of Applied Biology and Chemical Technology, The Hong Kong Polytechnic University, Hung Hom, Kowloon, Hong Kong SAR, China
[5] These authors contributed equally

E-mail: bhuang@polyu.edu.hk
E-mail: chmlx@nus.edu.sg

Received xxxxxx
Accepted for publication xxxxxx
Published xxxxxx

Abstract

The ability to convert low-energy quanta into a quantum of higher energy is of interest for a variety of applications, ranging from photovoltaics, volumetric display to bioimaging, multiplexing sensing, super-resolution imaging, optogenetics, and even phototherapies. Although photon upconversion can be achieved through the second harmonic generation and multiphoton absorption process, lanthanide-doped upconversion nanocrystal has emerged as an attractive alternative for non-linear upconversion of infrared light with pump intensities several orders of magnitude lower than required by conventional nonlinear crystals. Over the past, great efforts have been made to tune the photoluminescence of upconversion nanocrystals, and significant progress has been achieved. In this review, we focus on manipulation of the wavelength, emission intensity and lifetime of upconversion nanocrystals. An introduction to the fundamentals of the upconversion phenomenon would first be provided. Subsequently, we review recent experimental strategies used to control photon upconversion in lanthanide-doped nanocrystals, including conventional chemical routes and physical methods. Various crucial emerging applications using lanthanide-doped nanocrystals are highlighted in the third section. Lastly, some potential directions for challenging issues are suggested.

Keywords: lanthanide, upconversion, nanoparticles, anti-counterfeiting, security, biodetection, super-resolution imaging, optogenetics, phototherapy, photovoltaic, optoelectronic

1. Introduction

As a non-linear optical process, photon upconversion can convert the near infrared luminescence with low photon energy to higher energy ultraviolet and visible luminescence. After being discovered in bulk materials in the 1960s, photon upconversion has garnered enormous interest with potential applications in solid-state lasers, IR imaging, security markings, next-generation lighting, and three-dimensional displays, as well as biological imaging and optical therapeutics [1–5]. Unlike the emission properties of conventional quantum emitters (either molecules or quantum dots), lanthanide-doped upconversion nanoparticles (Ln-doped UCNPs) were minimally influenced by environment and exhibited non-photo-bleaching, and non-photoblinking behaviors since the upconversion luminescence (UCL) originates from well-shielded 4*f* electrons of the lanthanide ions embedded in photostable host crystals. Lanthanide-doped upconversion nanoparticles also feature numerous excellent properties, such as large anti-stokes shifts, sharp emission band, and finely controlled light emission [2]. Moreover, the capability of generating visible optical emissions under low irradiation doses of the near infrared light (*ca*. 10 W/cm^2) permits less photo-damage to biological tissues in living organisms, negligible background autofluorescence, and deep tissue penetration [6]. Such intrinsic unique features make Ln-doped UCNPs excellent optical labels for biological applications. On

the other hand, by converting sub-bandgap NIR photons into usable above-bandgap photons, the use of Ln-doped UCNPs can minimize the non-absorption energy losses in photovoltaic devices, providing a promising opportunity to break the Shockley–Queisser efficiency limit [7–9]. Since the excitation wavelengths for photon upconversion are typically in the technologically important telecom windows (0.8–1.8μm), which is of great importance in photonic applications, Ln-doped UCNPs can also serve as promising active materials to be integrated into silicon-based or other semiconductor materials for optoelectronic nanodevices as spectral converters to construct highly efficient optoelectronic nano-devices [1,3,10–14].

Due to the remarkable potential utility, considerable research efforts have been devoted to developing methods which can produce highly efficient upconversion nanocrystals and control the optical properties of upconversion nanocrystals in the past few decades. Precise control over the luminescence properties of upconversion nanocrystals as desired is not only crucial in turning their properties into a wide range of applications but also extremely important in fundamental studies of the photoluminescence mechanisms [15,16]. Previous studies have extensively focused on manipulation of the emission properties of Ln-doped UCNPs by conventional chemical routes, typically changing chemical compositions, core/shell structure, nanoscale integration, and others [17–21]. Theoretical calculations from early work of Crosswhite to the recent development of density functional theory (DFT) are beneficial for investigating the mechanism to control the luminescence properties [22–25]. Recently, innovative strategies through external stimuli have also been proposed to generate tunable upconversion luminescence [26]. So far, few attempts have been made to provide a systematic investigation of various strategies that have been successfully applied to tune the luminescence properties of upconversion nanocrystals and a broad overview of applications of these upconversion nanocrystals in diverse areas. In this review, we highlight different methods for tuning upconversion emission properties in lanthanide-doped nanocrystals. We begin with a brief introduction to the fundamental principles of the upconversion phenomenon. Subsequently, we provide a detailed description of recent experimental strategies to control the upconversion luminescence, including conventional chemical routes and those beyond chemical methods. Various significant emerging applications based on tunable upconversion luminescence are also highlighted in the third section. Finally, some potential future challenging issues and improvements in this field are suggested in the hope to deepen our understanding further.

1.1 Properties of upconversion nanoparticles

Typically, lanthanide-doped upconversion nanoparticles consist of an inorganic, photostable host embedded with various trivalent lanthanide ions (Figure 1a-d) [27]. Unlike conventional anti-Stoke processes, such as second-harmonic generation and multiphoton absorption, photon upconversion in lanthanides doped nanocrystals relies on the physically existing intermediary energy level, thus possessing higher frequency conversion efficiency. Upconversion emission originates from inner-shell 4*f* electrons which are well-shielded by the complete filled $5s^2$ and $5p^2$ sub-shells of lanthanide ions. This attribute renders upconversion emissions hardly influenced by environment, giving rise to unique optical properties like sharp emission bands, reliable photostability and long excited-state lifetimes [2]. In fact, the shielding effect that considers the $4f^n$ in electronic interactions with valence shells becomes necessary as well [28].The lanthanide's $4f^n$ electronic configuration can be split by the mutual repulsion from the coulombic interaction of the electrons and spin-orbit coupling among *f*-electrons, inducing a great diversity of energy-level arrangements. This feature made lanthanides ideal candidates for carrying out photon upconversion (Figure 1e) [29,30]. Theoretically, lanthanides feature substantially diverse energy levels and are capable of emitting light with any wavelength corresponding to the diverse distribution of the electrons within 4*f* sub-shells [31,32]. Figure 1f shows the typical luminescence photograph of colloidal solutions of representative Ln-UCNPs featuring the multicolor emission profiles [33]. Many theoretical works appeared in recent years have been used to explain the electronic structures of rare-earth materials. Based on vibronic coupling, Liu established a semi-empirical model to simulate the experimental spectra [23]. DFT with improved self-consistency calculation method is applied for further understanding and more accurate description of the energy levels of the lanthanide materials [25,28].

1.2 Upconversion luminescence process

Previous fundamental studies on lanthanide doped crystals allowed an improved comprehension of the underlying physical phenomenon in photon upconversion processes. With the abundant intrinsic energy levels of the *4f* electron configurations, trivalent lanthanide ions can undergo various upconversion processes. Typically, photon upconversion occurred through sequential absorption of two or more low-energy photons and converted the gain to a high-energy state. In principle, upconversion process in Ln-doped UCNPs can be categorized into four classes: Excited State Absorption (ESA), Energy Transfer Upconversion (ETU), Cooperative Sensitization Upconversion (CSU), and Photon Avalanche (PA) [34–36]. Figure 2 illustrates the proposed upconversion mechanisms, which will be described below.

These anti-stokes processes are realized by converting several photons within metastable energy levels into long-lived photon state of a dopant ion within the nanocrystals. ESA or ETU are the two common types of upconversion processes relying on the accumulation of the low-energy photons via the multiple intermediate states of lanthanide ions. In the ESA

process, two low energy photons sequentially absorbed are temporally stabilized in a real intermediary energy level of a single lanthanide ion, while in an ETU process, two low-energy photons of the same energy were absorbed by two adjacent sensitizer ions and successively transferred to a neighboring activator ion that can emit from a high energy level through a non-radiative energy transfer process. The major difference between ETU and CSU lies in the absence of a long-lived intermediate energy state of the activator, and thus the upconversion efficiency of CSU is very low. Unlike these three upconversion processes described, strong upconversion emissions from PA process do not depend on the synchronous progress with the ground state within lanthanide ions and could be generated when the power of the excitation exceeds a threshold value. On the other hand, there are four types of lanthanide ions involved in the EMU process within Gd-based core/shell nanoparticles. The excitation photon is first absorbed by a sensitizer, and the excited energy is subsequently transferred to the neighboring accumulator ion. Then the energy trapped in the accumulator ion is further transferred to a migrator ion to its high-lying excited state. After that, the excited energy can migrate across the interface at core-shell through the sub-lattice structure. Finally, the migrating energy stabilizes in the energy level of the activator, generating upconverted emitting photon when these excited ions return to the ground state. It should be noted that energy transfer upconversion (ETU) is known to be the most efficient frequency upconversion mechanism, which typically occurs in a sensitizer–activator system. After absorbing the excitation photons, resonant energy transfer from the sensitizer to the activator populates not only the ground state but also intermediate state of a nearby activator center. The energy transfer probability W_{S-A} between the sensitizer and activator ions can be described with the Förster-Dexter model:

$$W_{S-A} = \frac{3h^4c^4}{64\pi^5 n^4 \tau_S} \times \frac{Q_{abs}}{R_{S-A}^6} \times \int \frac{f_{em}^S(E) f_{abs}^A(E)}{E^4} dE \qquad (1)$$

Where h is the reduced Plank's constant, c is the speed of light in a vacuum, n is the refractive index of the host lattice medium, τ_S is the intrinsic lifetime of the sensitizer ions in the absence of activators, R_{S-A} is the distance between the sensitizer and activator ion, Q_{abs} is the integrated absorption cross section of the activator ion, the integral expresses the spectral overlap of sensitizer ion emission and activator ion absorption, as a function of photon energy E ($E=hc/\lambda$). Therefore, one can note that the R_{S-A} and the spectral overlap are the two critical parameters governing the energy transfer. In addition, high absorbance (Q_{abs}) by the activator at the emission wavelength of the sensitizer and sensitizer ions with lower τ_S are also beneficial for more efficient energy transfer. Moreover, from fundamental ESA process, highly efficient ETU process and to even EMU, accurate relative positions of electronic excitations within the host band structures to describe the optical transitions are highly desired. Recently, EMU model has been further improved based on DFT calculations, which revealed that a hidden energy level of Gd ions from level splitting due to close shell effect [37,38]. However, the present challenge for the systematical study of upconversion luminescence is to clarify and quantify the involvement of several mechanisms in one system.

2. The methodology of tuning photon upconversion in lanthanide-doped nanocrystals

Over the past decade, essential research on upconversion nanocrystals has made tremendous progress by leaps and bounds. The ability to precisely modulate the photophysical luminescence properties of upconversion nanocrystals on demand is vital in tuning their properties into real-world applications. A variety of empirical and academic studies on upconversion processes have greatly resulted in our fundamental understandings in various luminescence of upconversion nanocrystals, which provide meaningful indications for various techniques. In this section, we attempt to provide a systematic investigation of different strategies that have been successfully applied to tune upconversion luminescence in lanthanide-doped nanocrystals. Broadly, strategies used in tuning upconversion luminescence fall into either the "chemical method" or the "external stimuli method", as illustrated in Figure 3 and Figure 7. Numerous studies using conventional chemical routes have been reported, including dopant ions variation, host matrix manipulation, spatial confinement of dopants, and nanoscale integrations. Alternatively, innovative strategies beyond conventional chemical method have also been reported to tune the luminescence of upconversion nanocrystals, including electric and magnetic-field-induced tuning, photonic crystal engineering, surface plasmon coupling, altering pH environment, mechanical stress tuning, micro-lens light focusing, thermal phonon activation, varying excitation source a, d anisotropic polarization modulation. Detailed theoretical works on mechanism study combined with experimental works are also proposed to assist in controlling the upconversion luminescence.

2.1 Tuning by Chemical Methods

Chemical synthesis routes have been extensively employed to realize tunable upconversion emission for different possible applications [13,39–46]. The luminescence of lanthanide-doped nanocrystals primarily originates from the *f-f* transitions of lanthanide ions. Determined by the nature of *f-f* transitions, the UC emission efficiency is still below

expectation induced by the limited cross-section of lanthanide ions. Therefore, by manipulating the electron transitions of lanthanide elements between different energy levels, one can tune the emission profiles of upconversion nanocrystals in the form of emission wavelength, intensity, and dynamic decay rate.

2.1.1 Changing chemical composition and varying dopant concentration

By utilizing different dopant ions, adjusting dopant concentrations or co-doping activators with different emission wavelengths in the host material, multicolor emission of upconversion nanocrystals can be easily achieved. Our group reported the upconversion multicolor fine tuning from red-to-green emission based on $NaYF_4$:Yb^{3+}/Er^{3+} nanoparticles through controlling energy transfer of different lanthanide ions by varying Yb^{3+} concentration [47]. In addition, by carefully co-doping with Er^{3+} and Tm^{3+} in the $NaYF_4$ host material, we also able to manipulate the emission profiles of UCNPs (Figure 4a). It was found that a tiny change in the Er^{3+} concentration would cause significant changes in emission intensity balance between Er^{3+} and Tm^{3+}, resulting in a wide range of colors from blue to white. Yan's group has carefully studied another co-doped system $NaYF_4$:Yb^{3+}/Er^{3+} dependency on the ratio of both dopants, in which they determined the optimal concentration of Yb^{3+} and are 20% and 2% respectively [48]. Besides, several groups have confirmed that such dopant concentration enhancement on UCL is more favorable in high photon emission process [49–52].

In principle, the use of the high doping level of luminescent activator ions (Tm^{3+}, Er^{3+}, or Ho^{3+}) permits the maximization of the transfer of the excitation energy absorbed by the Yb^{3+} sensitizers. However, the interaction between different lanthanide activators in the host lattice is usually accompanied by a quenching effect due to deleterious cross-relaxations. In this context, a low dopant concentration is favorable since it can minimize the quenching effect. In another separate work, Jin and co-workers reported an intriguing design utilizing the concentration quenching effect to achieve broadly control over the luminescence kinetics [53]. Since the increase of doping concentration would cause increased energy migration rate due to the reduced ionic distances, a reduction in the emission lifetime of the nanocrystals will be induced. In this work, by varying the doping concentration of Tm^{3+} activator in the range 0.2–8 mol%, they achieved broadly tunable lifetimes from 25.6 μs to 662.4 μs in the blue emission band of Tm^{3+} (Figure 4b). A lifetime-based coding technique via lanthanide doping was also demonstrated, providing a new platform for time-domain optical multiplexing for security marking applications. In another theoretical work by Yan and Huang, the cluster effect induced by a high concentration of dopants, in which they conversely utilize the aforementioned quench-paths of upconversion energy transfer. Attributed to the homogeneous core@shell band offset at the interface region, the Er^{3+} UC luminescence with self-sensitization has been achieved through the additive energy transfer path [54].

Tailoring the local crystal field through point symmetry of the luminescent centers can loosen the parity-forbidden *4f–4f* intra-configurational transitions of Ln^{3+} ions. The involvement of Li^{+} ions in Ln-doped nanocrystals to tune the upconversion emission through the symmetry tailoring was accomplished by the alteration of the local crystal field around Ln^{3+} have been reported by several groups [55–58]. Moreover, Bi^{3+} and Fe^{3+} can also be applied to accomplish the local crystal field tailoring [59,60].

2.1.2 Host Matrix Screening

The host matrix also plays a critical role in determining the luminescence characteristics of upconversion nanocrystals since the excited energies of the dopant ions may interact with host materials through lattice vibration [21,61–63]. Estimation of quantum efficiency is highly dependent on the energy levels of the host material. P. Dorenbos has systematically derived the ground levels of Ln^{3+} ions within the bandgap of different host matrix that proved the overlap of excited states of with band structures [64,65]. The accurate location of the energy levels of divalent Ln ions relative to the valence and conduction band is proposed based on a three parameters model as follows:

$$E_{fd}(n, 2+, A) = E_{Afree}(n, 2+) - D(2+, A) \quad (2)$$

$$E_{Vf}(n+1, 2+, A) = E^{CT}(6,3+, A) + \Delta E_{CT}(n, 6, 3+) \quad (3)$$

where $E_{Afree}(n, 2+)$ and $\Delta E_{CT}(n, 6, 3+)$ are a constant value. $E_{Vf}(n+1, 2+, A)$ is the charge transfer (CT) energy between valence band maximum (VBM) and 4f ground state of divalent Ln ions and $D(2+, A)$ is the redshift.

The alteration of the host matrix would result in different phonon energy that will lead to different upconversion energy transfer pathways. There are numerous observations of structure-dependence of upconverting nanocrystals especially related to the lattice symmetry [39,43,45,66–68]. An enhancement of luminescence emission has been noted for ZnO: Er^{3+} in the monoclinic phase than the tetragonal phase [69]. Even with similar Er energy levels, upconversion intensity in Er-doped Lu_2O_3 is found to be much greater than Er-doped Y_2O_3, which can attribute to the allowance of mixing of 4f and 5d in the monoclinic structure rather than other structures [70].

In comparison with oxide materials, fluorides host materials usually have low phonon energies and are commonly used to achieve highly efficient upconversion luminescence. For instance, Zeng *et al.* have been reported the Mn^{2+} and Er^{3+} co-doped $KMnF_3$ nanocrystals [71]. They observed the strong interaction between different lanthanide ions in $KMnF_3$ host nanocrystals, leading to a decrease of the excitation energy at the $^4S_{3/2}$ level of Er^{3+}. This strong interaction subsequently caused the increased population at the $^4F_{9/2}$ level of Er^{3+} because of the low energy loss fluorides host materials and the energy transfer from Mn^{2+} to Er^{3+} ions. As a result, this design gives rise to an intensified upconversion luminescence.

2.1.3 Controlling size and utilizing core/shell architecture

Besides changing the chemical composition, controlling the size and architecting core/shell structure of nanocrystal can also achieve tailorable emission [63,72,73]. In the bulk phase of Ln-doped materials, the efficiency of the energy transfer for upconversion luminescence is usually low by the number of quenching effects between luminescence centers. These quenchers are usually assisted by the phonons or intrinsic defects in the bulk-sized Ln materials. Generally, as the size of the nanocrystal decreases, the concentrations of surface defects increase [74,75]. Moreover, those defects act as surface quenching sites and those emissions that require more phonons to bridge the energy gaps are readily susceptible to the defects. For example, owing to the surface quenching effect, the blue upconversion emission of Tm^{3+} ions was reduced when the crystalline size of $NaGdF_4:Yb^{3+}/Tm^{3+}$ nanoparticle became smaller [76]. Similar observations have been reported in $NaYF_4:Yb^{3+}/Er^{3+}$ nanoparticles. As a result of less quenching effect in green emission that requires more phonons, the ratio of green and red emissions and the emission decay time were reduced with decreasing crystalline size [73]. However, some DFT work has unraveled the potential contribution of the intrinsic defect and doping defects for achieving UC luminescence in CaS in terms of tuning energy levels [77].

Recently, spatially confinement of dopant ions by utilizing core/shell architecture structures as a self-protection strategy has proven to be effective to decrease deteriorative quenching effects among various dopants and thus control the luminescence of upconversion nanocrystals [27,78,79]. A perfect epitaxial shell layer should serve as blocking or suppressing the energy depletion channels from an activator to quenching sites (e.g., defects, impurities, solvent molecules, and capping ligands) on the core surface. This strategy offers a new route to achieve multicolor tuning of upconversion by integrating various dopant ions into a spatially confined nanoscopic region. Extensively, multilayer and heterogeneous core-shell structures have also been employed. For example, our group presented a core-shell structure with energy migration process to realize multicolor fine-tuning of upconversion emission (Figure 5) [27]. We also demonstrated that by harnessing various energy transfer or migration pathways, a wide range of color emission of upconversion nanocrystals could be achieved. By coating an inert $NaYF_4$ inert shell on the surface of $NaGdF_4:Yb^{3+}/Tm^{3+}@NaGdF_4:A$ ($A=Tb^{3+}$, Eu^{3+}, $Dy^{3+,}$ and Sm^{3+}) nanoparticles, we observed that the upconversion emission was dramatically enhanced in this multi-shell design [33]. A novel $LiLuF_4:Ln^{3+}$ core/shell UCNP system is also reported to remarkably approach quantum yield of 7.6% with new energy transfer routes [80]. In addition, by tuning the doping concentration of the activators in distinct layers, the optical emission will also be modulated as desired. Remarkably, Yan's group has achieved the simultaneous tuning of upconversion spectra and lifetime in a versatile nanoplatform based on a five-layer core/shell structure. They introduce the noninterfering luminescent regions in the nanosystem to correlate the spectra and lifetime orthogonally with excitation [40]. Till now, the upconversion efficiency of the core-shell system and the consequences caused dilemma between size and quenching of UCNPs still remain challenges for present research.

2.1.4 Incorporating various surface modifications

The capping ligand will be the cost of synthesizing UCNPs by reacting lanthanide precursors in an organic solvent to achieve the morphology and shape uniformity. Due to the hydrophobic nature of the capping ligands, UCNPs are very easy to aggregate in water solution. To alter the UCNPs to hydrophilic or biologically functionalized, there are many types of research the removal or change of the capping ligands. The direct method including strong acid or excess ethanol can remove the capping ligands [27,81]. The more efficient method is the ligand exchange or oxidation such as capping organic ligands. Capobianco and co-workers developed a surprising strategy that protonated the surface oleate ligand to alter the NCs from hydrophobic to hydrophilic and further enhance the UC emission [82]. In addition, organic dyes also have been used as broadband sensitizers for enlarging absorption cross section for upconversion process. In 2012, Zou and co-workers reported that incorporating a NIR dye to Yb^{3+} and Er^{3+} co-doped $NaYF_4$ nanoparticles would enable a broadband excitation of $NaYF_4:Yb^{3+}/Er^{3+}$ nanoparticles, resulting in 3,300-fold enhancement in total luminescence intensity [83].

As an alternative route, Yan's group demonstrated a strategy to realize the reversible tuning of UCL based on the combination of photosensitive organic molecules and upconversion nanoparticles [84]. The change in emission color and intensity of the upconversion nanocrystals are enabled by rapid energy transfer between dye molecules and upconversion nanocrystals. The photochromic molecule exhibits reversible transformation between the open-ring isomer and the closed-ring isomer under irradiation of appropriate UV and visible light (Figure 6a). These two isomers of photochromic molecules exhibit different optical absorption spectra. The change in the optical transmission surrounding the upconversion nanocrystals

can reversibly quench the green upconversion emission (Figure 6b). As a result, the upconversion photoluminescence can be modulated by utilizing the reversible absorption character of photochromic molecules. Alternatively, polymer encapsulation or coating inorganic quantum dots can bear further modification with various functional entities for biomedical applications [85,86]. When upconversion nanocrystals are near with external nanomaterials, the spectral overlapping of the emission band of upconversion nanocrystals with the absorption spectra of the outside nanomaterials may initiate energy transfer process, resulting in a selective wavelength tuning. For example, emission color tuning from green to pink is reported in a hybrid nanocomposite based on CdSe QDs coated $NaYF_4$:Yb^{3+}/Er^{3+} nanoparticles (Figure 6c and d) [87].

2.2 Strategies beyond Chemical Methods

Innovative routes in chemical synthesis enabled tailored emission profiles by modulating the intrinsic structures of upconversion nanocrystals with the host composition, dopants, and nanoscale integration. In concert with these approaches, utilizing an external stimulus has recently emerged as an effective method that allows for further manipulation of upconversion luminescence, which will be discussed in the following section (Figure 7).

2.2.1 Diverse excitation sources

For UCNPs, the selection of excitation source is limited that will constrain their further application, in which 980 nm laser is the most commonly used excitation source. Recently, more and more UCNPs have been applied to biomedical imagining applications. Owing to the relatively large absorption cross section around 980 nm, Yb^{3+} ions are usually used as sensitizers for upconversion luminescence. However, the 980 nm excitation will overlap with the absorption of water and cause overheat effect to the tissues. To solve this problem, novel excitation sources have been tried to minimize the heating effect. For instance, Nd^{3+} ions were employed to expand the excitation source due to the multiple NIR excitation bands at 730, 808, and 865 nm, respectively [44,88–90]. Similar excitation efficiency with 980 nm laser has been observed in work by Zhan and his co-workers. They proposed that employed a cost-effective 915 nm laser to replace the conventional 980 nm for deeper tissue imaging [91]. Therefore, upconversion nanoparticles doped with different sensitizers can yield various emissions in response to different NIR excitations.

In addition to NIR excitation, lanthanide-doped upconversion nanocrystals were also found to be excited by a beam of electrons. In 2015, our group demonstrated that a helium ion beam (α-beam) could be used as an effective form of excitation source for pumping upconversion process [92]. The luminescence intensity could be readily tuned by adjusting excitation voltage and current density. Unlike the conventional upconversion processes under NIR laser irradiation, the interaction between the α-beam and the crystal lattice causes the atomic ionization inside the crystal. Subsequently, the ionized secondary electrons can release their energy able to not only excite Yb^{3+} and Tm^{3+} ions but also allow energy transfer from the excited Yb^{3+} to its neighboring Tm^{3+} ions, populating the excited states of Tm^{3+} (Figure 8b). Importantly, this approach enables high-resolution luminescence imaging with a spatial resolution of sub-30 nm (Figure 8b).

Controllable emission color can also be achieved by carefully manipulating a non-steady state energy transfer upconversion process. Recently, our group demonstrated a novel strategy for dynamically fine-tuning the upconversion emission in the full-color range (Figure 8a) [93]. In this design, under the excitation of 808nm and 980nm, the upconversion nanocrystals with a multi-shell structure showed different emission colors. For example, when a continuous-wave laser with 808 nm excitation wavelength is used, the emission band appears mainly at 470nm, while altering the pulse width of the 980nm laser from 200 μs to 6 ms, the emission color was dynamically controlled within the visible range due to the varied ration between red and green emission. These findings provide a new opportunity for precisely controlling upconversion emission in a wide range of applications such as a volumetric display, multiplexed sensing, anti-counterfeiting and so on. In another intriguing demonstration, Zhang and co-workers reported an integrated core/shell/shell upconversion nanostructure which can emit a wide range of colors under different excitation power density (Figure 7d) [94]. This is realized by the investigation for the transition process within the lanthanide ions. Normally, different activators exhibit different sensitivity to the excitation power density of the laser. In this way, one can control the photon transfer process within the transition pathway and further manipulate the emission colors by varying the excitation laser power density. Especially, the white emission can be generated through the combination of several narrow spectral bands.

Very recently, stimulated emission depletion mechanisms have been adopted to control the upconversion luminescence. For instance, Jin and colleagues report a new approach for efficiently suppressing the fluorescent region of the UCNPs to realize super-resolved STED nanoscopy (Figure 8e) [95]. Upconversion nanoparticles with high doping concentration of Tm activator ions ($NaYF_4$: 20% Yb^{3+}/8% Tm^{3+}) were designed and synthesized as the luminescent probe since high doping level of activators often leads to drastically reduced ionic distance and thus strong cross-relaxation between neighbouring Tm^{3+} ions, resulting in photon avalanche and population inversion between the $_3H^4$ and $_3H^6$ states. Therefore, the amplified stimulated emission caused by the 808 nm beam can deplete the $_3H^4$ state and switch off the upconversion

emission efficiently. Similar observations have been reported in $NaYF_4$:Yb^{3+}/Er^{3+}/$NaYF_4$ core/shell nanoparticles [96]. Under illumination of 1540 nm infrared laser, the red emission (655 nm) intensity was reduced due to the emission depletion of the intermediary energy level that interacts resonantly with depletion beam. Zhan and He also proposed similar work on achieving super-resolution of bio-image based on $NaYF_4$:18% Yb^{3+}, 10% Tm^{3+} nanoparticles with even higher Tm doping concentration. They applied a single pair of excitation/depletion beam (810 nm) and acquired 96% depletion of blue emission (455 nm). Therefore, by switching on/off depletion beam, the upconversion emission could be modulated, which can significantly lower the intensity requirements of laser depletion [97].

2.2.2 Theoretic Investigation

Due to unique electronic structures of *f*-orbital in lanthanide elements, the dynamic of their upconversion luminescence properties has become more complicated because of variations in both chemical and electronic structures. Theoretical understanding is of great importance to achieve tuning of upconversion luminescence properties for further manipulation, which including the basic electronic structures, spectra properties, energy levels. Since 1960, the electronic structures of lanthanide solid materials have been well studied by pioneer works from Judd et al. [50–52,54,55]. These works have established the fundamental understanding of electron behaviors and benefit the later work of Crosswhite and Carnall, which have proposed and applied the empirical effective operator model in Ln-doped solids [22,98]. Carnall and his co-workers have systematically analyzed different Ln-doped LaF_3 in terms of transitions within $4f^n$ configurations. By combining energy matrices and free-ion terms with a crystal field, they have successfully correlated the transition energy with theoretical level structures. Hence, these basic models have allowed the calculation of the free ion energy levels and splitting in $4f^n$ [99].

Generally, the much higher phosphor efficiency with larger cross-sections in *4f-5d* transition than intra-*4f* transitions come from the parity allowed rule. The optical spectra can be modified by the presence of dopants based on the phonon-electron interactions. The vibronic transitions also have a great contribution to the broadband absorption and emission in Ln-doped materials. Hence, to control the upconversion luminescence dynamic, investigation of vibronic transition and phonon-assisted energy transfer are necessary. Chen and Liu have interpreted the spectrum of Er-doped Y_2O_2S under low temperature in terms of the confinement effects based on a study of phonon density of states(PDOS) [100]. They have estimated the population ratio of Er^{3+} on the two ground levels as follows:

$$\frac{N1}{N2} \approx \frac{W_{LIT} + W_{Raman,abs} + W_{21,abs}}{W_{Raman} + W_{21}} = e^{-\frac{\Delta E_{21}}{kT}} + \frac{W_{LIT}}{W_{Raman} + W_{21}} \quad (4)$$

where W_{LIT} is the rate of laser-induced thermalization through nonradiative relaxation on the excited states(populating), $W_{Raman,\ abs,}$ and W_{Raman} are the rates of two Raman phonon absorption and emission, respectively. W_{21} is the spontaneous phonon emission from ground level 2 to level 1. All these competition processes lead to the equilibrium population of the $^4I_{15/2}$ upper ground state. The nanocrystal size effect on PDOS and the phono-relaxation rates are calculated. The numerous hot bands in the spectrum from $^4I_{15/2}$ ground state to $^4F_{7/2}$ excited states can be attributed to the lack of low-energy phonon modes, which can reduce the energy transfer efficiency. This can explain the much lower upconversion efficiency from 20-50 nm nanocrystal to 400 nm nanocrystals. Later, Liu has established a semi-empirical model to simulate the experimental spectra based on vibronic modes [23]. Based on constrained frequency degeneracy modes as Eq. (5) and vibronic coupling strength with specific line width, the luminescence spectra of Ln-doped $Y_3Al_5O_{12}$ can be successfully generated from a calculation model for detailed analyzation of energy levels, vibronic modes, and coupling constants.

$$I(E) = \sum_k C_k(\Delta E_k) f_{m,n}(E, \omega_1, \omega_{2,k}) \quad (5)$$

Due to the quick development of computational resources, DFT calculation is an alternative method that can improve our understanding towards the energy transfer mechanism in Ln-doped UC luminescence to assist breaking the bottle-neck of quantum yield [38,61,101,102]. Start from the fundamental view of Yan and Huang's work towards the electronic structures of the β phase alkali-earth fluorides, which have analyzed the origins of the different observation on the basic band structures [37]. The understanding of EMU model has been improved with more accurate Gd *4f* levels based on the different overlap of F-Ln orbitals. The narrower bandgap of $NaGdF_4$ originated from a shifting 4f-empty state towards the bandgap. Within the first Brillouin zone, the local disorder can modulate the valence band near the Γ point. Recently, our group also proposed new route of energy transfer based on clustering effect from high dopant concentrations [54]. An Er-Yb-Er self-sensitized upconversion mechanism has been proposed to enhance the UC energy transfer based on the unusual absorption behaviors is determined by the Yb^{3+} dopants instead of sensitizers. Converse to the conventional idea, we utilize a conventional quench pathway to create an in-shell to in-core route assisted by the interface region. The interlayers showed evident potential difference arises from the band-offset effect that would de-excite the electrons from higher Yb_Y^{3+} levels to a lower Er_Y^{3+} level and reach red upconversion emission. Therefore, more details can be supplied from the different theoretical works that benefit our understanding of the upconversion energy transfer mechanism and create more possibilities in manipulating the upconversion luminescence in the future experiments.

2.2.3 Surface Plasmon Coupling

Beyond traditional surface modification, surface plasmon technique has great potential in optoelectronic controlling, which based on the coherent oscillation coupling of free electrons with the excitation light [103–106]. Commonly, plasmons in noble metals NPs with size much smaller than the incident wavelength (< 20 nm) are called localized surface plasmon resonance (LSPR), which can be adjusted by controlling their morphology, chemical composition, and spatial configuration. The plasmon damping dynamics is mainly dominated by three processes including electron-holes generation, thermalization, and photon emission. Especially, for metal size close to the quantum region, electron-electron interaction becomes important. When approaching the nano metal, the corresponding electric field distribution of NPs will be altered. Based on the approximation of quasistatic theories, the distortion of electron cloud induced by the altered electron field can be expressed by the metal polarizability with the scattering, absorption, and extinction cross-sections of a noble metal as follows [107]:

$$\alpha(\lambda) = V_{NP}\frac{\varepsilon(\lambda)-\varepsilon_m(\lambda)}{3\varepsilon_m(\lambda)+3L_i(\varepsilon(\lambda)-\varepsilon_m(\lambda))} \quad (6)$$

$$\mathrm{C_{abs,i}} = kIm(\propto(\lambda)) \quad (7)$$

$$\mathrm{C_{scat,i}} = \frac{k^4}{6\pi}|\propto(\lambda)|^4 \quad (8)$$

where λ represents the light wavelength, V_{NP} is the volume of nanoparticles, k is the wave vector, and L_i is the depolarization factor that varies with the metal morphology. ε and ε_m are the dielectric constant of metal and the non-absorbing surrounding material, respectively. Because of this local field effect, the excitation field as well as the emission decay rate can be enhanced, but also quenching by energy back-transfer from emission center to metal structures is possible. Thus, this local field effect shows potentials for manipulating upconversion emission in terms of emission intensity, wavelength and decay rate [108–111].

In different situations, plasmonic resonances structure can extend the upconversion emission in various level when the resonance wavelength matched with absorption band or emission band of UC luminescence. For instance, with noble metal NPs nearby, the absorption cross-section of the UCNPs can be expressed as [112]:

$$\sigma_{abs} \propto \omega Im[\alpha](\frac{E_{Loc}}{E_0})^2\cos^2\theta \quad (9)$$

Moreover, the expression of quantum yield (Q) will also be affected with contribution from the LSPR induced by Au NPs as follows [113,114]:

$$\mathrm{Q} = \frac{\Gamma_{Rad}+\Gamma_{Rad}^{M}}{\Gamma_{Rad}+\Gamma_{Rad}^{M}+\Gamma_{NRad}+\Gamma_{NRad}^{M}} \quad (10)$$

Where Γ_{Rad} and Γ_{NRad} represents the radiative rates and non-radiative rates, respectively. The Γ_{Rad}^{M} term is the contribution from plasmon resonance influence, which can increase the emission rate by the local electromagnetic field enhancement. For high quantum yield fluorescence materials, the influence from Γ_{Rad}^{M} is limited. However, for low quantum yield fluorescence materials, the Γ_{Rad}^{M} can enhance value of Q evidently.

Especially, Au is the best candidate for coupling with UCNPs since the surface plasmon band of Au NPs can be visible-to-near-infrared tunable and cover a large range of spectral range that can largely enhance the light absorption and scattering. It has been summarized that the main causes of the LSPR modulation on upconversion luminescence including the amplification of the local electromagnetic field and enhancement of recombination rate. In 2009, first work about applying LSPR in enhancing upconversion luminescence intensity had been reported by Yan's group based on Ag nanowires coupling with $NaYF_4$:Yb,Er nanocrystals [115]. Both green and red emission intensity has been improved with an increase factor of 2.3 and 3.7, respectively.

Recently, there are some research works focused on the coupling structure on single particle level to tune upconversion emission properties and investigate the mechanism in detail [116–118]. The LSPR properties are mainly determined by the nanostructure and local environment, in which different geometry of the noble metals have shown distinct effects. For example, Hartschuh and colleagues reported a system comprised a good nanotip with $NaYF_4$:Yb^{3+}/Er^{3+} nanoparticles, demonstrating how the locally enhanced electric fields in the vicinity of a sharp metal tip can amplify the excitation and emission rates of a nearby upconversion nanoparticle, as shown in Figure 9a [119]. In this case, when a gold nanotip was put closed to one single $NaYF_4$:Yb^{3+}/Er^{3+} nanoparticles, both the green emission and red emission was enhanced as can be seen in the tip up/down spectra in Figure 9b and 9c. Besides, Au or Ag arrays and grating films [120], Au nanohole array [121], gold pyramid array [122], Au nanocavity array [123] are also investigated by different groups for improving the upconversion emissions. In core-shell structures, the spatial parameter is another important effect for LSPR properties. Optimization on the distance between noble metals and UCNPs have been carried out by many research groups as well

[124,125]. These results suggested that upconversion emission profiles can be modulated by varying the distance between the nanoparticle and the plasmonic center.

In another separate work, Lee and co-works developed a novel hybrid structure with an asymmetric nanocrescent antenna on upconversion nanoparticle (ANAU). This plasmonic antenna is able to deliver excitation light effectively to the upconversion nanoparticle by nanofocusing light, giving rise to asymmetric frequency upconverted emission concentrated toward the tip region [126]. The single upconversion nanoparticle was confined in the asymmetric nanocrescent antenna and exhibited directionality-dependent frequency upconverted emission (Figure 9d and e). In this system, a 16.1 times enhancement of photon emission toward the nanocrescent antenna tip region were generated by ANAU, whereas photon emission is reduced by half toward the nanocrescent antenna body (Figure 9f).

2.2.4 Magnetic and Electric-Field-Induced Tuning

Compared to the conventional chemical tuning strategies, dynamically adjusting energy level splitting or crystal lattice initiating the energy pathways are alternative routes that allow for dynamic and in-situ modulation of upconversion luminescence. For example, Hao's group reported an electric field induced modulation of upconversion emission [127]. By applying a bias voltage to the ferroelectric host material $BaTiO_3$ with Yb^{3+} and Er^{3+}, dynamically luminescence tuning and enhanced upconversion emission were observed through the converse piezoelectric effect (Figure 10). The enhancement and modulation of upconversion photoluminescence can be attributed to the increased variation of Er^{3+} site symmetry because of the distinct structure symmetry of the $BaTiO_3$ host effected by an electric field.

The extra big bandgap and local non-crystallization of surface structures of UCNPs can largely influence their upconversion emission. A clearer understanding and clever utilization on the energy levels can assist modulating the upconversion optical properties. Meijerink's group has observed the effect of the electric dipole and magnetic dipole to the emitters [128]. Different dependence index in cavity model of Eu-doped and Gd-doped $NaYF_4$ has been measured and calculated to describe the radiative transition probability between different energy levels. Based on such theoretical fundamental and preliminary experiment results, further modulation on upconversion emission can be achieved. Li's group developed a similar strategy to tune upconversion luminescence by introducing a magnetic field. The external magnetic field was used to manipulate the energy level of the doped lanthanide ions to control upconversion luminescence [129]. The magnetic tuning mechanism of the green emission is due to the Zeeman splitting of $^4S_{3/2}$ energy levels of the Er^{3+} ions. A general schematic diagram for energy levels splitting of Er^{3+} ions is explained in Figure 11, especially the $^4S_{3/2}$ and $^4I_{15/2}$ energy states are often available for the stabilization of the excited ions. Induced by applied magnetic field, $^4S_{3/2}$ of Er^{3+} cracks to four different energy levels: |+3/2>, |-3/2>, |+1/2>, |-1/2>. And when the external magnetic field gets stronger, the distance between |-3/2> and |-1/2> is increased, resulting in that |3/2> doublet state is further splitting. Meanwhile, the chance for the slight radiative transition from |+3/2> to |3/2> will be increased. Since most upconversion luminescence comes from the lowest |-3/2> state of Er^{3+} ions, so in this way, the upconversion emission in visible range would be reduced. Similar observations have been reported by recent work [130].

2.2.5 Photonic Crystal Engineering

Photonic crystals (PCs) have widely announced to manipulate the emission intensity and lifetime of the upconverters within the structure [131–136]. Especially, periodic dielectric structures based three-dimensional photonic crystals permit the manipulation of the flow of light and generate photonic band-gaps. By making an optimal factor, the photonic crystals can provide high stored electric field intensity within the structure. Thus, it can affect the spontaneous and stimulated emission process through the interaction between the upconversion emitter and its local electromagnetic state, resulting in enhanced emission without quenching effects. Recently, several groups achieved the obvious enhancements of upconversion emission by depositing UCNPs on the surface of the photonic crystal. Different modulating effects can come from the different position of emitters within the 3D structure, various types of photonic crystal and different refractive index of the building blocks. For instance, Song's group investigated the coupling effect between UCNPs and photonic crystal structure composed of polymethyl methacrylate (PMMA) opals with periodic structures by depositing $NaYF_4$:Yb^{3+}/Tm^{3+} nanoparticles on the surface of PCs (Figure 12) [137]. As a result, more than 30-folds of UC emission enhancement is realized when the excitation frequency matched well with the stop band of photonic crystals. It was found that the stop band of PMMA photonic crystals strongly contributed to the degree of upconversion enhancement.

2.2.6 Altering pH environment

The upconversion photoluminescence can also be affected by changing their surrounding pH environment. The pH value is a general parameter which is determined by the concentration of hydrogen ions in solution. The hydrogen ions may affect the interaction among the emitter ions directly or change the upconversion emission indirectly by tuning the parameters which can determine upconversion luminescence. For example, Capobianco's group observed that upconversion luminescence could be changed by tuning the pH environment of oleate ligand-free $NaYF_4$: Yb^{3+}/Er^{3+} nanoparticles through

making an acid treatment to the as-synthesized UCNPs. In this case, the red emission changed when pH is decreased. This phenomenon may attribute to different multi-phonon relaxation processes among several excited states of the emitter ions when surface OH groups in water have been affected by tuning pH [82].

In another study, Hao's group showed a hybrid system composed of silica-coated $NaYF_4$: Yb^{3+}/Er^{3+} nanoparticles and cysteine–Au NPs. The pH value can control the assembly process of AuNPs and further modulate the upconversion emission [138]. In this way, upconversion luminescence may be switched depending on the changes of OH ions concentration in the reaction system. For mechanism, the cysteine linking the AuNPs is pH sensitive so the reversible assembly of AuNPs can be controlled by destroying and rebuilding the linkage. And meanwhile, the plasmon absorption band of these AuNPs matches with the emission band of UCNPs, and by changing the size and morphology of AuNPs, the absorption bands can be red-shifted to some extent. As a result, upon tuning the pH value, the green and red upconversion photoluminescence are finally affected. Wolfbeis and his co-workers also observed such a phenomenon in the $NaYF_4$: Yb^{3+}/Er^{3+} nanorod system, which can be applied to a biomedical pH sensor [139].

2.2.7 Micro-lens light focusing

Micro-lens has been widely used for increasing the light concentration efficiency of solar cells or light extraction efficiency of LED [140–144]. The light field confinement by the micro-lens provides an exciting possibility for fluorescence enhancement. Recently, Li and co-works reported that spherical or discal shape bio-cells, such as yeast cell and human cell are able to focus light into a confined region, which can act as a biological micro-lens to enhance the fluorescence of UCNPs (Figure 13) [145]. It was found that the NIR excitation light was confined in a subwavelength region due to the photonic nanojet effect of the bio-micro-lens, resulting in a 100-fold enhancement of upconversion luminescence. They further experimentally demonstrated single-cell imaging and real-time detection of pathogenic bacteria, which is difficult to achieve by using conventional methods, mainly due to the small sizes of pathogenic bacteria and high motilities in dark environments.

2.2.8 Thermal phonon activation

A phonon represents an excited state of vibrations of elastic structures of materials, playing a major role in governing electrical and thermal conductivities of a material. Previous reports showed that the process of upconversion luminescence involves various non-radiative transitions whose non-radiative transition rates usually depend on the environmental temperature [146–148]. Therefore, since the gaps among energy levels of lanthanide ions can be changed under different temperature, the upconversion emission is acceptable to be tuned according to distinct temperature. For example, Li and colleagues investigated the temperature-related upconversion emission properties of Yb^{3+}, Er^{3+} co-doped $NaYF_4$ UCNPs with different particle phases and sizes [149]. They discovered the intensity of upconversion emission within β-phase UCNPs showed the largest value at about 100 K, while that of α-phase UCNPs exhibited emission quenching problem when the temperature is increased.

In another case, Jin and co-workers reported an unprecedented enhancement of upconversion emission from small-sized UCNPs with increasing temperature [150]. They proposed that the vibrations of surface-bound molecules through Yb–O chelating can work as surface phonons to broaden the excited-state energy band of the Yb^{3+} sensitizer and reduce the energy mismatch between the sensitizer and activator, as illustrated in Figure 14a. This principle facilitates the energy transfer from Yb^{3+} to adjacent activators and permits the luminescence of an upconversion process to be greatly intensified (Figure 14b). It was found that this anomalous upconversion emission enhancement effect related to the changing of temperature is depending on the size of UCNPs when the temperature is high, and this relationship becomes weak when the size of UCNPs gets larger. This thermally enhanced upconversion phenomena due to surface phonon-assisted energy transfer process of UCNPs with the relatively smaller size indicated that the surface phonon engineering could be used to overtake the thermal quenching effect of small-sized UCNPs.

Thermal activation combined with upconversion is found to be useful in enhancing solar energy efficiency by altering the poor response to low solar energy photon. Yan and Wang have unraveled a novel route for altering the unabsorbed low-energy photons into a high-energy one, which can reach a 16% power upconversion efficiency in Yb^{3+} doped ZrO_2 [151]. They also supplied guidelines for finding proper host matrix to achieve higher upconversion emission including high melting points, low thermal conductivities and strong absorption to infrared light.

2.2.9 Mechanical Stress-Induced Tuning

Upconversion luminescence mainly originates from the parity-forbidden *f-f* electron transition of lanthanide ions. Relaxing this selection rule where electric dipole transitions are weakly allowed could lead to increased probability of the electric dipole transitions and improved upconversion quantum efficiency [18,152]. Therefore, tailored emission properties can be achieved by carefully engineering the surrounding crystal field environments of the lanthanide ions. For instance, Dionne and co-workers found a strain-induced enhancement in upconversion emission in the $NaYF_4$ system by altering the geometry of the $NaYF_4$ host matrix. By manipulating the local symmetry to relax the Laporte selection rule and distances

between Ln ions to increase the electron transitions probability, a 2-fold enhancement in upconversion emission from α-$NaYF_4$:Yb^{3+}/Er^{3+} nanoparticle with 1 % reduction in lattice constant was observed, as shown in Figure 15 [153].

Alternatively, since the transition metals with *d–d* transitions are very sensitive to the surrounding environment, doping transition metals inside UCNPs is expected to be a promising approach to tune the upconversion emission. Recently, the same research team reported a mechanical force induced tuning of upconversion luminescence from a Mn^{2+}, Yb^{3+}, Er^{3+} co-doped $NaYF_4$ system for nano and micro force-sensing [154]. In this system, Mn^{2+} ion was used to substitute Y^{3+} ion partially and further serves as a pressure sensor to the lanthanide pair. Thereafter, an alternative energetic pathway is created when Mn^{2+} is coupled to the green and red emission peaks of Er^{3+} ions, leading to photons from Er^{3+} green states into the red state. Consequently, external forces will lead to changes in the external crystal field of Mn^{2+} and further alter the energy transfer processes, resulting in the changes of the relative intensities of green and red peaks in the upconversion emission spectra.

Many materials that can exhibit both mechanoluminescence (ML) and upconversion luminescence are potential candidates for applications in monitoring pressure and temperature distribution. Piezoelectric semiconductor CaZnOS with high stability and the wide band gap is considered to be a good multifunctional host matrix to introduce rare-earth doping to realize upconversion luminescence. Pan's group has reported green emission of Er-Doped CaZnOS, which intensity can be modified by applied pressure [155]. Simultaneously, the near-infrared (980 nm) excitation also show bright red emission. They utilize the high sensitivity of the fluorescence intensity ratio of $^2H_{11/2}$ and $^4S_{3/2} \rightarrow {}^4I_{15/2}$ of Er^{3+} in the upconversion process for the temperature sensor. In the same host system, Peng and his co-workers also discovered the external force induced upconversion luminescence in NIR region that covered the first and second tissue-penetrating bioimaging window, which has potential application for bioimaging [156].

2.2.10 Anisotropic polarization modulation

The physical and mechanical properties of a single crystalline material often differ with crystallographic orientations, which is said to be anisotropic. Luminescence from anisotropic crystals often exhibits polarization behavior [157,158]. Polarization can largely affect the surrounding environment of Ln dopants by lower the symmetry with uneven composition, which can enhance *4f−4f* transition probabilities for better upconversion emission. It can be seen by looking at the dependence of the luminescence intensity on the polarization angle of the excitation source. The polarized upconversion behavior from a single hexagonal-phase $NaYF_4$:Yb^{3+}/Tm^{3+} microrods was first demonstrated by Qiu and co-workers in 2013 [159]. Under a 980 nm linearly polarized laser excitation, the upconversion luminescence is also polarized, and different transitions exhibit the same polarization dependence (Figure 16a and b). By rotating a half wave plate located close to the polarizer, polarized upconversion emission was recorded as a function of the polarization angle, as shown in Figure 16c. Similar observations have been reported in $NaYF_4$:Yb^{3+}/Er^{3+} nanodisks by the same research team [160]. The linearly polarized laser beam was focused onto two nanodisks with face-up and side-up configurations, and it was found that for the side-up form, the upconversion luminescence intensity changes periodically and exhibits a sinusoidal dependence on the polarization of excitation light. In contrast, the upconversion luminescence intensity was independent of the polarization angle in the case of the face-up form. These results revealed that the polarization of upconversion luminescence depends upon the orientation of the nano-disk with respect to the polarization angle of the excitation light.

Besides normal upconversion materials, the perovskite oxide materials have also been considered as a possible host matrix for upconversion luminescence with excellent physical properties, low phonon energy. Most importantly, the crystal structure can be adjusted through different techniques. Han's group has found both green and red emission in Er-doped $PbTiO_3$ are highly enhanced around 43 times and 8 times at 523 nm and 656 nm, respectively [161]. This evident increase in upconversion emission can be ascribed to the lowering of naturally high tetragonality and polarization of $PbTiO_3$ by the introduction of Er dopant. The tailorable effect of the low-energy E(1TO) phonon will assist the overall upconversion emission. Moreover, Er^{3+} dopants occupy a Ti^{3+} position with reasonable crystal field environment for further adjustment.

2.2.11 High throughput techniques

Lanthanide-doped upconversion materials exhibit diverse optical properties, which are mainly determined by the combination of Ln dopants, nanoparticle morphology, host matrix, and the surface configuration. However, to achieve certainly expected upconversion luminescence with identified synthesis condition, it will be a tedious and time-consuming job based on large amounts of parameters and database. Hence, the high throughput techniques will be ideal for rapid screening and enhance the upconversion luminescence. Ostrowski and his co-workers utilized WANDA LTMR reactors to optimize the synthesis parameters of $NaYF_4$, which revealed that ammonium fluoride and oleylamine surfactant could promote to reduce particle size to 5 nm [162].

In the previous chapter, we have demonstrated the importance of dopants combination and concentration for tuning the upconversion luminescence in Ln-doped materials. Chan's group has proposed an approach that using microplate-based

reactions, which include arrays of glass vials arranged in metal blocks (microplates) that are heated to reaction temperature with magnetic stirring or shaking. In average, this method displays a 24 times faster synthesis speed with 20 times saving on reagents [163]. Even though the HT method has shown many advantages in UCNPs optimization, the best candidate materials still need to be validated by conventional techniques rigorously. Moreover, the HT technique is still limited in flexibility and depth of information for understanding the mechanism of upconversion luminescence.

3. Capitalizing upconversion luminescence for new emerging applications

Lanthanide-doped upconversion nanoparticles and their extraordinary photophysical properties have attracted many to research upon in the scientific community. Crucially, many innovative and fundamental research on these unique lanthanide-doped upconversion materials has progressed substantially recently. This is evident in various research disciplines such as anti-counterfeiting and security, biodetection, super-resolution imaging, photovoltaics, and optoelectronic devices, optogenetics, phototherapies and bioimaging for various biological applications (Figure 17). Given the tremendous wide scope of emerging applications, we instead propose to highlight selected significant emerging developments to readers on various important research areas that are the current popular research.

3.1 Anti-counterfeiting and security applications

An analytical approach to identify exogenous and endogenous chemicals compounds accumulated in latent fingerprints is of utmost value to forensic science as it provides crucial evidence that criminal investigators need. From forensic literature records, the motif of friction ridge skin found on the palms of hands is unique to every single individual. As such, this strategy provides valuable evidence in forensic science analyses for ascertaining the identities based on latent fingerprints. Notwithstanding, a significant issue arises because they are invisible to criminal investigators and usually necessitates physical or chemical treatments to scrutinize them. Generally, iron and aluminum flakes, magnetic powder and other powder treatments have been used [164]. Yet, at present, the fluorescence background selectivity is an extensive limitation for use in latent fingerprint forensic work. Therefore, Ln-doped UCNPs with its superior and proven low background performances can resolve this issue.

One of the first few emerging and prominent discoveries was by Jin's group. They developed a tunable lifetime multiplexing Ln-doped UCNPs not just for data security applications but also for life sciences (Figure 18a). In their work, the three merged patterns were annotated with various thulium τ-dots of different dopant concentrations, and upon intensity-based luminescence irradiation, they gave complex images. The patterns were also separated by their lifetime components of every pixel using time-resolved scanning. Crucially, an authentic multiplexing data were included in the same merged boundaries of the document and therefore can be decoded with negligible crosstalk. Remarkably, it could potentially open-up avenues for potential high-density data storage and anti-counterfeiting document security against forgery. Next, Yuan's group constructed a novel aptamer functionalized on the surface of Ln-doped UCNPs that binds specifically to the fingerprint ridges lysozymes [165]. Under 980-nm laser irradiation, negligible background luminescence was observed. Of importance is that their work showed a proof-of-concept to confirm the possibility of identifying fingerprints stained with cocaine powder using the developed Ln-doped UCNPs modified with a cocaine-binding aptamer (Figure 18b). Our group also reported the synthesis of Ln-doped upconversion microrods as the unique potential for used as optical barcodes in anti-counterfeiting applications (Figure 18c top) [166]. This uniquely designed bottom-up synthetic method can readily access multicolor microrods in gram-scale. Crucially, such an end-on growth approach utilizing one-dimensional microrods as the template affords easy multicolor tuning in a single nanocrystal, which is inaccessible in traditional upconversion nanomaterials. Of importance, we revealed dual-color spatially coded microrods which can serve as enhanced security protection and allow immediate authentication of patterned features. In another vital work was reported by Doyle's group, which utilized a judicious multi-scale design approach to access robust encoding that is amenable to high-throughput particle synthesis and easily decoded by a portable charged-coupled device (Figure 18c bottom) [167]. They discovered that their architecture structure showed significant insensitivity towards various particle chemistries, enable modulation of encoding storage and verified that the decoding error rate was not correlated to the characteristics of the particle material. Vitally, there is also a prospect for direct magnetic manipulation. Their work expanded the potential of encoded Ln-doped UCNPs as a novel approach to manufacture long-lasting and hidden anti-counterfeiting designs with unprecedented encoding capacity from a small set of exclusively-encoded particles, which is highly valuable. Another unique work in security applications using Ln-doped UCNPs was established by May's group in which they showed that an RGB additive-color printing system which generates high-resolution pre-defined patterns that are invisible under ambient lighting (Figure 18d) [168]. Interestingly, they were viewable as luminescent multi-color images under NIR laser excitation, which made it possible for use in security printing applications. It is known surface plasmon modulation to enhance the upconversion luminescence (UCL) can be a new approach. Song's group tapped onto the use of Au-Ag alloy/$NaYF_4$:Yb,Tm Ln-doped UCNPs composite films for fingerprint identification studies and demonstrated unprecedented optical contrast, which for the first time showed a large detection sensitivity because of an enhancement of 180-times of the overall UCL intensity [169]. Remarkably, their research allowed unique opportunities to study novel insights based on the utilization of a hybrid material of metal/upconversion

device for fingerprint identification applications. Another pioneering work was Li's group, which use an 808-nm laser to excite Nd-sensitized multi-shell Ln-doped UCNPs for downshifting infrared luminescence for fingerprint bioimaging [170]. Relative to 980-nm laser excitation, 808-nm laser reduced the overheating effect on the delicate fingerprint samples.

To safeguard vital security information ranging from currencies, products, and even defense intelligence data from being fraudulently used, various strategies and approaches have been worked out and utilized. These include holographic methods, quick response codes (QR), plasmatic security labels and visible luminescent ink [171]. In recent times, materials such as cadmium telluride (CdTe) and cadmium selenide (CdSe) have been exploited as luminescent security ink. Nonetheless, the intrinsic metallic toxicity, which only dissolves in organic solvents and wide emission bands has curbed their widespread applications. On the contrary, a great prospect in Ln-doped UCNPs is their down-shifting luminescence especially in their downshifting luminescences in the NIR wavelengths. Besides, they offer sharp emission peaks, low cellular toxicity, and solubility due to the ease of accessing various surface modifications have enabled them to be outstandingly used for transparent security ink applications [172]. One of the prominent research was the used of highly luminescent lanthanide-doped nanomaterials by Shanker and co-workers [173]. The uniquely designed enabled dual upconversion and downshifting luminescence modality to be demonstrated using a single 980-nm excitation source. Notably, their work demonstrated a photoluminescence decay time within a few milliseconds, which is sufficient for applications in various luminescent security applications. In another renowned work was reported by Wang's group [174]. They established a one-pot hydrothermal strategy to access various hollow lanthanide-doped $NaYbF_4$ microrods containing isolated holes along the longitudinal axis via kinetic morphology control with facilitation from selective adhesion of citrate ligands (Figure 18e Top). Of importance is the fundamental mechanistic study showing that the presence of structural void enabled light intensity across the microrods to be altered in the solid matter because of the light scattering and reflection effects within the inner walls. Crucially, this synthetic study of a 1D hollow microstructure single microrod crystal doped with lanthanide upconverting ions can spatially be resolved and produced optical codes upon NIR excitation which has the potential to be used for low-cost manufacturing anti-counterfeiting applications. Recently, our group illustrated the use of integrating both long-lived Mn^{2+} upconversion emission and a short-lived lanthanide upconversion in a nanoparticulate system which enabled us to generate uniquely binary temporal codes for effective data encoding applications (Figure 18e Bottom) [175]. By precisely controlling the nanoparticle structure, we verified the excitation usefulness under NIR excitation of both 808-nm and 980-nm irradiation. Interestingly, we discovered that the designed Mn^{2+}-doped Ln-doped UCNPs are valuable for multilevel anti-counterfeiting with efficient high-throughput authentication rates without the requirement for sophisticated time-gated decoding equipment.

3.2. Biodetection applications

The uniquely photophysical properties that Ln-doped UCNPs possess were also harnessed and employed widely in various biological studies. One of which is biodetection applications. A valuable approach is to use the conceptual resonance energy transfer (RET) phenomenon in these Ln-doped UCNPs. In RET, energy is transferred from an excited luminescent donor to a close proximity acceptor, resulting in diminished luminescence emission intensity of the donor and an increase in the corresponding acceptor [176]. In recent years, several RET systems have utilized various Ln-doped UCNPs as they possess optical superiority and versatility to serve as either a quencher or donor. Besides, their intrinsic large anti-stokes shifts, negligible autofluorescence when irradiated under NIR light excitation and long luminescence lifetimes have been highly useful for RET applications. Tapping into the strengths of Ln-doped UCNPs would increase the performance and allow the prospects of multiple excitation sources to be selected. Undeniably, such RET-based Ln-doped UCNPs can respond with high sensitivity, specificity, rapidly and dynamically to the complex *in situ* biological environments. Particularly, various organic molecules, biological moieties, metal−organic complexes, or even inorganic nanoparticles have been rationally designed and carefully selected and conjugated to the surface of Ln-doped UCNPs for the preparation of novel RET-based biodetection applications.

An important work in biological detection using Ln-doped UCNPs was reported by Li and Huang's groups. They established a rationale biosensor using biocompatible Ln-doped UCNPs to target and detect a specific DNA sequence [177]. As illustrated in Figure 19, they utilized the specific interaction between biotin and streptavidin to perform RET. The biotinylated captured DNA was conjugated to streptavidin-Ln-doped UCNPs and used to target the desired DNA sequence with the subsequent addition of a reporter-DNA sequence that was functionalized with a fluorophore N,N,N',N'-tetramethyl-6-carboxyrhodamine (TAMRA). TAMRA has an absorbance that overlaps with the green upconversion luminescence of the Ln-doped UCNPs. By spectrometrically measuring the luminescence intensity ratio of (I_{580}/I_{540} or I_{540}/I_{654}), the biosensor can quantitatively identify the target oligonucleotide. The detection limit was measured with a threshold value of nanomole per liter which was sensitive enough for the general bioanalytical methods. In another valuable work for highly efficient luminescence sensing and biodetection was reported by Li's group. They established a novel absorption-shifting technique by chemically functionalized the Ru(II) complex which is chromophoric onto the surface of $NaYF_4$:Yb,Er,Tm UCNPs via a coordination reaction (Figure 20) [178]. The designed nanomaterials demonstrated a highly selective water-soluble detection tool using upconversion luminescence sensing and bioimaging of highly toxic mercury ions (Hg^{2+}) intracellularly. Of significance was that by using a ratiometric upconversion luminescence as the detection signal, they showed that the

detection limit of mercury ions in water was around 1.95 ppb, which was lower than the maximum threshold level of 2.00 ppb in drinking water as established by the United States Environmental Protection Agency (EPA). Finally, the nanoprobe N719-Ln-doped UCNPs can detect the regulated dynamic changes in the distribution of mercury ions in living cells via upconversion luminescence bioimaging. The prospects of the biologically sensing capability of Ln-doped UCNPs based on RET can also be used in animals for *in vivo* analyte monitoring. Li's group showed that by using a neodymium-sensitized upconversion nanomaterial, a higher contrast probe for biodetection of hypochlorite ions (ClO^-) in living cells and arthritis in vivo rodent model [179]. They utilized a cyanine dye, hCy3 which is known to be sensitive to ClO^- ions via luminescent resonance energy transfer and inner filter mechanism. They discovered that by using the ratiometric upconversion emission of I_{540}/I_{654} as the ratiometric detection signal, the nanosystem could detect ClO^- ions with a threshold low detection limit of 27 ppb. Significantly, the feasibility of such tailored-made nanoprobes was ascertained in an *in the vivo* arthritis animal model, demonstrating that these Ln-doped UCNP nanoprobes have the immense potential to be translated and applied for *in vivo* biodetection of vital biological analytes in the future.

3.3. Super-resolution imaging applications

The presence of optical microscopy has evolved tremendously since its first discovery in the 17th century [180]. Even though both scanning-based and electron-based microscopy techniques have overcome the challenges of resolving power, optical microscopy remains an instrumental method for many scientific disciplines. In this context, far-field optical microscopy provides a valuable and unique three-dimensional imaging of biological samples. Besides, the technique offers biomolecular specificity and minimal disruption when fluorescence imaging is integrated [181]. Despite the outlined advantages, a severe limitation is the light diffraction barrier, which restricts high-resolution of traditional light microscopy imaging to around 200-nm to 300-nm in the lateral dimensions. This has serious implications especially on the imaging of molecular structures and intracellular organelles as they are unresolvable, which in turn can be crucial to elucidate real-time important and minute biological functions. This major diffraction problem, however, has been overcome in recent years with the advent of several major super-resolution methods such as reversible saturable optically linear fluorescent transitions (RESOLFT), photoactivated localization microscopy (PALM), stimulated emission depletion (STED) and stochastic optical reconstruction microscopy (STORM). These highly useful methods have improved resolutions up to the range of 20-nm to 50-nm [182]. Crucially, the recent popular STED method utilizes stimulated emission to reduce the spontaneous fluorescent emission of materials that fluorescent to the central sub-region of an observation volume via de-excitation of fluorophores in the periphery regions. This is done by overlapping a focused excitation beam with a "doughnut"- a shaped beam that de-excites emitters to the ground state with the exception for the plane by reducing the full-width at half-maximum (FWHM) of the point spread function [183,184]. The area within the boundaries of the center of the doughnut can render unlimited high resolution in the transverse plane and thus enable super-resolution imaging.

In the context of super-resolution imaging applications, Ln-doped UCNPs signifies an entirely novel type of multi-photon luminescent probes. It is dependent on the immense densities of multi-photon emitters localized within the miniature nanoparticles [1]. Embedded in each nanoparticle are several thousands of various co-doped lanthanide ions that establish a structure of photon activators and sensitizers which give rise to upconversion emission upon absorbing near-infrared photons via various mechanisms (Figure 2). Recent research demonstrated that thousands of emitters embedded in each Ln-doped UCNPs could be stimulated by microscopes and generate a highly bright luminescence, which enables an attractive and promising single molecule nanoprobes [185,186]. These highly concentrated dopants in UCNPs render seamless optical population inversion at their intermediate energy metastable levels [95]. Consequently, a minimal saturation intensity of approximately 0.19 MW/cm^2 in upconversion STED was documented with a maximum threshold resolution of 28 nm ($\lambda/36$) for optical imaging of single 13 nm Ln-doped UCNPs. Of significance in super-resolution imaging would be the work by Jin's group which established Ln-doped UCNPs with unusually high thulium ion (Tm^{3+}) doping concentration to attain low-powered super-resolution stimulated emission depletion (STED) microscopy [95]. Two Ln-doped UCNP samples were prepared with an average size of 39.8 and 12.9 nm and were co-doped with similar dopant compositions of 8% Tm and 20% Yb prior to STED microscopy. Under 808-nm laser irradiation of 9.75 mW/cm^2, a 48.3 nm spot FWHW was attained in 39.8 nm UCNPs while a 13-fold enhancement over the optical diffraction limit was measured by FWHM after Gaussian fitting analyses (Figure 8e). On the other, a 31.2 nm spot FWHM was seen in the 12.9 nm UCNPs and a similar high contrasting improvement in resolution was discovered relative to traditional confocal imaging studies. Remarkably, their results demonstrated that utilizing low-powered laser radiation on lanthanide-doped UCNPs can effectively overcome the major problems limiting super-resolution imaging due to heat and cost.

In another notable work was shown by He's group, which tapped onto the intrinsic cross relaxation between the lanthanide dopants embedded within the Ln-doped UCNPs to generate a supplementary route for optical depletion of blue UCL at 455 nm using highly doped Tm^{3+}-$NaYF_4$:Yb^{3+}/Tm^{3+} with improved interactions between adjacent thulium ions [97]. This resulted in a near complete silencing of blue emission using the induced stimulated emission from a second laser beam source and concurrently abolish the synergistic emission enhancement effect of the same laser beam. Such an innovative emission depletion strategy is amenable to super-resolution microscopy and facilitates nanoscopic cytoskeleton imaging at

high-speed (100 μs dwelling time) with super-resolution imaging of cellular cytoskeleton protein structures with a resolution of 80 nm (Figure 21a and b).

3.4. Display technological applications

The eventual goal in encoding and modulating colors in material science research is to realize a universal sensitive and responsive material which has the potential to be accessed remotely on demand using extrinsic stimuli. These can range from pressure, magnetic, light and electric fields. Of importance, these useful optical materials can potentially be translated into displays that possess high resolution than existing red-green-blue (RGB) pixilated color display counterparts. Significantly, both two-dimensional pixelated RGB and three-dimensional volumetric full-color displays require the mixing of individual RGB elements as one color pixel which is necessitated by the specifications for devices with unique pixel manufacture and configuration [93]. Given the multitude of fundamental studies on color tuning strategies in lanthanide-doped nanomaterials that have been addressed and improved our understandings, it is without a doubt that they can represent the next generation of luminescent materials for display technology applications. One of the attractive features of these nanomaterials is the possibility to modulate emission color under a single wavelength excitation. This can be performed by controlling the intensity ratio of emission peaks and enable high spatial resolution [187].

In this context, our group pioneered a novel concept which showcases a dynamic fine-tuning emission of core-shell lanthanide-doped nanomaterials to generate the entire visible wavelength range and have the grand possibility to manufacture true three-dimensionalm full-color display devices with high spatial resolution and locally addressable color gamut for commercialization [93]. We discovered and attributed to the ability to attain such unique and superior luminescence via tuning the pulse width of NIR laser beams (Figure 22a). The lanthanide-doped nanoparticles were synthesized via an epitaxial layer-by-layer approach with low phonon β-hexagonal phase $NaYF_4$ as the host structure, and five groups of activated lanthanide ions (Tm^{3+}, Yb^{3+}, Nd^{3+}, $Ce^{3+,}$ and Ho^{3+}) were doped into several layers to afford color-tunable multi-shell nanoparticles. The incorporation of these designed lanthanide-doped nanoparticles into polydimethylsiloxane (PDMS) monolith to manufacture a transparent display and a conceptual proof of multi-perspective color images with the immense resolution was achieved by laser excitation with both 980-nm and 800-nm (Figure 22b). Crucially, equal mixtures of each Ln-doped UCNPs with balanced monochromatic RGB elements over a solution or solid-state substrate can emit white color.

Another notable display application using lanthanide-doped nanomaterials was reported by Zhang's group [94]. In their research, they established an upconversion nanomaterial system which can generate RGB emission colors that include the entire electromagnetic visible spectrum and when mixed together, they can produce white light (Figure 8d). Significantly, by simply tuning the excitation power density, they showed that the upconversion emission colors could be changed. This auxiliary strategy can be amenable to display technological applications via modulating the output of the emission colors through a facile excitation source. They designed a lanthanide-doped nanoplatform in which six different lanthanide dopant ions were doped (Tm^{3+}, Yb^{3+}, Y^{3+}, Er^{3+}, $Gd^{3+,}$ and Eu^{3+}). They showed that upon irradiation by 980-nm NIR laser, origins of blue light was generated by Tm^{3+}, green light by Er^{3+} and red light by Eu^{3+} dopant ions were observed. Surprisingly, they discovered that the emission colors could be dynamically modulated by changing the 980-nm laser excitation power density, which from the range of 3 to 30W/cm^2, showed a color evolution from green to cyan to white and finally to red. Crucially, this discovery was similarly observed when the colloidal nanocrystals were incorporated into the polystyrene microbeads. As a proof-of-concept, the authors developed a prototype flat-panel display that contains the designed lanthanide-doped nanocrystal-coated substrate, and it can generate different emission visible colors via a rapid scanning laser that is synchronously tuned by modulating the pump current (Figures 22c and d).

3.5. Photovoltaic and Optoelectronic applications

Photovoltaic which is also known as solar cells are semiconductor devices that create electricity via transforming solar radiation directly into electricity through the photovoltaic effect [12]. Notwithstanding, the main issue in the widespread application is the efficiency in energy conversion because they are selectively responsive to a minute population of solar photons with photonic energy higher than the threshold bandgap of the system. As such, there are the intrinsic fundamental disadvantages in maximizing the efficiency threshold of these solar cells. To further enhance such conversion efficiency, a promising strategic approach is to tap onto lanthanide-doped upconversion nanomaterials to establish productive spectral conversion because of the rich multiple energy level structures native to the lanthanide ions. This would enable facile photon management useful for photovoltaic applications [5,188]. Since they have the potential to convert two or more sub-bandgap NIR photons into one usable above-bandgap photon, it is also highly valuable as this can reduce non-absorption energy losses in various photovoltaic devices [12].

One of the emerging photovoltaic applications is the use of multi-component heterostructures that comprises two or more nanoscale components organized in a structured way that was reported by Rosei and Perepichka's groups. They discovered that the interaction between the integrated components can tremendously enhance the intrinsic electronic properties and developed a nanoheterostructure system that integrates lanthanide-doped upconversion nanoparticles with

CdSe quantum dots (QDs) – CdSe/$NaYF_4$:Yb/Er (CSNY) [86]. This hybrid nanoheterostructure which comprises both upconverting and semiconducting properties gave rise to sub-band-gap photoconductivity. They illustrated the utility of CSNY photoconductivity in electronic devices by assembling two contact devices via a spin-coating solution of CSNY particles in solution onto Si/SiO_2 substrates pre-patterned with gold electrodes (Figure 23a Top). Upon 980-nm irradiation, the upconverted photons generated excitons and further created charge carriers within the CdSe-based films. Consequently, this leads to a reversible and durable NIR photoconductivity switch as exemplified in the photocurrent-time graph (Figure 23a Bottom). Significantly, this novel concept being conceived in electronic devices can be applied in photovoltaics to accumulate photons with sub-band-gap energies. In another notable work were performed by Yan's group in which they showcased a photon energy upconversion via the thermal radiation route that resulted in the highest power upconversion efficiency achieved around 16% [151]. They introduced various lanthanide and transition metals as ionic sensitizers into oxide hosts in order for the infrared photons to be absorbed, and subsequently the energy being transferred to the host lattice structure via multi-phonon relaxation. As such, the accumulation of phonon in the host lattice increases the temperature and exacerbates the thermal radiation, in which a huge number of photons possess higher energy than the incident photons. Importantly, this strategy tapped into multiphonon relaxation and attained relatively high upconversion efficiencies. Besides, they identified and achieved an upconversion power efficiency of 16% under continuous wave 976-nm laser excitation with the most optimal hybrid lanthanide-transition metal co-doped upconversion nanomaterials – 28 mol% Yb^{3+}sensitized ZrO_2 (Figure 23b Top) They concluded with the establishment of thermal radiation photon energy upconversion under concentrated exposure to sunlight radiation and also under a 976-nm laser radiation source in which the upconverted white light is absorbed by Si solar cells to create electrical current, drive optical and electrical devices for potential photovoltaic and optoelectronic applications (Figure 23b Bottom).

The concept of light-induced thermal heating of various noble metal nanomaterials has been a strategic approach in recent years that have found its use in many applications, especially in photovoltaic and plasmonic research. One of the significant emerging works of plasmonic-induced nano heaters was accounted by Rocha and Carlos's groups in which they developed a novel all-in-one nanoheterostructures comprising a lanthanide-doped oxide $(Gd,Yb,Er)_2O_3$ as temperature sensors and a surface decorated gold nanoparticles as heaters for utilization as local-temperature sensing capabilities. It has the potential to cover a wide temperature range from 300 – 2000 K (Figure 23c Top and Bottom) [189]. In their designed nanoplatform, a continuous wave 980-nm laser-induced would generate heat due to absorption by AuNPs and also render thermometer capability based on the Er^{3+}-upconverted green region intensity ratios $(Gd,Yb,Er)_2O_3$ for the range of 300-1050 K and using Planck's law for the white-light emission for the range of 1200 – 2000 K. Remarkably, upon incrementing the amount of AuNPs, they discovered that both surface temperature and operating range of the nanothermometers increased and an obvious attribution of the white-light emission to an incandescence process. Mechanistically, the thermal-sensing principle was discovered to have a close association with the cooperative effect of thermal equilibrium in the population of excited states on Er^{3+} upconversion nanorods. This provides much prospects not just for photovoltaics research but also have the possibility to be used for controlled hyperthermia and deep-tissue optical bioimaging without causing over-heating damage to the adjacent normal tissues.

In another significant work for optoelectronic devices operating at NIR wavelength was reported by Wang and Zhou's group in which synthesized a novel NIR upconversion lasing Erbium-Yttrium chloride nanowires (Er-Y) (Figure 23d Top) [190]. They demonstrated that upon 1476-nm laser irradiation on a single-crystal Er-Y chloride nanowire, an ultra-narrow linewidth of 980-nm lasing properties was observed with a well-resolved sharp emission line (0.25nm at 77K) within the wavelength range of 400-nm to 1000-nm (Figure 23d Bottom). Besides, they showed that at the highest Er/Y ratio in these nanowires would result in a blue shift of the strongest peak. Importantly, the ability to generate 980-nm lasing properties of these ER-Y chloride nanowires upon irradiation by 1476-nm would enable their utilization to attain tunable NIR laser and have prospects in nanoscale optoelectronic devices that can perform at NIR wavelengths.

3.6. Optogenetics applications

Ln-doped UCNPs have also conjured considerable attention in various potential biological applications. Relative to the traditional luminescent probes such as quantum dots, fluorescent proteins or organic dyes, they had superior photophysical properties such as resistance to photobleaching and minimized photoblinking, autofluorescence and cross-talked emissions [188]. The NIR excitation source such as 808-nm and 980-nm of these Ln-doped UCNPs also enabled deeper tissue penetration than the conventional bioimaging probes that often rely on UV and visible range excitation. One of the most important strengths of Ln-doped UCNPs is that only a low powered continuous-wave laser operating at a power density of (1-1000 W/cm^2) have demonstrated to have efficient enough to initiate the lanthanide upconversion mechanism and the ability to serve as nanotransducers to convert NIR-to-UV/Vis wavelengths [191]. Taking advantage of these extraordinary photophysical behaviors, they have considered valuable and high-performance tools for life sciences in areas such as

optogenetics [192,193], photodynamic and photothermal therapies [194,195]. Also, these Ln-doped UNCPs can have down-shifting optical properties that are highly valuable since these NIR emissions are situated in what was known as the "second transparent biological window" where minimal biological tissue scattering occurs [196].

The field of optogenetics has been revolutionized by innovative optical techniques. This intriguing and extraordinary field uses genetic engineering methods to selectively insert opsins and its related family of proteins such as halorhodopsin, bacteriorhodopsin, and channelrhodopsin into any randomly marked sub-population of neurons in the brain [197]. Upon irradiation with light via fiberoptics or other light-guiding instruments, those neurons marked can be modulated to activate or inactivate with millisecond timing [198–200]. The ultimate goal of optogenetics is to allowed scientists within the neuroscience field to harness the use of optical control of these neurons in various organism models to deepen our understanding how the brain functions and possibility design novel therapeutics to treat various neurodegenerative diseases. Generally, various fundamental studies have shown that visible light in the regions of 430-nm to 630-nm are used to modulate the biological activities of the corresponding light-gated and light-driven ion pumps found in opsins, which cause a cascade of events to happen and leads to the genetically engineered neurons to be activated or inhibited [201]. Yet, direct blue light excitation has limited tissue penetration depth due to severe light tissue scattering (Figure 24a). Also, invasive fiber insertion method can overcome the tissue penetration depth, but this approach has limitations in that the experimental mouse subject's movement is restricted and may result in tissue damage during experiments (Figure 24b). Therefore, much research has been working on extending the wavelength excitation towards the red and NIR region because of the intrinsic deeper tissue penetration at this wavelengths. However, designing and genetically engineering opsins in the visible red region has yet to be identified and presents a challenge. A promising strategy to overcome this major limitation is to tap onto the nanotransudcing capabilities of these lanthanide-doped UCNPs, which have the extraordinary potential to convert low-energy NIR laser stimulation into UV/Visible wavelengths (Figure 24c) [188,202]. This has a tremendous clinical impact for *in vivo* deep-tissue optogenetic studies since the optical fiber tethering is removed.

One of the first notable optogenetic work using Ln-doped UCNPs was reported by Han's group in 2016 [193]. They developed a state-of-the-art IR-806 dye-sensitized core-shell nanoparticles which have a wide absorption range and an enhanced seven-fold upconversion luminescence efficiency due to the conjugated IR-806 antenna effect on the surfaces of the core-shell Ln-doped UCNPs (Figure 25a). A proof-of-concept using optogenetics controlling of the neuronal activity in cultured hippocampal neurons that expressed red-activatable channelrhodopsins (ReaChR) was attained when subjecting these dye-sensitized core-shell nanoparticles that have been embedded in poly(methyl methyacrylate) matrix in upon 800-nm NIR laser excitation (Figure 25b-e). Significantly, the as-synthesized Ln-doped UCNPs demonstrated good water solubility with Pluronic F127 for used in future bioimaging applications. In another extraordinary work on optogenetics research was reported by McHugh and our group. We established that Ln-doped UCNPs could serve as optogenetic actuators for transcranial NIR light stimulation of deep brain neurons (Figures 26a-c) [192]. The proof-of-concept was achieved by utilizing transgenic mice infused with Ln-doped UCNPs to locally activate light-gated ion channels and modulate neuronal activity, deep inside the brain of the mouse. Remarkably, this led to stimulation of brain oscillations via activation of inhibitory neurons in the medial septum, silenced seizure through blocking the hippocampal excitatory cells and enabled memory recall through hippocampal engram experiments. Most importantly, we demonstrated that an extraordinary nano-transducer capable of converting deep tissue NIR laser irradiation to blue light would enable fast increases in dopamine release in deep brain and could give rise to the possibility of incorporating such UCNP-mediated neuronal modulation tools to be integrated or expand traditional approaches to deep brain stimulation and find new strategies to overcome neurological disorder that have not been successfully addressed at the present moment.

3.7. Phototherapy and Bioimaging applications

Ln-doped UCNPs have also found its prospects prominently for phototherapies and diagnostic bioimaging. In the context of phototherapies, this would include photodynamic therapy (PDT) and photothermal therapy (PTT). In PDT, it taps onto photosensitizers to generate lethal cytotoxic reactive oxygen species (ROS) to cause cell death with the facilitation of Ln-doped UCNPs as nanotransducers to convert NIR-to-visible light wavelengths to photoactivate the visible-light activated photosensitizers [203]. This is highly efficacious and has been used widely for a range of cancers because of its minimal chronic cellular cytotoxicity, accurate targeting by a localized irradiation source, and low cost involved [194].

One of the significant early work using PDT was demonstrated by Liu's group. They developed a UCNP-Ce6 Ln-doped UCNP (Ce6 represents Chlorin e6) and discovered that the NIR light could permeate an 8 mm thick pork and yield obvious PDT cellular effects to reduce tumor growth rate (Figure 27a) [204]. However, the visible red light was unable to initiate the PDT process as it was totally filtered off. Another similar work was reported by Gu's group in which they developed an Ln-doped UCNP based on ZnPc photosensitizer (ZnPC represents Zinc Phthalocyanine) for efficacious treatment of tumors buried 1 cm deep into the tissue (Figure 27b) [205]. At present, most Ln-doped UCNP systems used single photosensitizers to effect the PDT. To further improved on the PDT efficacy, Zhang's group developed a dual-sensitized photosensitizer using Er^{3+}-based silica-coated Ln-doped UCNP which can be activated both by green and red light upon a single NIR irradiation in

tumor-bearing mice and has achieved effective non-invasive deep-cancer therapy (Figure 27c) [206]. The same group also achieved another notable milestone in PDT application in which they developed and use titania coated Ln-doped UCNPs (Figure 27d) [207]. This was rationally designed to overcome the major issue of limited photosensitizer loading efficiency by replacing the organic photosensitizers with a uniformly coated stable titanium dioxide (TiO_2). Through doping with Tm^{3+} ions, the upconverted UV light generated would photoexcites the electrons in the valence band (VB) of the TiO_2 shell and promotes to the conduction band (CB), which leads to the generation of electron-hole pair and evoke redox reactions with molecular oxygen and water to produce reactive oxygen species and leads to tumor cell death.

Another useful phototherapy would be Photothermal therapy (PTT). This non-invasive therapeutic approach employs photothermal agents to absorb light to generate heat and leads to the denaturation of the proteins found inside the cells, resulting in cell death. It can also result in thermal ablation of cancers [203]. This strategy creates several advantages such as being selective and accurate since it relies on the spot in which the laser is irradiated on, and only those regions which contain the photothermal agents would result in elevated temperature. Also, similar to photodynamic therapy, PTT can be considered flexible and cost-effective for potential efficacious treatment against cancer. In the context of lanthanide-doped upconversion nanoparticles for PTT applications, it is usually integrated with other types of photothermal agents that possess high extinction coefficient from gold, transition metal sulfides or indocyanine green, or even polydopamine because of the intrinsic low extinction coefficient of lanthanide ions. One of the prominent PTT application is the work reported by Song's group. They developed a multifunctional Ag-Ln-doped UCNP nanocomposite. Due to surface plasmon resonance (SPR) absorption of 980-nm NIR laser irradiation, the tuned outer silver shell can be absorbed and perform upconversion luminescence concurrently. This led to photothermal ablation on human liver and breast cancer cell lines of HepG2 and BCap-37 cells respectively [208]. In another significant work was published by Liu's group. They designed and synthesized a layer-by-layer assembly of core-multi-shell nanocomposite termed as (MFNPs) comprising an Ln-doped UCNP core, a layer of iron oxide nanoparticles (IONPs) that serves as the intermediate shell and a gold nanoparticle layer as the outermost shell (Figure 28a) [209]. Remarkably, the amount of MFNPs that localized in the tumor tissue regions when subjected to an external magnetic field was about 8-times higher than the non-magnetic field control group. Besides, due to the large NIR optical absorption coefficients of the Au nanoparticle layer, near complete thermal ablation of tumors in mice were achieved when irradiated with NIR laser. This resulted in a longer duration life-span to the maximum (Figures 28b and c). Hence, the MFNPs could enhance the efficiency of thermal ablation with the assistance from an external magnetic field for magnetic targeting and a dual-imaging modality consisting of magnetic resonance imaging and upconversion luminescence bioimaging. In another promising PTT, the agent was reported by Hilderbrand in which they developed an Ln-doped UCNPs and carbocyanine organic dyes being co-loaded into the nanostructure [210]. They synthesized a silica shell Er^{3+}-based Ln-doped UCNPs, and the carbocyanine dyes were adsorbed within the silica layer. When subjected to 980-nm laser irradiation, superior cellular imaging was observed. Independently, with 750-nm irradiation for 2 minutes at 2.5 W/cm^2, the temperature of the nanostructures increased by 21ºC. Crucially in this work, they showed that about 42% of murine leukemia (RAW) cells were thermally killed which demonstrated the efficacy of PTT treatment.

To further enhance therapeutic efficacy, researchers continued to explore and develop multifunctional nanomaterials that combine several functionalities into one heterogeneous system. This novel paradigm shift was proposed to overcome the intrinsic tumor complexity and heterogeneity, leading to multi-drug resistance and tumor recurrence [211]. As such, the possibility of incorporating multiple therapies within Ln-doped UCNPs have continued to progress in this direction in the hope to developed more efficacious nanoplatforms and reduce side effects [212]. A notable work showcasing this multifunctional concept was demonstrated by Zhang's group. They designed and synthesized a poly(allylamine)-coated Ln-doped UCNPs and covalently conjugate it with graphene oxide and subsequently functionalized with ZnPc photosensitizers on the surface of graphene oxide (Figure 28d) [213]. In this system, the graphene oxide functions as the photothermal agent to give PTT which absorbs NIR 808-nm wavelength while the ZnPc absorbs 630-nm laser and generates ROS such as cellular cytotoxic singlet oxygen $^1O_2$. The results obtained supported the synergistic multifunctional of PDT and PTT on Ln-doped nanocomposite, which gave rise to an enhanced therapeutic efficacy on those labeled cancer cells (Figure 28e). In a more recent work was accomplished by Shi's group in which they developed a trimode image-guided synergistic photothermal therapy and radiation therapy [214]. In their research, they combined a silica-coated Ln-doped UCNPs based on $NaGdF_4$:Yb,Er and CuS nanoparticles which functions as the PTT photothermal agent (Figure 28f). The proof-of-concept of radiation therapy was confirmed upon subjecting the nanocomposite to high X-ray irradiation since lanthanide ions have a large X-ray absorption coefficient. The intrinsic extraordinary imaging properties of the nanocomposite which possess upconversion luminescence, magnetic resonance and computed tomography tri-modal imaging were used to facilitate the image-guided multifunctional synergistic treatment which led a tumor growth inhibition of about 79% when subjected to PTT under *in vivo* conditions (Figure 28g). Crucially, application of radiation therapy to the 4T1 tumor resulted in totally ablated in 4 days and no observable tumor recurrence for accounted during a longitudinal 120 days experimental study.

Outlook and perspectives

Photon upconversion in lanthanide-doped upconversion nanomaterials has drawn much considerable attention over recent years as highlighted in this review and elsewhere. Many fundamental studies, as well as a diversity of emerging applications, have been demonstrated using these extraordinary class of luminescent nanomaterials. These examples illustrated the promising prospects for commercialization and translation for various industries. Besides; these nanoprobes can enable various scientists working in different disciplines to gain a deeper understanding of the scientifically observed phenomenon when they apply these nanomaterials in their research work. With a repertoire of experimental methods available to tune photon upconversion in these lanthanide-doped upconversion nanomaterials, either through chemical or other physical strategies as outlined above, these nanomaterials have great prospects and can be tailored-made exquisitely and transformed to meet the stringent requirements that each scientific application requires. These are especially observed in energy-related applications from volumetric three-dimensional displays to lightings or even photovoltaic and optoelectronic applications.

Worth mentioning would be the characteristics of these lanthanide-doped upconversion nanomaterials. They are amenable with ease to be deposited as layered films from liquid solutions using a variety of available methods. Furthermore, in the context of microelectronic use, the reorganization of the films is adaptable with traditional lithographic steps that are commonly used in various semiconductor industry which is due to the high thermal stability and photostability of these Ln-doped UCNPs [1]. Also, these nanomaterials can be used directly molded using a flexible elastomeric stamp that is a unique property for photonic amalgamation on thin and malleable substrates. Concurrently, these Ln-doped UCNPs have demonstrated extraordinary photophysical and photochemical properties in various biological applications such as bioimaging, and phototherapeutic applications. As for the emerging fields such as optogenetics and super-resolution imaging, the present significant achievements by various research groups are encouraging. For example, the recent optogenetics research appears to suggest that neural circuitry optical modulation by lanthanide-doped upconversion-assisted optogenetics have evolved to a non-invasive, remote and optical examination of genetic-modified neurons that possess tremendously enhanced spatial resolution and sensitivity. Furthermore, in the context of super-resolution imaging, lanthanide-doped upconversion nanoparticles possess superior luminescence properties in which the large anti-stokes spectral differences between the emission and excitation wavelengths which renders these luminescence probes ideal for background-free and photostable imaging applications.

Nonetheless, Ln-doped UCNPs also has several intrinsic limitations. First and foremost, their low upconversion quantum yield which is usually less than 1% have limited their widespread use in various applications. Thus, one of the major problems faced by material scientists working with these luminescent Ln-doped nanomaterials is to rectify the severely low quantum yield. At present, the highest measured upconversion quantum yield efficiencies for NIR-to-visible were around 5% for irradiation power densities of less than 100 W/cm^2 [215,216]. A few possible strategic approaches can be proposed to enhance radiative rates in these lanthanide-based upconverters. This can be done by coupling Ln-doped UCNPs to organic dye molecules which have broadband sensitization or through other various strategies such as host-lattice manipulation, energy transfer modulation, surface passivation or even photonic crystal engineering [26]. Another research challenge is to address the possibility of unconventional excitation wavelengths that have high extinction coefficients instead of the traditional 808-nm and 980-nm NIR excitation source. A probable approach is to tap onto organic dyes which have broadband excitation and can serve as antennas to mechanistically energy transfer to the lanthanide dopant ions embedded in the host lattice of Ln-doped UCNPs [217]. Ironically, more fundamental studies need to be established to obtain clarity and understanding of the mechanisms underlying such dye-sensitized upconversion process since they are rather inconclusive at present. Also, an alternative recently explored optical excitation source using helium ion beam excited upconversion luminescence can be exploited for new possibilities [92].

To this end, we and others have pioneered the paradigm shift and conceptually shift the excitation wavelength to 808-nm by using Nd^{3+}-based or NIR-dye as sensitizers from the conventional 980-nm Yb^{3+}-based sensitizers to prevent over-heating effects and improved tissue penetration depth [90]. While such 808-nm wavelengths are useful and valuable especially for biological applications, there is still the need to improve since there can be the possibility that the dye-sensitized can suffer from photobleaching upon long-term exposure to the NIR laser excitation, which is intrinsically found in most organic dyes. Besides, organic dyes may dissociate from the surfaces of the Ln-doped UCNPs to which they are coupled onto or enzymatically degraded by the high expression levels of native enzymes present in living organisms. Worth noting is that most of the experimental settings are often performed in organic media which makes it challenging for biological studies. Although the dispersion of these Ln-doped UCNPs in the micelle or amphiphilic polymeric encapsulation can overcome the solubility issue, the intrinsic upconversion emission may be reduced as energy can be transferred to the aqueous biological milieu [193]. Thus, there is a pressing need to circumvent these complex issues that are linked with dye-based sensitization of Ln-doped UCNPs.

In parallel would be the need to build commercial luminescent instrumentation that would enable successful commercialization and translation of these Ln-doped UCNPs for useful real-world applications, given that various significant examples in the emerging applications outlined in this review have demonstrated their feasibility. At present, most research

laboratories working on Ln-doped UCNPs often utilize customized setup since these equipment are often a rather niche research area where specific excitation laser wavelengths using continuous wave laser diodes or optical parametric oscillator-based (OPO) lasers sources, which are frequently not available with commercial equipment packages [218]. As such, there is a huge unmet need for easy accessibility of this commercial equipment that would further facilitate research groups working in this field to possess a standardized instrument. This can resolve various major issues such as the robustness and reproducibility of the obtained results such as quantum yield, lifetime measurements, spectroscopic measurements to be compared with greater precision in the hope that with such advancement, it can drive these Ln-doped UCNPs for commercialization.

Another major area worth resolving in these lanthanide-doped upconversion nanoparticles would be gearing these extraordinary nanomaterials towards translation purposes for various industries. Well-established and routine synthetic pathways and rational surface engineering approaches of these Ln-doped UCNPs are crucial and form the basis for consistent quality nanomaterials for commercialization. They have to be comprehensively verified using various physicochemical and photophysical techniques much like the quality assurance checks performed on manufactured drugs in pharmaceutical industries. Establishment and regulation of standard protocols for sturdy particle surface modifications with various important macro-biomolecules is of utmost importance. Besides, complementing the synthesis strategy are the novel techniques afforded in the bioconjugation chemistries, which would result in high quality and high-performance nanomaterials for next-generation research.

Finally would be the rational and thorough examination of the long-term chronic toxicity studies of these Ln-doped UCNPs used in biological studies, especially those that have the potential to be translated. A crucial challenge for possible translation into the clinics is the great uncertainties of these lanthanide-doped upconversion nanoparticles in not just systemic toxicity but also they are biological in situ route movements, ability to be eliminated from the body and the chronic long-term effects. Even though multiple reports have shown that rationale surface-modified lanthanide-doped nanoparticles did not have acute safety under in vitro and in vivo experiments along with their biodistribution, in-depth longitudinal chronic toxicity studies remained largely elusive. Besides, the probable interactions of these lanthanide-doped upconversion nanoparticles with the immune system and the possible illicit immune response remained unexplored. Such immunological studies may shed light into the extent of biological toxicity and assess its feasibility for the ultimate translation for clinical studies. Hence, more systematic with clear objectives needed to be performed to ascertain the safety profiles of these surface-modified Ln-doped UCNPs.

Acknowledgments

Funding

This work is supported by the Singapore Ministry of Education (Grant R143000627112, R143000642112), National Research Foundation, Prime Minister's Office, Singapore under its Competitive Research Program (CRP Award No. NRF-CRP15-2015-03), National Basic Research Program of China (973 Program, Grant 2015CB932200), National Natural Science Foundation of China (11774133, 21771135, 21471109, 21210001, 21701119), and CAS/SAFEA International Partnership Program for Creative Research Teams.

Notes

The authors declare no competing financial interest.

References

[1] Zhou B, Shi B, Jin D and Liu X 2015 Controlling upconversion nanocrystals for emerging applications *Nat. Nanotechnol.* **10** 924–36

[2] Wang F, Banerjee D, Liu Y, Chen X and Liu X 2010 Upconversion nanoparticles in biological labeling, imaging, and therapy *Analyst* **135** 1839–54

[3] Huang X, Han S, Huang W and Liu X 2013 Enhancing solar cell efficiency: The search for luminescent materials as spectral converters *Chem. Soc. Rev.* **42** 173–201

[4] González-Béjar M and Pérez-Prieto J 2015 Upconversion luminescent nanoparticles in physical sensing and in monitoring physical processes in biological samples *Methods Appl. Fluoresc.* **3** 042002

[5] Auzel F 2004 Upconversion and Anti-Stokes Processes with f and d Ions in Solids *Chem. Rev.* **104** 139–73

[6] Yang D, Ma P, Hou Z, Cheng Z, Li C and Lin J 2015 *Current advances in lanthanide ion (Ln^{3+})-based upconversion*

nanomaterials for drug delivery vol 44 (Royal Society of Chemistry)
[7] Liu X, Su L T, Karuturi S K, Luo J, Liu L, Liu X, Guo J, Sum T C, Deng R, Fan H J and Tok A I Y 2013 Photon upconversion in hetero-nanostructured photoanodes for enhanced near-infrared light harvesting *Adv. Mater.* **25** 1603–7
[8] Shang Y, Hao S, Yang C and Chen G 2015 Enhancing Solar Cell Efficiency Using Photon Upconversion Materials *Nanomaterials* **5** 1782–809
[9] Ramasamy P, Manivasakan P and Kim J 2014 Upconversion nanophosphors for solar cell applications *RSC Adv.* **4** 34873–95
[10] Chen G, Ågren H, Ohulchanskyy T Y and Prasad P N 2015 Light upconverting core-shell nanostructures: Nanophotonic control for emerging applications *Chem. Soc. Rev.* **44** 1680–713
[11] Zhou J and Qiu J 2016 Upconversion luminescence behavior of single nanoparticles *Phosphors, Up Convers. Nano Part. Quantum Dots Their Appl.* **2** 311–31
[12] Yang W, Li X, Chi D, Zhang H and Liu X 2014 Lanthanide-doped upconversion materials: Emerging applications for photovoltaics and photocatalysis *Nanotechnology* **25**
[13] Wang F and Liu X 2014 Multicolor tuning of lanthanide-doped nanoparticles by single wavelength excitation *Acc. Chem. Res.* **47** 1378–85
[14] Zhou J, Liu Q, Feng W, Sun Y and Li F 2015 Upconversion luminescent materials: Advances and applications *Chem. Rev.* **115** 395–465
[15] Tsang M-K, Bai G and Hao J 2015 Stimuli responsive upconversion luminescence nanomaterials and films for various applications *Chem. Soc. Rev.* **44** 1585–607
[16] Bai G, Tsang M K and Hao J 2015 Tuning the luminescence of phosphors: Beyond conventional chemical method *Adv. Opt. Mater.* **3** 431–62
[17] Wang G, Peng Q and Li Y 2010 Luminescence tuning of upconversion nanocrystals *Chem. - A Eur. J.* **16** 4923–31
[18] Wang F, Han Y, Lim C S, Lu Y, Wang J, Xu J, Chen H, Zhang C, Hong M and Liu X 2010 Simultaneous phase and size control of upconversion nanocrystals through lanthanide doping *Nature* **463** 1061–5
[19] Chang H, Xie J, Zhao B, Liu B, Xu S, Ren N, Xie X, Huang L and Huang W 2014 Rare Earth Ion-Doped Upconversion Nanocrystals: Synthesis and Surface Modification *Nanomaterials* **5** 1–25
[20] Chen D, Lei L, Yang A, Wang Z and Wang Y 2012 Ultra-broadband near-infrared excitable upconversion core/shell nanocrystals *Chem. Commun.* **48** 5898–900
[21] Wang J, Song H, Xu W, Dong B, Xu S, Chen B, Yu W and Zhang S 2013 Phase transition, size control and color tuning of $NaREF_4$:Yb^{3+}, Er^{3+}(RE = Y, Lu) nanocrystals *Nanoscale* **5** 3412–20
[22] Grosswhite H M and Crosswhite H 1984 Parametric model for f-shell configurations. I. The effective-operator Hamiltonian *J. Opt. Soc. Am. B* **1** 246–54
[23] Liu G 2014 A degenerate model of vibronic transitions for analyzing 4f-5d spectra *J. Lumin.* **152** 7–10
[24] Huang B 2016 Energy harvesting and conversion mechanisms for intrinsic upconverted mechano-persistent luminescence in CaZnOS *Phys. Chem. Chem. Phys.* **18** 25946–74
[25] Huang B 2017 The screened pseudo-charge repulsive potential in perturbed orbitals for band calculations by DFT+U *Phys. Chem. Chem. Phys.* **19** 8008–25
[26] Han S, Deng R, Xie X and Liu X 2014 Enhancing luminescence in lanthanide-doped upconversion nanoparticles *Angew. Chemie - Int. Ed.* **53** 11702–15
[27] Wang F, Deng R, Wang J, Wang Q, Han Y, Zhu H, Chen X and Liu X 2011 Tuning upconversion through energy migration in core-shell nanoparticles *Nat. Mater.* **10** 968–73
[28] Huang B 2016 4f fine-structure levels as the dominant error in the electronic structures of binary lanthanide oxides *J. Comput. Chem.* **37** 825–35
[29] LIU; G and JACQUIER B 2005 *Spectroscopic Properties of Rare Earths in Optical Materials* vol 83
[30] Dieke G H, Crosswhite H M and Dunn B 1961 Emission Spectra of the Doubly and Triply Ionized Rare Earths* *J. Opt. Soc. Am.* **51** 820
[31] Qin X, Liu X, Huang W, Bettinelli M and Liu X 2017 Lanthanide-Activated Phosphors Based on 4f-5d Optical Transitions: Theoretical and Experimental Aspects *Chem. Rev.* **117** 4488–527
[32] Dong H, Sun L-D and Yan C-H 2013 Basic understanding of the lanthanide related upconversion emissions *Nanoscale* **5** 5703
[33] Su Q, Han S, Xie X, Zhu H, Chen H, Chen C K, Liu R S, Chen X, Wang F and Liu X 2012 The effect of surface coating on energy migration-mediated upconversion *J. Am. Chem. Soc.* **134** 20849–57
[34] Bünzli J-C G and Piguet C 2005 Taking advantage of luminescent lanthanide ions *Chem. Soc. Rev.* **34** 1048
[35] Yan C, Zhao H, Perepichka D F and Rosei F 2016 Lanthanide Ion Doped Upconverting Nanoparticles: Synthesis, Structure and Properties *Small* 3888–907
[36] Dong H, Sun L D and Yan C H 2013 Basic understanding of the lanthanide related upconversion emissions *Nanoscale* **5** 5703–14
[37] Huang B, Dong H, Wong K L, Sun L D and Yan C H 2016 Fundamental View of Electronic Structures of β-$NaYF_4$, β-$NaGdF_4$, and β-$NaLuF_4$ *J. Phys. Chem. C* **120** 18858–70
[38] HUANG B, DONG H, Wong K-L, SUN L and YAN C 2017 Interface formation energy, bonding, energy band alignment in α-$NaYF_4$ related core shell models: For future multi-layer core shell luminescence materials *J. Rare Earths* **35** 315–34
[39] Zhao J, Jin D, Schartner E P, Lu Y, Liu Y, Zvyagin A V., Zhang L, Dawes J M, Xi P, Piper J A, Goldys E M and Monro T M 2013 Single-nanocrystal sensitivity achieved by enhanced upconversion luminescence *Nat. Nanotechnol.* **8** 729–34
[40] Dong H, Sun L D, Feng W, Gu Y, Li F and Yan C H 2017 Versatile Spectral and Lifetime Multiplexing Nanoplatform with Excitation Orthogonalized Upconversion Luminescence *ACS Nano* **11** 3289–97
[41] Han S, Qin X, An Z, Zhu Y, Liang L, Han Y, Huang W and Liu X 2016 Multicolour synthesis in lanthanide-doped nanocrystals through cation exchange in water *Nat. Commun.* **7** 1–7

[42] Wang H, Lu W, Yi Z, Rao L, Zeng S and Li Z 2015 Enhanced upconversion luminescence and single-band red emission of $NaErF_4$nanocrystals via Mn^{2+} doping *J. Alloys Compd.* **618** 776–80
[43] Tian G, Gu Z, Zhou L, Yin W, Liu X, Yan L, Jin S, Ren W, Xing G, Li S and Zhao Y 2012 Mn^{2+} Dopant-Controlled Synthesis of $NaYF_4$:Yb/Er Upconversion Nanoparticles for in vivo Imaging and Drug Delivery *Adv. Mater.* **24** 1226–31
[44] Xie X, Gao N, Deng R, Sun Q, Xu Q H and Liu X 2013 Mechanistic investigation of photon upconversion in Nd^{3+}- sensitized core-shell nanoparticles *J. Am. Chem. Soc.* **135** 12608–11
[45] Chen D, Lei L, Zhang R, Yang A, Xu J and Wang Y 2012 Intrinsic single-band upconversion emission in colloidal Yb/Er(Tm):$Na_3Zr(Hf)F_7$nanocrystals *Chem. Commun.* **48** 10630–2
[46] Chen D and Wang Y 2013 Impurity doping: A novel strategy for controllable synthesis of functional lanthanide nanomaterials *Nanoscale* **5** 4621–37
[47] Wang F and Liu X 2008 Upconversion multicolor fine-tuning: Visible to near-infrared emission from lanthanide-doped NaYF4 nanoparticles *J. Am. Chem. Soc.* **130** 5642–3
[48] Mai H X, Zhang Y W, Sun L D and Yan C H 2007 Highly efficient multicolor up-conversion emissions and their mechanisms of monodisperse $NaYF_4$:Yb,Er core and core/shell-structured nanocrystals *J. Phys. Chem. C* **111** 13721–9
[49] Yin A, Zhang Y, Sun L and Yan C 2010 Colloidal synthesis and blue based multicolor upconversion emissions of size and composition controlled monodisperse hexagonal $NaYF_4$:Yb,Tm nanocrystals *Nanoscale* **2** 953–9
[50] Shen J, Chen G, Ohulchanskyy T Y, Kesseli S J, Buchholz S, Li Z, Prasad P N and Han G 2013 Tunable near infrared to ultraviolet upconversion luminescence enhancement in (α-$NaYF_4$:Yb,Tm)/CaF_2core/shell nanoparticles for in situ real-time recorded biocompatible photoactivation *Small* **9** 3213–7
[51] Zhai X, Liu S, Zhang Y, Qin G and Qin W 2014 Controlled synthesis of ultrasmall hexagonal $NaTm_{0.02}Lu_{0.98-x}Yb_xF_4$ nanocrystals with enhanced upconversion luminescence *J. Mater. Chem. C* **2** 2037–44
[52] Qiu H, Chen G, Fan R, Yang L, Liu C, Hao S, Sailor M J, Ågren H, Yang C and Prasad P N 2014 Intense ultraviolet upconversion emission from water-dispersed colloidal YF_3:Yb^{3+}/Tm^{3+} rhombic nanodisks *Nanoscale* **6** 753–7
[53] Lu Y, Zhao J, Zhang R, Liu Y, Liu D, Goldys E M, Yang X, Xi P, Sunna A, Lu J, Shi Y, Leif R C, Huo Y, Shen J, Piper J A, Robinson J P and Jin D 2014 Tunable lifetime multiplexing using luminescent nanocrystals *Nat. Photonics* **8** 32–6
[54] Huang B, Sun M, Dougherty A W, Dong H, Xu Y-J, Sun L-D and Yan C-H 2017 Unravelling the energy transfer of Er^{3+}-self-sensitized upconversion in Er^{3+}-Yb^{3+}-Er^{3+} clustered core@shell nanoparticles *Nanoscale* **9**
[55] Bai Y, Wang Y, Yang K, Zhang X, Peng G, Song Y, Pan Z and Wang C H 2008 The effect of Li on the spectrum of Er^{3+} in Li- and Er-codoped ZnO nanocrystals *J. Phys. Chem. C* **112** 12259–63
[56] Yin W, Zhao L, Zhou L, Gu Z, Liu X, Tian G, Jin S, Yan L, Ren W, Xing G and Zhao Y 2012 Enhanced Red Emission from GdF_3:Yb^{3+},Er^{3+} Upconversion Nanocrystals by Li^+ Doping and Their Application for Bioimaging *Chem.- A Eur. J.* **18** 9239–45
[57] Chen G, Liu H, Liang H, Somesfalean G and Zhang Z 2008 Upconversion Emission Enhancement in Yb^{3+}/Er^{3+}-Codoped Y_2O_3 Nanocrystals by Tridoping with Li + Ions *J. Phys. Chem. C* **112** 12030–6
[58] Liang H, Chen G, Liu H and Zhang Z 2009 Ultraviolet upconversion luminescence enhancement in Yb^{3+}/Er^{3+}-codoped Y_2O_3 nanocrystals induced by tridoping with Li+ ions *J. Lumin.* **129** 197–202
[59] Jiang L, Xiao S, Yang X, Ding J and Dong K 2012 Enhancement of up-conversion luminescence in Zn_2SiO_4:Yb^{3+},Er^{3+} by co-doping with Li^+or Bi^{3+} *Appl. Phys. B Lasers Opt.* **107**
[60] Ramasamy P, Chandra P, Rhee S W and Kim J 2013 Enhanced upconversion luminescence in $NaGdF_4$:Yb,Er nanocrystals by Fe^{3+} doping and their application in bioimaging *Nanoscale* **5** 8711–7
[61] Wang J, Deng R, Macdonald M A, Chen B, Yuan J, Wang F, Chi D, Andy Hor T S, Zhang P, Liu G, Han Y and Liu X 2014 Enhancing multiphoton upconversion through energy clustering at sublattice level *Nat. Mater.* **13** 157–62
[62] Wang L, Li X, Li Z, Chu W, Li R, Lin K, Qian H, Wang Y, Wu C, Li J, Tu D, Zhang Q, Song L, Jiang J, Chen X, Luo Y, Xie Y and Xiong Y 2015 A New Cubic Phase for a $NaYF_4$ Host Matrix Offering High Upconversion Luminescence Efficiency *Adv. Mater.* **27** 5528–33
[63] Chen G, Qiu H, Fan R, Hao S, Tan S, Yang C and Han G 2012 Lanthanide-doped ultrasmall yttrium fluoride nanoparticles with enhanced multicolor upconversion photoluminescence *J. Mater. Chem.* **22** 20190–6
[64] Dorenbos P 2005 Valence stability of lanthanide ions in inorganic compounds *Chem. Mater.* **17** 6452–6
[65] Dorenbos P 2004 Locating lanthanide impurity levels in the forbidden band of host crystals *Journal of Luminescence* vol 108 pp 301–5
[66] Zhang Y, Lin J D, Vijayaragavan V, Bhakoo K K and Tan T T Y 2012 Tuning sub-10 nm single-phase NaMnF3nanocrystals as ultrasensitive hosts for pure intense fluorescence and excellent T1magnetic resonance imaging *Chem. Commun.* **48** 10322–4
[67] Huang Z, Yi M, Gao H, Zhang Z and Mao Y 2017 Enhancing single red band upconversion luminescence of $KMnF_3$:Yb^{3+}/Er^{3+} nanocrystals by Mg^{2+} doping *J. Alloys Compd.* **694** 241–5
[68] Wang J, Wang F, Wang C, Liu Z and Liu X 2011 Single-Band Upconversion Emission in Lanthanide-Doped $KMnF_3$ Nanocrystals *Angew. Chemie Int. Ed.* **50** 10369–72
[69] Patra A, Friend C S, Kapoor R and Prasad P N 2003 Effect of crystal nature on upconversion luminescence in Er^{3+}: ZrO_2 nanocrystals *Appl. Phys. Lett.* **83** 284–6
[70] Vetrone F, Boyer J C, Capobianco J A, Speghini A and Bettinelli M 2002 NIR to visible upconversion in nanocrystalline and bulk Lu_2O_3:Er^{3+} *J. Phys. Chem. B* **106** 5622–8
[71] Zeng J H, Xie T, Li Z H and Li Y 2007 Monodispersed nanocrystalline fluoroperovskite up-conversion phosphors *Cryst. Growth Des.* **7** 2774–7
[72] Chen X, Jin L, Kong W, Sun T, Zhang W, Liu X, Fan J, Yu S F and Wang F 2016 Confining energy migration in upconversion nanoparticles towards deep ultraviolet lasing *Nat. Commun.* **7** 1–6
[73] Zhao J, Lu Z, Yin Y, McRae C, Piper J A, Dawes J M, Jin D and Goldys E M 2013 Upconversion luminescence with tunable

lifetime in $NaYF_4$:Yb,Er nanocrystals: Role of nanocrystal size *Nanoscale* **5** 944–52
[74] Michalet X, Pinaud F F, Bentolila L A, Tsay J M, Doose S, Li J J, Sundaresan G, Wu A M, Gambhir S S and Weiss S 2005 Quantum dots for live cells, in vivo imaging, and diagnostics *Science* **307** 538–44
[75] Xue X, Uechi S, Tiwari R N, Duan Z, Liao M, Yoshimura M, Suzuki T and Ohishi Y 2013 Size-dependent upconversion luminescence and quenching mechanism of $LiYF_4:Er^{3+}/Yb^{3+}$ nanocrystals with oleate ligand adsorbed *Opt. Mater. Express* **3** 989
[76] Wang F, Wang J and Liu X 2010 Direct evidence of a surface quenching effect on size-dependent luminescence of upconversion nanoparticles *Angew. Chemie - Int. Ed.* **49** 7456–60
[77] Huang B 2015 Native Point Defects in CaS: Focus on Intrinsic Defects and Rare Earth Ion Dopant Levels for Up-converted Persistent Luminescence *Inorg. Chem.* **54** 11423–40
[78] Zhou B, Yang W, Han S, Sun Q and Liu X 2015 Photon Upconversion Through Tb^{3+}-Mediated Interfacial Energy Transfer *Adv. Mater.* **27** 6208–12
[79] Zhou B, Tao L, Chai Y, Lau S P, Zhang Q and Tsang Y H 2016 Constructing Interfacial Energy Transfer for Photon Up- and Down-Conversion from Lanthanides in a Core–Shell Nanostructure *Angew. Chemie - Int. Ed.* **55** 12356–60
[80] Huang P, Zheng W, Zhou S, Tu D, Chen Z, Zhu H, Li R, Ma E, Huang M and Chen X 2014 Lanthanide-doped $LiLuF_4$ upconversion nanoprobes for the detection of disease biomarkers. *Angew. Chemie - Int. Ed.* **53** 1252–7
[81] Kumar R, Nyk M, Ohulchanskyy T Y, Flask C a and Prasad P N 2009 Combined Optical and MR Bioimaging Using Rare Earth Ion Doped $NaYF_4$ Nanocrystals *Adv. Funct. Mater.* **19** 853–9
[82] Bogdan N, Vetrone F, Ozin G A and Capobianco J A 2011 Synthesis of ligand-free colloidally stable water dispersible brightly luminescent lanthanide-doped upconverting nanoparticles *Nano Lett.* **11** 835–40
[83] Zou W, Visser C, Maduro J A, Pshenichnikov M S and Hummelen J C 2012 Broadband dye-sensitized upconversion of near-infrared light *Nat. Photonics* **6** 560–4
[84] Zhang C, Ou H P, Liao L Y, Feng W, Sun W, Li Z X, Xu C H, Fang C J, Sun L D, Zhang Y W and Yan C H 2010 Luminescence modulation of ordered upconversion nanopatterns by a photochromic diarylethene: Rewritable optical storage with nondestructive readout *Adv. Mater.* **22** 633–7
[85] Yi G and Chow G-M 2007 Water-Soluble $NaYF_4$:Yb,Er(Tm)/$NaYF_4$ / Polymer Core/Shell/Shell Nanoparticles with Significant Enhancement of Upconversion Fluorescence *Chem. Mater.* **19** 341–3
[86] Li Z and Zhang Y 2006 Monodisperse silica-coated polyvinyl-pyrrolidone/$NaYF_4$ nanocrystals with multicolor upconversion fluorescence emission *Angew. Chemie - Int. Ed.* **45** 7732–5
[87] Yan C, Dadvand A, Rosei F and Perepichka D F 2010 Near-IR photoresponse in new up-converting CdSe/$NaYF_4$:Yb,Er nanoheterostructures *J. Am. Chem. Soc.* **132** 8868–9
[88] Xu B, Zhang X, Huang W, Yang Y, Ma Y, Gu Z, Zhai T and Zhao Y 2016 Nd^{3+} sensitized dumbbell-like upconversion nanoparticles for photodynamic therapy application *J. Mater. Chem. B* **4** 2776–84
[89] Wang Y F, Liu G Y, Sun L D, Xiao J W, Zhou J C and Yan C H 2013 Nd^{3+}-sensitized upconversion nanophosphors: Efficient in vivo bioimaging probes with minimized heating effect *ACS Nano* **7** 7200–6
[90] Xie X, Li Z, Zhang Y, Guo S, Pendharkar A I, Lu M, Huang L, Huang W and Han G 2017 Emerging ≈800 nm Excited Lanthanide-Doped Upconversion Nanoparticles *Small* **13**
[91] Zhan Q, Qian J, Liang H, Somesfalean G, Wang D, He S, Zhang Z and Andersson-Engels S 2011 Using 915 nm laser excited $Tm^{3+}/Er^{3+}/Ho^{3+}$-doped $NaYbF_4$ upconversion nanoparticles for in vitro and deeper in vivo bioimaging without overheating irradiation *ACS Nano* **5** 3744–57
[92] Mi Z, Zhang Y, Vanga S K, Chen C B, Tan H Q, Watt F, Liu X and Bettiol A A 2015 Subwavelength imaging through ion-beam-induced upconversion *Nat. Commun.* **6**
[93] Deng R, Qin F, Chen R, Huang W, Hong M and Liu X 2015 Temporal full-colour tuning through non-steady-state upconversion *Nat. Nanotechnol.* **10** 237–42
[94] Zhang C, Yang L, Zhao J, Liu B, Han M Y and Zhang Z 2015 White-Light Emission from an Integrated Upconversion Nanostructure: Toward Multicolor Displays Modulated by Laser Power *Angew. Chemie - Int. Ed.* **54** 11531–5
[95] Liu Y, Lu Y, Yang X, Zheng X, Wen S, Wang F, Vidal X, Zhao J, Liu D, Zhou Z, Ma C, Zhou J, Piper J A, Xi P and Jin D 2017 Amplified stimulated emission in upconversion nanoparticles for super-resolution nanoscopy *Nature* **543** 229–33
[96] Shin K, Jung T, Lee E, Lee G, Goh Y, Heo J, Jung M, Jo E-J, Lee H, Kim M-G and Lee K T 2017 Distinct mechanisms for the upconversion of $NaYF_4$:Yb^{3+},Er^{3+} nanoparticles revealed by stimulated emission depletion *Phys. Chem. Chem. Phys.* **19** 9739–44
[97] Zhan Q, Liu H, Wang B, Wu Q, Pu R, Zhou C, Huang B, Peng X, Ågren H and He S 2017 Achieving high-efficiency emission depletion nanoscopy by employing cross relaxation in upconversion nanoparticles *Nat. Commun.* **8**
[98] Carnall W T, Goodman G L, Rana R S, Vandevelde P, Fluyt L and GÖrller-Walrand C 1986 Crystal-field analysis of Ho^{3+} LaF_3 and $Er^{3+}LaF_3$ in C2v site symmetry *J. Less-Common Met.* **116**
[99] Carnall W T, Goodman G L, Rajnak K and Rana R S 1989 A systematic analysis of the spectra of the lanthanides doped into single crystal LaF_3 *J. Chem. Phys.* **90** 3443–57
[100] Liu G K, Zhuang H Z and Chen X Y 2002 Restricted Phonon Relaxation and Anomalous Thermalization of Rare Earth Ions in Nanocrystals *Nano Lett.* **2** 535–9
[101] Auzel F 2005 Up-conversion in RE-doped Solids *Spectroscopic Properties of Rare Earths in Optical Materials* vol 83 pp 266–319
[102] Yang D, Ma P, Hou Z, Cheng Z, Li C and Lin J 2015 Current advances in lanthanide ion (Ln^{3+})-based upconversion nanomaterials for drug delivery *Chem. Soc. Rev.* **44** 1416–48
[103] Liz-Marzán L M, Murphy C J and Wang J 2014 Nanoplasmonics *Chem. Soc. Rev.* **43** 3820–2
[104] Linic S, Christopher P and Ingram D B 2011 Plasmonic-metal nanostructures for efficient conversion of solar to chemical energy *Nat. Mater.* **10** 911–21

[105] Jain P K and El-Sayed M A 2010 Plasmonic coupling in noble metal nanostructures *Chem. Phys. Lett.* **487** 153–64
[106] Schuller J A, Barnard E S, Cai W, Jun Y C, White J S and Brongersma M L 2010 Plasmonics for extreme light concentration and manipulation *Nat. Mater.* **9** 193–204
[107] Buffman D R, Matter B, Of O P, Bohren C F, Huffman D R M R, Stevens W L, Silvonen K, Purcell E M, Rev A, Astrophys A, Of O P, Modes S, Matter B, Matrix S, Huffman D R M R, Buffman D R, Bohren C F, Huffman D R M R, Buffman D R, Bohren C F, Huffman D R M R, Buffman D R, Purcell E M, Rev A, Astrophys A, Buffman D R, Silvonen K, Bohren C F, Huffman D R M R, Of F, Mie G, Bohren C F, Huffman D R M R, Matrix S and Stevens W L 2007 *Absorption and Scattering of Light by Small Particles* vol 38
[108] Xu W, Chen X and Song H 2017 Upconversion manipulation by local electromagnetic field *Nano Today* **17** 54–78
[109] Liu X and Lei D Y 2015 Simultaneous excitation and emission enhancements in upconversion luminescence using plasmonic double-resonant gold nanorods *Sci. Rep.* **5**
[110] Zhang W, Ding F and Chou S Y 2012 Large enhancement of upconversion luminescence of $NaYF_4$:Yb^{3+}/Er^{3+} Nanocrystal by 3D plasmonic nano-antennas *Adv. Mater.* **24** OP236-OP241
[111] Wang Y L, Estakhri N M, Johnson A, Li H Y, Xu L X, Zhang Z, Alù A, Wang Q Q and Shih C K 2015 Tailoring plasmonic enhanced upconversion in single $NaYF_4$: Yb^{3+}/Er^{3+} nanocrystals *Sci. Rep.* **5**
[112] Park W, Lu D and Ahn S 2015 Plasmon enhancement of luminescence upconversion *Chem. Soc. Rev.*
[113] Lakowicz J R 2001 Radiative decay engineering: Biophysical and biomedical applications *Anal. Biochem.* **298** 1–24
[114] Wu D M, García-Etxarri A, Salleo A and Dionne J A 2014 Plasmon-enhanced upconversion *J. Phys. Chem. Lett.* **5** 4020–31
[115] Feng W, Sun L D and Yan C H 2009 Ag nanowires enhanced upconversion emission of $NaYF_4$:Yb,Er nanocrystals via a direct assembly method *Chem. Commun.* 4393–5
[116] Schietinger S, Aichele T, Wang H Q, Nann T and Benson O 2010 Plasmon-enhanced upconversion in single $NaYF_4$:Yb^{3+}/Er^{3+} codoped nanocrystals *Nano Lett.* **10** 134–8
[117] Greybush N J, Saboktakin M, Ye X, Della Giovampaola C, Oh S J, Berry N E, Engheta N, Murray C B and Kagan C R 2014 Plasmon-enhanced upconversion luminescence in single nanophosphor-nanorod heterodimers formed through template-assisted self-assembly *ACS Nano* **8** 9482–91
[118] He J, Zheng W, Ligmajer F, Chan C, Bao Z, Wong K, Chen X, Hao J, Dai J, Yu S and Lei D Y 2017 Plasmonic enhancement and polarization dependence of nonlinear upconversion emissions from single gold satellite nanostructures *Light Sci. Appl.* **6** e16217
[119] Mauser N, Piatkowski D, Mancabelli T, Nyk M, Mackowski S and Hartschuh A 2015 Tip Enhancement of Upconversion Photoluminescence from Rare Earth Ion Doped Nanocrystals *ACS Nano* **9** 3617–26
[120] Xu W, Song H, Chen X, Wang H, Cui S, Zhou D, Zhou P and Xu S 2015 Upconversion luminescence enhancement of Yb^{3+},Nd^{3+} sensitized $NaYF_4$ core–shell nanocrystals on Ag grating films *Chem. Commun.* **51** 1502–5
[121] Saboktakin M, Ye X, Chettiar U K, Engheta N, Murray C B and Kagan C R 2013 Plasmonic enhancement of nanophosphor upconversion luminescence in Au nanohole arrays *ACS Nano* **7** 7186–92
[122] Sun Q C, Mundoor H, Ribot J C, Singh V, Smalyukh I I and Nagpal P 2014 Plasmon-enhanced energy transfer for improved upconversion of infrared radiation in doped-lanthanide nanocrystals *Nano Lett.* **14** 101–6
[123] Fisher J, Zhao B, Lin C, Berry M, May P S and Smith S 2015 Spectroscopic Imaging and Power Dependence of Near-Infrared to Visible Upconversion Luminescence from $NaYF_4$:Yb^{3+},Er^{3+} Nanoparticles on Nanocavity Arrays *J. Phys. Chem. C* **119** 24976–82
[124] Saboktakin M, Ye X, Oh S J, Hong S H, Fafarman A T, Chettiar U K, Engheta N, Murray C B and Kagan C R 2012 Metal-enhanced upconversion luminescence tunable through metal nanoparticle-nanophosphor separation *ACS Nano* **6** 8758–66
[125] Yuan P, Lee Y H, Gnanasammandhan M K, Guan Z, Zhang Y and Xu Q-H 2012 Plasmon enhanced upconversion luminescence of $NaYF_4$:Yb,Er@SiO_2@Ag core–shell nanocomposites for cell imaging *Nanoscale* **4** 5132
[126] Bang D, Jo E J, Hong S, Byun J Y, Lee J Y, Kim M G and Lee L P 2017 Asymmetric Nanocrescent Antenna on Upconversion Nanocrystal *Nano Lett.* **17** 6583–90
[127] Hao J, Zhang Y and Wei X 2011 Electric-induced enhancement and modulation of upconversion photoluminescence in epitaxial $BaTiO_3$:Yb/Er thin films *Angew. Chemie - Int. Ed.* **50** 6876–80
[128] Wang Z, Senden T and Meijerink A 2017 Photonic Effects for Magnetic Dipole Transitions *J. Phys. Chem. Lett.* **8** 5689–94
[129] Liu Y, Wang D, Shi J, Peng Q and Li Y 2013 Magnetic tuning of upconversion luminescence in lanthanide-doped bifunctional nanocrystals *Angew. Chemie - Int. Ed.* **52** 4366–9
[130] Xiao Q, Zhang Y, Zhang H, Dong G, Han J and Qiu J 2016 Dynamically Tuning the Up-conversion Luminescence of Er^{3+}/Yb^{3+} Co-doped Sodium Niobate Nano-crystals through Magnetic Field *Sci. Rep.* **6** 1–9
[131] Li Z X, Li L Le, Zhou H P, Yuan Q, Chen C, Sun L D and Yan C H 2009 Colour modification action of an upconversion photonic crystal *Chem. Commun.* 6616–8
[132] Yin Z, Li H, Xu W, Cui S, Zhou D, Chen X, Zhu Y, Qin G and Song H 2016 Local Field Modulation Induced Three-Order Upconversion Enhancement: Combining Surface Plasmon Effect and Photonic Crystal Effect *Adv. Mater.* **28** 2518–25
[133] Gan X, Yao X, Shiue R-J, Hatami F and Englund D 2015 Photonic crystal cavity-assisted upconversion infrared photodetector *Opt. Express* **23** 12998
[134] Marques-Hueso J, Peretti R, Abargues R, Richards B S, Seassal C and Martínez-Pastor J P 2015 Photonic crystal-driven spectral concentration for upconversion photovoltaics *Adv. Opt. Mater.* **3** 568–74
[135] Yang Z, Yan D, Zhu K, Song Z, Yu X, Zhou D, Yin Z and Qiu J 2012 Modification of the upconversion spontaneous emission in photonic crystals *Mater. Chem. Phys.* **133** 584–7
[136] Niu W, Su L T, Chen R, Chen H, Wang Y, Palaniappan A, Sun H and Yoong Tok A I 2014 3-Dimensional photonic crystal surface enhanced upconversion emission for improved near-infrared photoresponse *Nanoscale* **6** 817–24
[137] Yin Z, Zhu Y, Xu W, Wang J, Xu S, Dong B, Xu L, Zhang S and Song H 2013 Remarkable enhancement of upconversion fluorescence and confocal imaging of PMMA Opal/$NaYF_4$:Yb^{3+}, Tm^{3+}/Er^{3+} nanocrystals *Chem. Commun.* **49** 3781–3

[138] Zhang S Z, Sun L D, Tian H, Liu Y, Wang J F and Yan C H 2009 Reversible luminescence switching of $NaYF_4$:Yb,Er nanoparticles with controlled assembly of gold nanoparticles *Chem. Commun.* 2547–9
[139] Sun L N, Peng H, Stich M I J, Achatz D and Wolfbeis O S 2009 PH sensor based on upconverting luminescent lanthanide nanorods *Chem. Commun.* 5000–2
[140] Tvingstedt K, Dal Zilio S, Inganäs O and Tormen M 2008 Trapping light with micro lenses in thin film organic photovoltaic cells *Opt. Express* **16** 21608
[141] Cho C and Lee J-Y 2013 Multi-scale and angular analysis of ray-optical light trapping schemes in thin-film solar cells: Micro lens array, V-shaped configuration, and double parabolic trapper *Opt. Express* **21** A276
[142] Peer A, Biswas R, Park J-M, Shinar R and Shinar J 2017 Light management in perovskite solar cells and organic LEDs with microlens arrays *Opt. Express* **25** 10704
[143] Lin H-Y, Ho Y-H, Lee J-H, Chen K-Y, Fang J-H, Hsu S-C, Wei M-K, Lin H-Y, Tsai J-H and Wu T-C 2008 Patterned microlens array for efficiency improvement of small-pixelated organic light-emitting devices. *Opt. Express* **16** 11044–51
[144] Wrzesniewski E, Eom S H, Cao W, Hammond W T, Lee S, Douglas E P and Xue J 2012 Enhancing light extraction in top-emitting organic light-emitting devices using molded transparent polymer microlens arrays *Small* **8** 2647–51
[145] Li Y, Liu X, Yang X, Lei H, Zhang Y and Li B 2017 Enhancing Upconversion Fluorescence with a Natural Bio-microlens *ACS Nano* **11** 10672–80
[146] Brites C D S, Xie X, Debasu M L, Qin X, Chen R, Huang W, Rocha J, Liu X and Carlos L D 2016 Instantaneous ballistic velocity of suspended Brownian nanocrystals measured by upconversion nanothermometry *Nat. Nanotechnol.* **11** 851–6
[147] Geitenbeek R G, Prins P T, Albrecht W, Van Blaaderen A, Weckhuysen B M and Meijerink A 2017 $NaYF_4$:Er^{3+},Yb^{3+}/SiO_2Core/Shell Upconverting Nanocrystals for Luminescence Thermometry up to 900 K *J. Phys. Chem. C* **121** 3503–10
[148] Fischer L H, Harms G S and Wolfbeis O S 2011 Upconverting nanoparticles for nanoscale thermometry *Angew. Chemie - Int. Ed.* **50** 4546–51
[149] Yu W, Xu W, Song H and Zhang S 2014 Temperature-dependent upconversion luminescence and dynamics of $NaYF_4$:Yb^{3+}/Er^{3+} nanocrystals: influence of particle size and crystalline phase *Dalt. Trans.* **43** 6139–47
[150] Zhou J, Wen S, Liao J, Clarke C, Tawfik S A, Ren W, Mi C, Wang F and Jin D 2018 Activation of the surface dark-layer to enhance upconversion in a thermal field *Nat. Photonics* **12** 154–8
[151] Wang J, Ming T, Jin Z, Wang J, Sun L D and Yan C H 2014 Photon energy upconversion through thermal radiation with the power efficiency reaching 16% *Nat. Commun.* **5**
[152] Dou Q and Zhang Y 2011 Tuning of the structure and emission spectra of upconversion nanocrystals by alkali ion doping *Langmuir* **27** 13236–41
[153] Wisser M D, Chea M, Lin Y, Wu D M, Mao W L, Salleo A and Dionne J A 2015 Strain-induced modification of optical selection rules in lanthanide-based upconverting nanoparticles *Nano Lett.* **15** 1891–7
[154] Lay A, Wang D S, Wisser M D, Mehlenbacher R D, Lin Y, Goodman M B, Mao W L and Dionne J A 2017 Upconverting Nanoparticles as Optical Sensors of Nano- to Micro-Newton Forces *Nano Lett.* **17** 4172–7
[155] Zhang H, Peng D, Wang W, Dong L and Pan C 2015 Mechanically Induced Light Emission and Infrared-Laser-Induced Upconversion in the Er-Doped CaZnOS Multifunctional Piezoelectric Semiconductor for Optical Pressure and Temperature Sensing *J. Phys. Chem. C* **119** 28136–42
[156] Li L, Wondraczek L, Li L, Zhang Y, Zhu Y, Peng M and Mao C 2018 CaZnOS:Nd^{3+} Emits Tissue-Penetrating near-Infrared Light upon Force Loading *ACS Appl. Mater. Interfaces* **10** 14509–16
[157] Ting T C T 1992 *Anisotropic Elasticity: Theory and Applications*
[158] Hermannstädter C, Witzany M, Heldmaier M, Hafenbrak R, Jöns K D, Beirne G J and Michler P 2012 Polarization anisotropic luminescence of tunable single lateral quantum dot molecules *J. Appl. Phys.* **111**
[159] Zhou J, Chen G, Wu E, Bi G, Wu B, Teng Y, Zhou S and Qiu J 2013 Ultrasensitive Polarized Up-Conversion of Tm^{3+}–Yb^{3+} Doped β-$NaYF_4$ Single Nanorod *Nano Lett.* **13** 2241–6
[160] Chen P, Song M, Wu E, Wu B, Zhou J, Zeng H, Liu X and Qiu J 2015 Polarization modulated upconversion luminescence: Single particle vs. few-particle aggregates *Nanoscale* **7** 6462–6
[161] Gong S, Ren Z, Jiang S, Li M, Li X, Wei X, Xu G, Shen G and Han G 2014 Phase-modified Up-conversion luminescence in Er-doped single-crystal $PbTiO_3$nanofibers *J. Phys. Chem. C* **118** 5486–93
[162] Ostrowski A D, Chan E M, Gargas D J, Katz E M, Han G, Schuck P J, Milliron D J and Cohen B E 2012 Controlled synthesis and single-particle imaging of bright, sub-10 nm lanthanide-doped upconverting nanocrystals *ACS Nano* **6** 2686–92
[163] Chan E M, Han G, Goldberg J D, Gargas D J, Ostrowski A D, Schuck P J, Cohen B E and Milliron D J 2012 Combinatorial discovery of lanthanide-doped nanocrystals with spectrally pure upconverted emission *Nano Lett.* **12** 3839–45
[164] Hazarika P and Russell D A 2012 Advances in fingerprint analysis *Angew. Chemie - Int. Ed.* **51** 3524–31
[165] Wang J, Wei T, Li X, Zhang B, Wang J, Huang C and Yuan Q 2014 Near-infrared-light-mediated imaging of latent fingerprints based on molecular recognition *Angew. Chemie - Int. Ed.* **53** 1616–20
[166] Zhang Y, Zhang L, Deng R, Tian J, Zong Y, Jin D and Liu X 2014 Multicolor barcoding in a single upconversion crystal *J. Am. Chem. Soc.* **136** 4893–6
[167] Lee J, Bisso P W, Srinivas R L, Kim J J, Swiston A J and Doyle P S 2014 Universal process-inert encoding architecture for polymer microparticles *Nat. Mater.* **13** 524–9
[168] Meruga J M, Baride A, Cross W, Kellar J J and May P S 2014 Red-green-blue printing using luminescence-upconversion inks *J. Mater. Chem. C* **2** 2221–7
[169] Chen X, Xu W, Zhang L, Bai X, Cui S, Zhou D, Yin Z, Song H and Kim D H 2015 Large Upconversion Enhancement in the "islands" Au-Ag Alloy/$NaYF_4$:Tm^{3+}/ Yb^{3+}, Tm^{3+}/Er^{3+} Composite Films, and Fingerprint Identification *Adv. Funct. Mater.* **25**

5462–71
[170] Li J, Zhu X, Xue M, Feng W, Ma R and Li F 2016 Nd^{3+}-Sensitized Upconversion Nanostructure as a Dual-Channel Emitting Optical Probe for Near Infrared-to-Near Infrared Fingerprint Imaging *Inorg. Chem.* **55** 10278–83
[171] Zhou D, Liu D, Xu W, Chen X, Yin Z, Bai X, Dong B, Xu L and Song H 2017 Synergistic Upconversion Enhancement Induced by Multiple Physical Effects and an Angle-Dependent Anticounterfeit Application *Chem. Mater.* **29** 6799–809
[172] Gupta B K, Haranath D, Saini S, Singh V N and Shanker V 2010 Synthesis and characterization of ultra-fine Y_2O_3:Eu^{3+}nanophosphors for luminescent security ink applications *Nanotechnology* **21**
[173] Kumar P, Dwivedi J and Gupta B K 2014 Highly luminescent dual mode rare-earth nanorod assisted multi-stage excitable security ink for anti-counterfeiting applications *J. Mater. Chem. C* **2** 10468–75
[174] Chen B, Kong W, Liu Y, Lu Y, Li M, Qiao X, Fan X and Wang F 2017 Crystalline Hollow Microrods for Site-Selective Enhancement of Nonlinear Photoluminescence *Angew. Chemie - Int. Ed.* **56** 10383–7
[175] Liu X, Wang Y, Li X, Yi Z, Deng R, Liang L, Xie X, Loong D T B, Song S, Fan Di, All A H, Zhang H, Huang L and Liu X 2017 Binary temporal upconversion codes of Mn^{2+}-activated nanoparticles for multilevel anti-counterfeiting *Nat. Commun.* **8**
[176] Su Q, Feng W, Yang D and Li F 2017 Resonance energy transfer in upconversion nanoplatforms for selective biodetection *Acc. Chem. Res.* **50** 32–40
[177] Chen Z, Chen H, Hu H, Yu M, Li F, Zhang Q, Zhou Z, Yi T and Huang C 2008 Versatile synthesis strategy for carboxylic acid-functionalized upconverting nanophosphors as biological labels *J. Am. Chem. Soc.* **130** 3023–9
[178] Liu Q, Peng J, Sun L and Li F 2011 High-efficiency upconversion luminescent sensing and bioimaging of Hg(II) by chromophoric ruthenium complex-assembled nanophosphors *ACS Nano* **5** 8040–8
[179] Zou X, Liu Y, Zhu X, Chen M, Yao L, Feng W and Li F 2015 An Nd^{3+}-sensitized upconversion nanophosphor modified with a cyanine dye for the ratiometric upconversion luminescence bioimaging of hypochlorite *Nanoscale* **7** 4105–13
[180] Smolyaninov I I, Elliott J, Zayats A V. and Davis C C 2005 Far-field optical microscopy with a nanometer-scale resolution based on the in-plane image magnification by surface plasmon polaritons *Phys. Rev. Lett.* **94**
[181] Huang B, Wang W, Bates M and Zhuang X 2008 Three-dimensional super-resolution imaging by stochastic optical reconstruction microscopy *Science* **319** 810–3
[182] Huang B, Babcock H and Zhuang X 2010 Breaking the diffraction barrier: Super-resolution imaging of cells *Cell* **143** 1047–58
[183] Rittweger E, Han K Y, Irvine S E, Eggeling C and Hell S W 2009 STED microscopy reveals crystal colour centres with nanometric resolution *Nat. Photonics* **3** 144–7
[184] Gao P, Prunsche B, Zhou L, Nienhaus K and Nienhaus G U 2017 Background suppression in fluorescence nanoscopy with stimulated emission double depletion *Nat. Photonics* **11** 163–9
[185] Zhao J, Jin D, Schartner E P, Lu Y, Liu Y, Zvyagin A V., Zhang L, Dawes J M, Xi P, Piper J A, Goldys E M and Monro T M 2013 Single-nanocrystal sensitivity achieved by enhanced upconversion luminescence *Nat. Nanotechnol.* **8** 729–34
[186] Gargas D J, Chan E M, Ostrowski A D, Aloni S, Altoe M V P, Barnard E S, Sanii B, Urban J J, Milliron D J, Cohen B E and Schuck P J 2014 Engineering bright sub-10-nm upconverting nanocrystals for single-molecule imaging *Nat. Nanotechnol.* **9** 300–5
[187] Mahalingam V, Mangiarini F, Vetrone F, Venkatramu V, Bettinelli M, Speghini A and Capobianco J A 2008 Bright white upconversion emission from Tm^{3+}/Yb^{3+}/Er^{3+}-doped $Lu_3Ga_5O_{12}$ nanocrystals *J. Phys. Chem. C* **112** 17745–9
[188] Wang F and Liu X 2009 Recent advances in the chemistry of lanthanide-doped upconversion nanocrystals *Chem. Soc. Rev.* **38** 976–89
[189] Debasu M L, Ananias D, Pastoriza-Santos I, Liz-Marzán L M, Rocha J and Carlos L D 2013 All-in-one optical heater-thermometer nanoplatform operative from 300 to 2000 K based on Er^{3+} emission and blackbody radiation *Adv. Mater.* **25** 4868–74
[190] Ye R, Xu C, Wang X, Cui J and Zhou Z 2016 Room-temperature near-infrared up-conversion lasing in single-crystal Er-Y chloride silicate nanowires *Sci. Rep.* **6**
[191] Wu S, Han G, Milliron D J, Aloni S, Altoe V, Talapin D V., Cohen B E and Schuck P J 2009 Non-blinking and photostable upconverted luminescence from single lanthanide-doped nanocrystals *Proc. Natl. Acad. Sci.* **106** 10917–21
[192] Chen S, Weitemier A Z, Zeng X, He L, Wang X, Tao Y, Huang A J Y, Hashimotodani Y, Kano M, Iwasaki H, Parajuli L K, Okabe S, Loong Teh D B, All A H, Tsutsui-Kimura I, Tanaka K F, Liu X and McHugh T J 2018 Near-infrared deep brain stimulation via upconversion nanoparticle–mediated optogenetics *Science* **359** 679–84
[193] Wu X, Zhang Y, Takle K, Bilsel O, Li Z, Lee H, Zhang Z, Li D, Fan W, Duan C, Chan E M, Lois C, Xiang Y and Han G 2016 Dye-sensitized core/active shell upconversion nanoparticles for optogenetics and bioimaging applications *ACS Nano* **10** 1060–6
[194] Lucky S S, Soo K C and Zhang Y 2015 Nanoparticles in photodynamic therapy *Chem. Rev.* **115** 1990–2042
[195] Cheng L, Wang C and Liu Z 2014 Functional nanomaterials for phototherapies of cancer *Chinese J. Clin. Oncol.* **41** 18–26
[196] Frangioni J V. 2003 In vivo near-infrared fluorescence imaging *Curr. Opin. Chem. Biol.* **7** 626–34
[197] Williams S C P and Deisseroth K 2013 Optogenetics *Proc. Natl. Acad. Sci.* **110** 16287–16287
[198] Deisseroth K 2011 Optogenetics *Nat. Methods* **8** 26–9
[199] Zhang F, Vierock J, Yizhar O, Fenno L E, Tsunoda S, Kianianmomeni A, Prigge M, Berndt A, Cushman J, Polle J, Magnuson J, Hegemann P and Deisseroth K 2011 The microbial opsin family of optogenetic tools *Cell* **147** 1446–57
[200] Packer A M, Roska B and Häuser M 2013 Targeting neurons and photons for optogenetics *Nat. Neurosci.* **16** 805–15
[201] Nagel G, Szellas T, Huhn W, Kateriya S, Adeishvili N, Berthold P, Ollig D, Hegemann P and Bamberg E 2003 Channelrhodopsin-2, a directly light-gated cation-selective membrane channel *Proc. Natl. Acad. Sci.* **100** 13940–5
[202] Haase M and Schäfer H 2011 Upconverting nanoparticles *Angew. Chemie - Int. Ed.* **50** 5808–29
[203] Liu B, Li C, Yang P, Hou Z and Lin J 2017 808-nm-Light-Excited Lanthanide-Doped Nanoparticles: Rational Design, Luminescence Control and Theranostic Applications *Adv. Mater.* **29**
[204] Wang C, Tao H, Cheng L and Liu Z 2011 Near-infrared light induced in vivo photodynamic therapy of cancer based on upconversion nanoparticles *Biomaterials* **32** 6145–54

[205] Cui S, Yin D, Chen Y, Di Y, Chen H, Ma Y, Achilefu S and Gu Y 2013 In vivo targeted deep-tissue photodynamic therapy based on near-infrared light triggered upconversion nanoconstruct *ACS Nano* **7** 676–88
[206] Idris N M, Gnanasammandhan M K, Zhang J, Ho P C, Mahendran R and Zhang Y 2012 In vivo photodynamic therapy using upconversion nanoparticles as remote-controlled nanotransducers *Nat. Med.* **18** 1580–5
[207] Lucky S S, Muhammad Idris N, Li Z, Huang K, Soo K C and Zhang Y 2015 Titania coated upconversion nanoparticles for near-infrared light triggered photodynamic therapy *ACS Nano* **9** 191–205
[208] Dong B, Xu S, Sun J, Bi S, Li D, Bai X, Wang Y, Wang L and Song H 2011 Multifunctional $NaYF_4:Yb^{3+},Er^{3+}$@Ag core/shell nanocomposites: integration of upconversion imaging and photothermal therapy *J. Mater. Chem.* **21** 6193
[209] Cheng L, Yang K, Li Y, Zeng X, Shao M, Lee S T and Liu Z 2012 Multifunctional nanoparticles for upconversion luminescence/MR multimodal imaging and magnetically targeted photothermal therapy *Biomaterials* **33** 2215–22
[210] Shan G, Weissleder R and Hilderbrand S A 2013 Upconverting organic dye doped core-shell nano-composites for dual-modality NIR imaging and photo-thermal therapy *Theranostics* **3** 267–74
[211] Meacham C E and Morrison S J 2013 Tumour heterogeneity and cancer cell plasticity *Nature* **501** 328–37
[212] Tian G, Zhang X, Gu Z and Zhao Y 2015 Recent Advances in Upconversion Nanoparticles-Based Multifunctional Nanocomposites for Combined Cancer Therapy *Adv. Mater.* **27** 7692–712
[213] Wang Y, Wang H, Liu D, Song S, Wang X and Zhang H 2013 Graphene oxide covalently grafted upconversion nanoparticles for combined NIR mediated imaging and photothermal/photodynamic cancer therapy *Biomaterials* **34** 7715–24
[214] Xiao Q, Zheng X, Bu W, Ge W, Zhang S, Chen F, Xing H, Ren Q, Fan W, Zhao K, Hua Y and Shi J 2013 A core/satellite multifunctional nanotheranostic for in vivo imaging and tumor eradication by radiation/photothermal synergistic therapy *J. Am. Chem. Soc.* **135** 13041–8
[215] Fischer S, Bronstein N D, Swabeck J K, Chan E M and Alivisatos A P 2016 Precise Tuning of Surface Quenching for Luminescence Enhancement in Core-Shell Lanthanide-Doped Nanocrystals *Nano Lett.* **16** 7241–7
[216] Johnson N J J, He S, Diao S, Chan E M, Dai H and Almutairi A 2017 Direct Evidence for Coupled Surface and Concentration Quenching Dynamics in Lanthanide-Doped Nanocrystals *J. Am. Chem. Soc.* **139** 3275–82
[217] Zou W, Visser C, Maduro J A, Pshenichnikov M S and Hummelen J C 2012 Broadband dye-sensitized upconversion of near-infrared light *Nat. Photonics*
[218] Wilhelm S 2017 Perspectives for Upconverting Nanoparticles *ACS Nano* **11** 10644–53

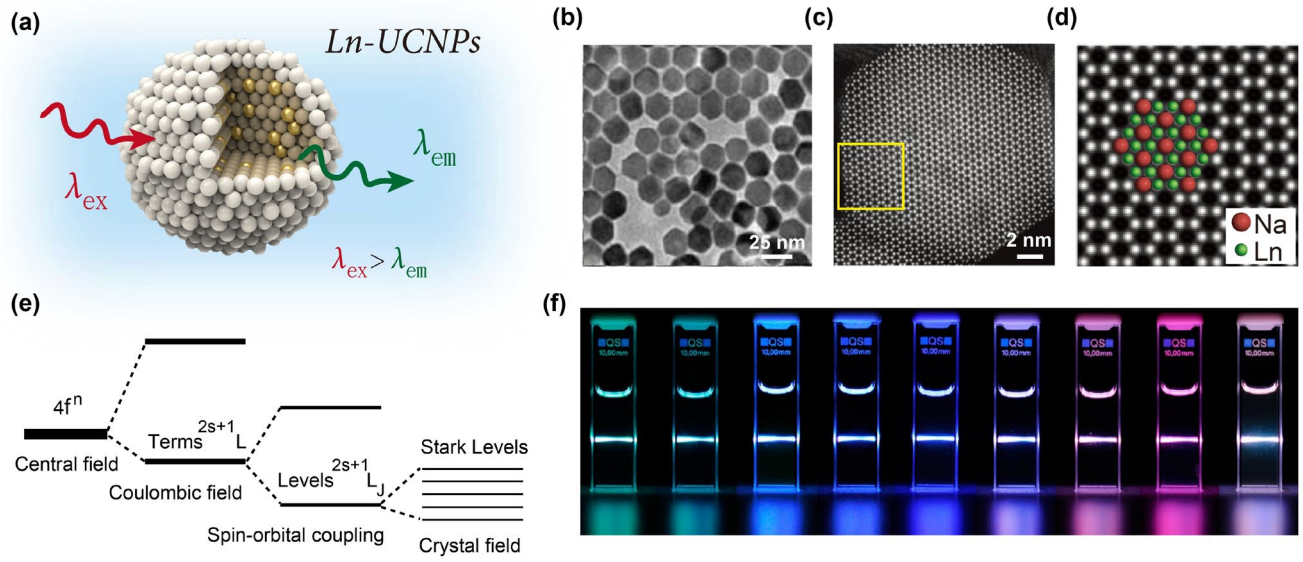

Figure 1. (a) Schematic illustration of upconversion nanoparticle composed of an inorganic crystalline host embedded with trivalent lanthanide dopant ions; (b-c) TEM and High-resolution STEM image of a typical upconversion nanoparticle comprising a $NaGdF_4$:Yb/Tm(49/1%) core and a $NaGdF_4$:Tb (15%) shell, revealing the single-crystalline nature of the crystal. (d) An enlarged view of the selected area in (c), indicated by a yellow box, showing lanthanide ions were uniformly embedded in crystalline host; (e) Simplified illustration of the effect of Coulombic field, spin–orbital coupling, and crystal field interaction on the electronic configurations of lanthanide atoms; (f) Typical luminescence photograph of colloidal solutions of representative samples showing the upconversion multicolor tuning. Figure reproduced with permission from: (b-c), [27], Springer Nature; (f), [33], American Chemical Society.

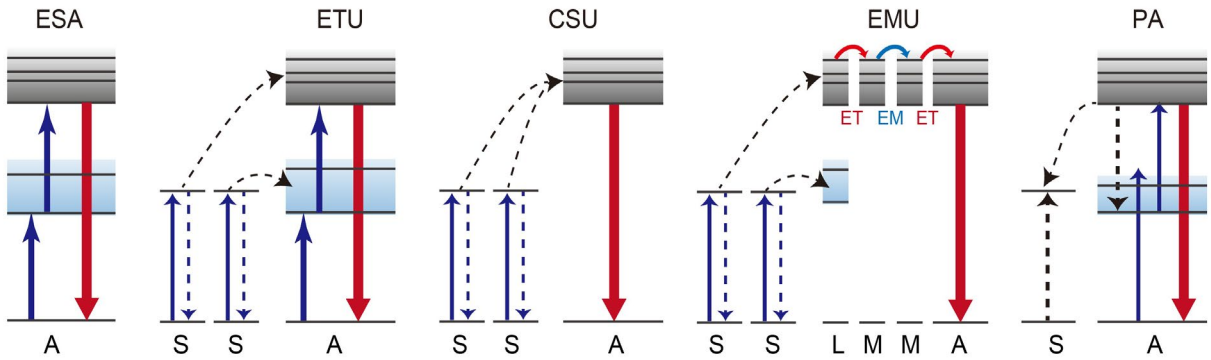

Figure 2. Simplified energy level diagrams depicting upconversion processes including excited-state absorption (ESA), energy transfer upconversion (ETU), cooperative sensitization upconversion (CSU), energy migration upconversion (EMU) and photon avalanche (PA).

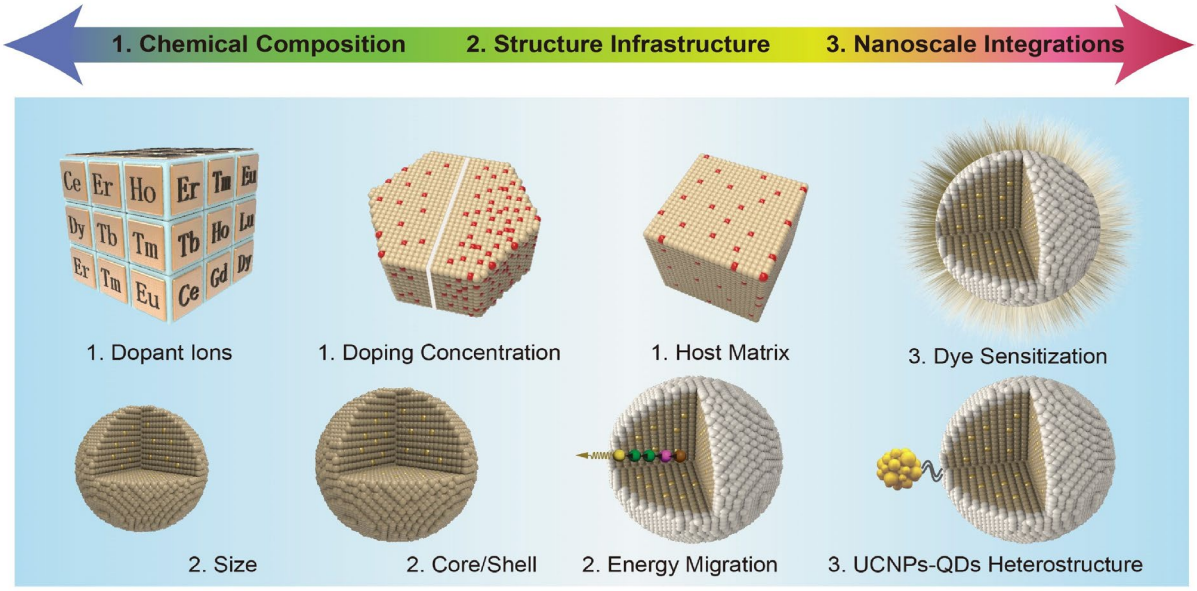

Figure 3. Tuning the luminescence of lanthanide-doped upconversion nanoparticles by conventional chemical methods.

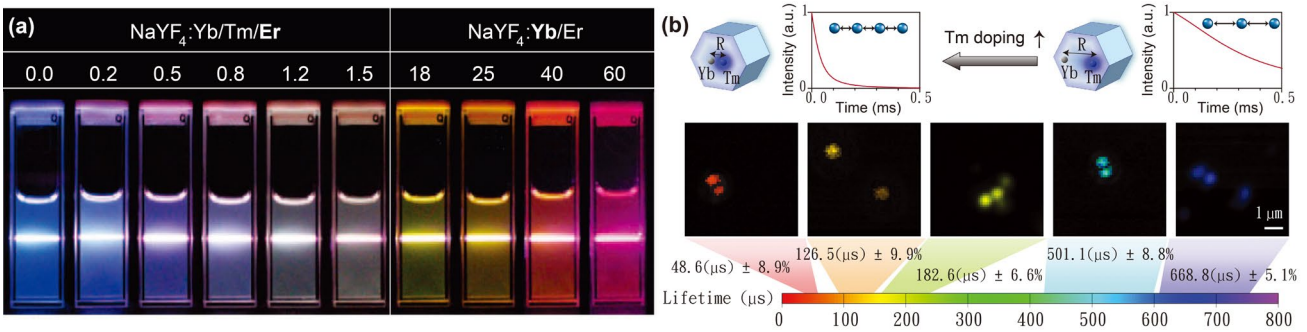

Figure 4. (a) Upconversion multicolor emission photos of $NaYF_4:Yb^{3+}/Tm^{3+}/Er^{3+}$ (20/0.2/0.2–1.5 mol%) and $NaYF_4:Yb^{3+}/Er^{3+}$ (18–60/2 mol%) nanoparticles in ethanol solutions under 980 nm laser illumination [47]. (b) Schematic illustration of lifetime tuning and time-resolved confocal images for $NaYF_4:Yb^{3+}/Tm^{3+}$ (20/0.2-4 mol%) upconversion nanocrystals. The images from left to right represent that nanoparticles with Tm doping concentrations of 4, 2, 1, 0.5 and 0.2 mol%, respectively [53]. Figure reproduced with permission from: (a), [47], American Chemical Society; (b), [53], Springer Nature.

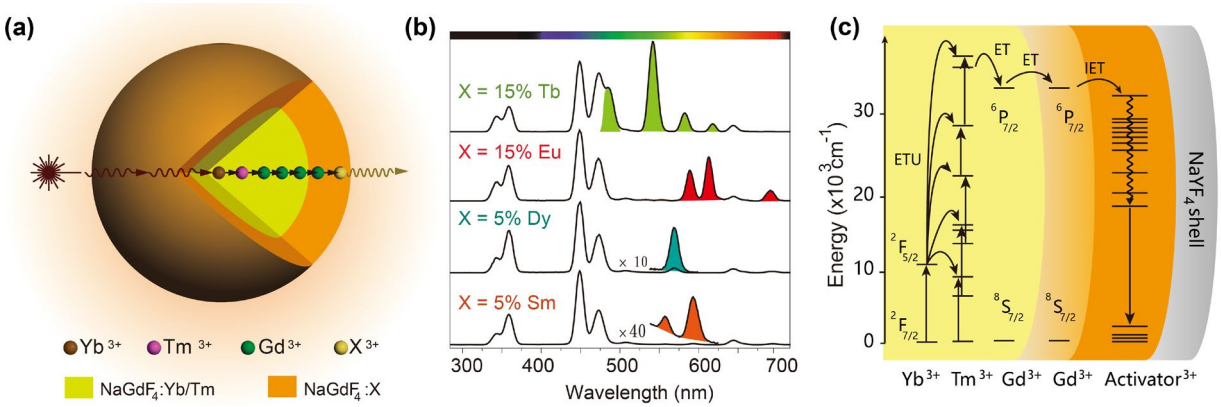

Figure 5. (a) Schematic design of core/shell structured nanoparticles to control upconversion photoluminescence through energy migration-mediated upconversion mechanism. (b) Emission spectra of core/shell structured nanoparticles doped with different activators (Tb^{3+}, Eu^{3+}, Dy^{3+} and Sm^{3+}); (c) Simplified energy level diagrams representing energy migration-mediated upconversion processes; (d) Luminescence photographs of $NaGdF_4$:Yb/Tm@$NaGdF_4$:A@$NaYF_4$ nanoparticles with different activator concentrations in cyclohexane solution under irradiation of a 980 nm laser. Figure reproduced with permission from: (a-b), [27], Springer Nature; (c-d), [33], American Chemical Society.

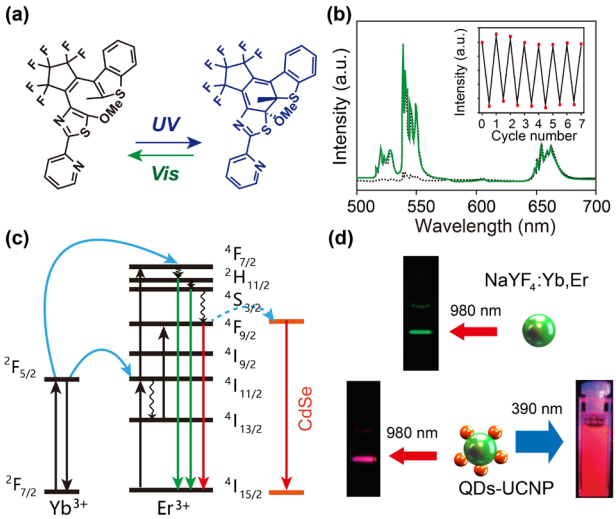

Figure 6. (a) Chemical structures of the diarylethene molecule in the open-ring and closed-ring isomers upon photoisomerization reactions. (b) Composite film based on diarylethene dye engineered $NaYF_4$:Yb^{3+}/Er^{3+} upconversion nanoparticles exhibiting photoswitching behaviour. Inset shows reversible fluorescence on/off cycles under alternating UV/vis irradiation [84]. (c) Schematic of the excitation and energy transfer in CdSe quantum dots coated $NaYF_4$:Yb^{3+}/Er^{3+} nanocrystals. (d) Photographs of the emission from $NaYF_4$:Yb^{3+}/Er^{3+} nanocrystals (top) and CdSe QDs coated $NaYF_4$:Yb^{3+}/Er^{3+} nanoheterostructures (bottom) [87]. Figure reproduced with permission from: (a-b), [84], Wiley; (c-d), [87], American Chemical Society.

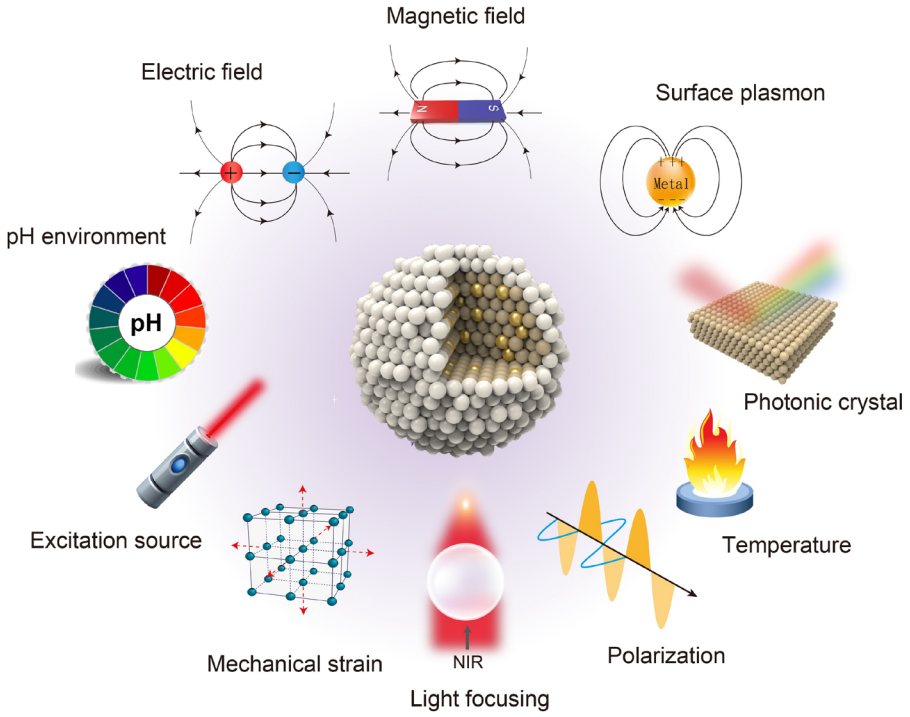

Figure 7. Tuning the luminescence of lanthanide-doped upconversion nanoparticles by engineering external stimulus.

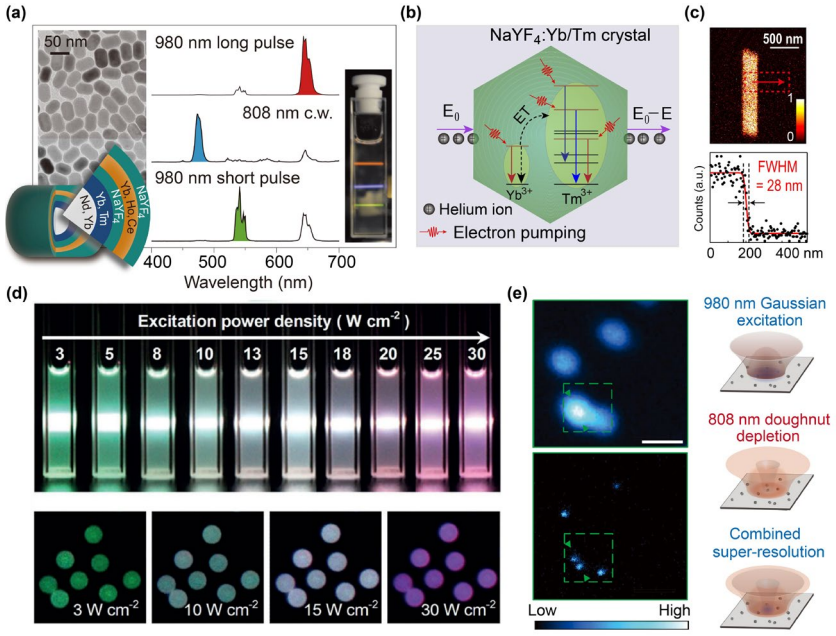

Figure 8. Excitation light-induced multicolour fine tuning in upconversion nanocrystals. (a) Core/shell structured $NaYF_4$-based nanocrystals exhibiting three primary colours emitting capability under NIR lasers excitation [93]. (b) Proposed upconversion mechanisms of Yb/Tm codoped system under 980 nm laser and ion-beam stimulation. (c) Iono-luminescence image of a single nanorod and the corresponding line-scanning profile extracted from the intensity counting at the red region long the arrow, indicating an imaging resolution of about 28 nm [92]. (d) Luminescence photographs of $NaYF_4$ coated $NaGdF_4$:Yb/Tm/Er@$NaGdF_4$:Eu nanoparticles in cyclohexane solution and polystyrene microbeads loaded with the nanocrystals under irradiation of a 980 nm laser with a power density of 3 to 30 W/cm^2 [94]. (e) schematic illustration of $NaYF_4$:Yb^{3+}/Tm^{3+} (20/8%) UCNPs upon 980 nm, 808 nm and dual excitations and the respective confocal and upconversion-STED super-resolution images [95]. Figure reproduced with permission from: (a), [93], Springer Nature; (b-c), [92], Springer Nature; (d), [94], Wiley; (e), [95], Springer Nature.

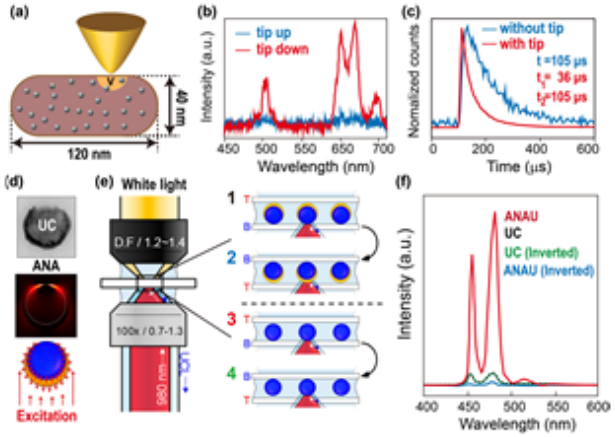

Figure 9. (a) Schematic illustration of tip enhanced photoluminescence of upconversion nanocrystal. (b,c) Manipulating upconversion photoluminescence of the **$NaYF_4$:Yb^{3+}/Er^{3+}** nanoparticle by moving a gold nanotip to the upconversion nanoparticle and the respective upconversion emission spectra and lifetime of the **$NaYF_4$: Yb^{3+}/Er^{3+}** near the gold nanotip (blue) and away from gold nanotip [119]. (d) TEM image and schematic diagram of ANAUs depicting nanofocusing of excitation light of ANAUs with nanocrescent antenna. (e) Schematic diagram of experimental setup used to measure the asymmetric emission characteristics of various samples. The sample was vertically mounted (1 and 3) to measure the emission toward the nanocrescent antenna tip region, while for the measurement of emission toward the body region, the sample was mounted in an inverted direction (2 and 4). (f) Emission spectra of an ANAU toward the tip region (black), an ANAU toward the body region (blue), a UC toward the bottom (red), and a UC toward the top (green) [126]. Figure reproduced with permission from: (a-c), [119], American Chemical Society; (d-f), [126], American Chemical Society.

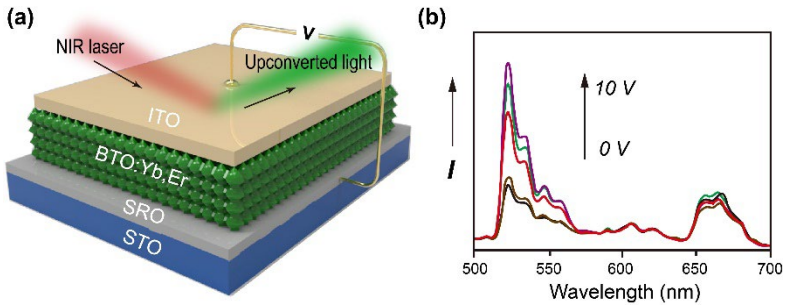

Figure 10. (a) Schematic illustration of opto-electrical device based on Yb^{3+} and Er^{3+} co-doped ferroelectric host material ($BaTiO_3$). The active matrix was sandwiched between two transparent conductive electrodes. (b) Upconversion photoluminescence can be modulated by adjusting the applied bias voltage to the ferroelectric $BaTiO_3$ thin film. Figure reproduced with permission from [127], Wiley.

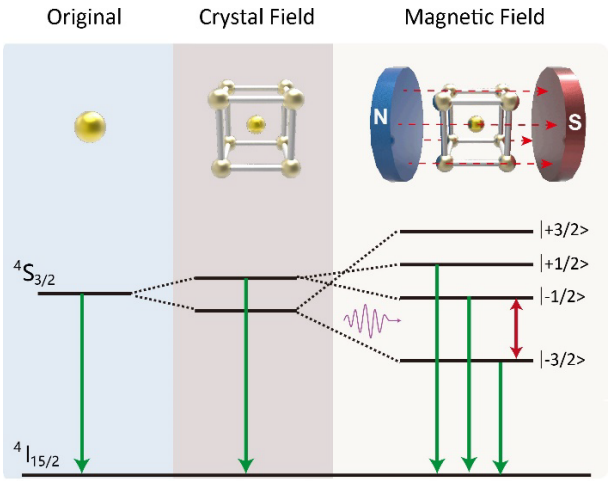

Figure 11. General schematic diagram for the splitting energy levels of $_4S^{3/2}$ of the Er^{3+} ions in which the gap between the Zeeman levels |-1/2> and |-3/2> increases with applied magnetic field. Figure reproduced with permission from [129], Wiley.

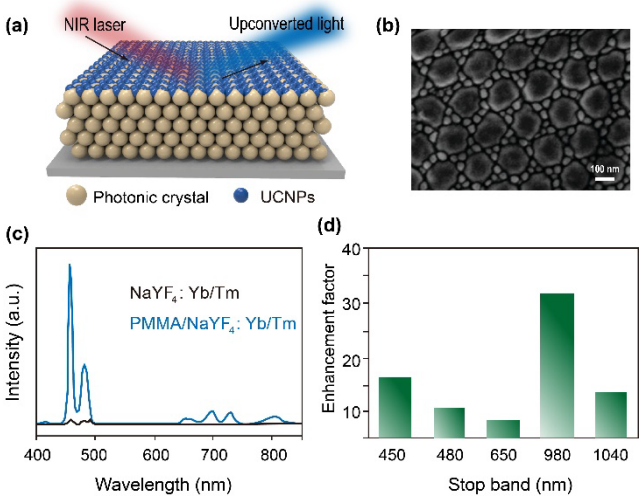

Figure 12. (a) Scheme illustration of photonic crystals deposited with upconversion nanoparticles. (b) SEM image of the as-prepared PMMA photonic crystal structure with $NaYF_4:Yb^{3+}/Tm^{3+}$ nanoparticles deposited in the gaps. (c) Upconversion emission spectra of $NaYF_4:Yb^{3+}/Tm^{3+}$ nanoparticles obtained with and without the PMMA photonic crystal. (d) Different emission enhancement factors by using PMMA photonic crystals with different photonic stop band. Figure reproduced with permission from [137], The Royal Society of Chemistry.

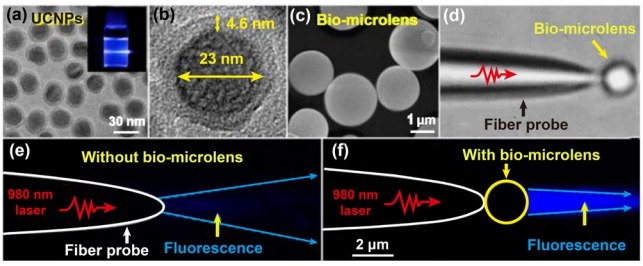

Figure 13. (a,b) TEM image of the core-shell UCNPs with an overall diameter of 28 ± 3 nm. (c) SEM image of the yeast cell bio-microlenses with an average diameter of 2.0 μm. (d) Optical image showing a bio-microlens was trapped at the tip of an optical fiber probe. (e,f) Fluorescent images of output light from a fiber probe without a bio-microlens and with a bio-microlens, which were obtained by 980 nm laser excitation into the fiber and illuminating the upconversion fluorescence of a UCNP suspension. Figure reproduced with permission from [145], American Chemical Society.

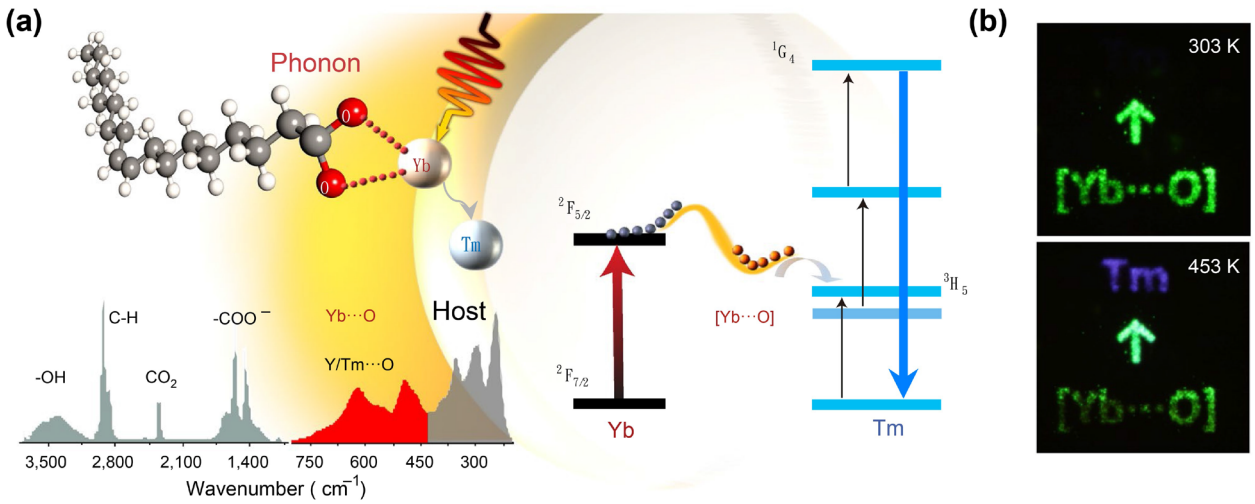

Figure 14. (a) Schematic illustration of the surface-phonon-enhanced upconversion process; (b) Temperature-responsive anti-counterfeiting security patterns at 453 K and 303 K. Figure reproduced with permission from [150], Springer Nature.

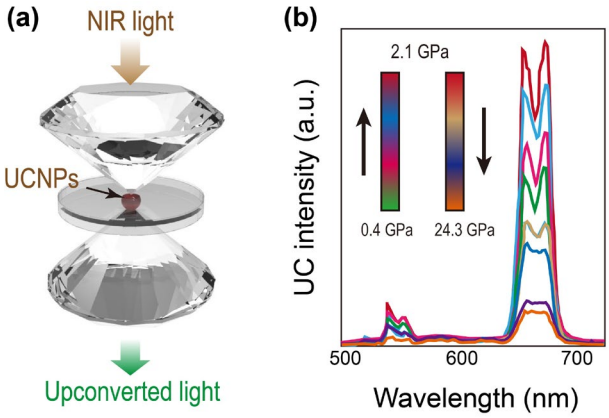

Figure 15. (a) Illustration of the experimental approach used in pressure-dependent spectra measurement. (b) Pressure-dependent emission spectra of α-$NaYF_4$:Yb^{3+}/Er^{3+} UCNPs on 980 nm excitation. Figure reproduced with permission from [153], American Chemical Society.

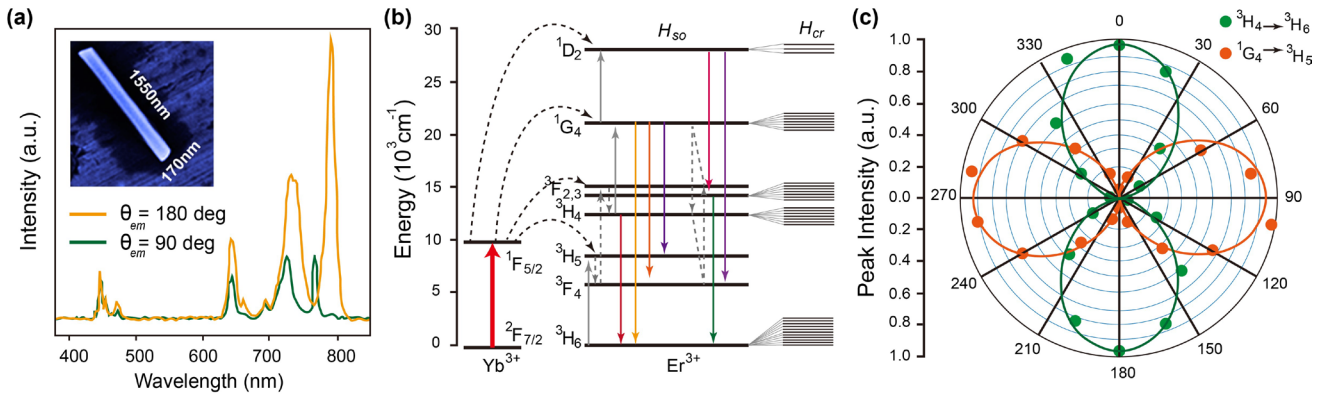

Figure 16. (a) Upconversion emission spectra of a $NaYF_4$:Yb^{3+}/Tm^{3+} single rod, recorded at different polarization angles. Inset is the scanning electron microscopic image of the single rod. (b) Proposed energy transfer pathways from Yb^{3+} to Tm^{3+}, alongside schematic splitting levels of Tm^{3+} because of crystal field interaction. (c) Polar plots of the upconversion peak intensity (according to the $_3H^4 \rightarrow {}_3H^6$ and $_1G^4 \rightarrow {}_3H^5$ transitions of Tm^{3+}) as a function of the emission polarization angle. Figure reproduced with permission from [159], American Chemical Society.

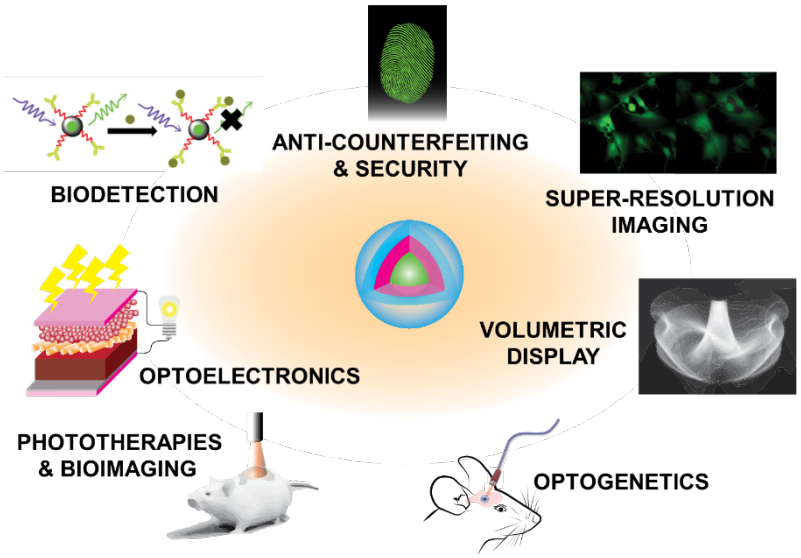

Figure 17. Overview of the emerging applications that capitalize on lanthanide-doped upconversion nanoparticles.

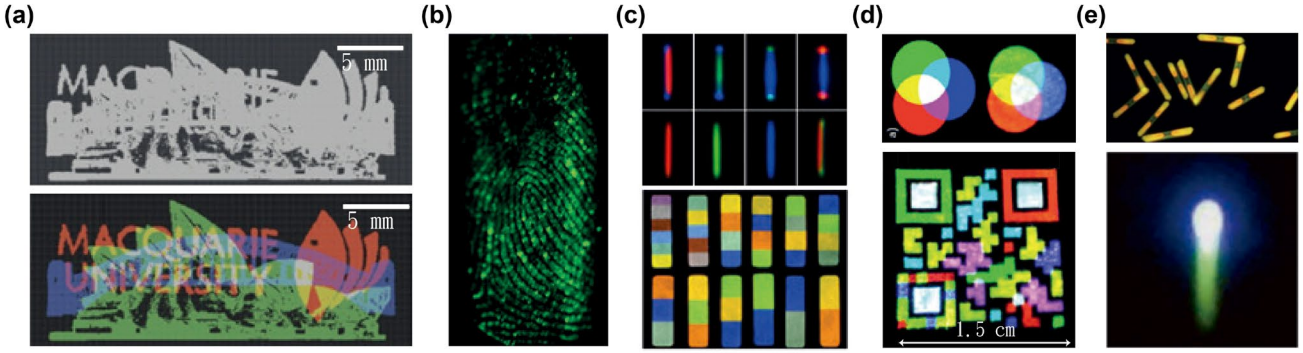

Figure 18. Significant milestones of selected multifunctional lanthanide-doped upconversion nanoparticles for evolving anti-counterfeiting and security applications. (a) Illustration of document security printing via lifetime-encoding which was achieved via three types of lifetime encoded $NaYF_4$:Yb/Tm nanoparticles [53]. (b) Application of $NaYF_4$:Yb/Er lanthanide-doped nanocrystals for latent fingerprinting [165]. (c) Achieving multicolour barcoding via single lanthanide-doped nanoparticles (Top) Optical micrograph photos of dual-coloured-band single-crystalline microrods [166] (Bottom) Luminescence pictures of multicoloured band rod-shaped nanoparticles synthesized via microfluidic devices [167]. (d) Red-green-blue (RGB) printing of lanthanide-doped nanoparticles [168]. (e) (Top) Upconversion micrographs of the $NaYbF_4$:Er (5 mol%) microrods dispersed on a glass substrate [174] (Bottom) Multilevel anti-counterfeiting application using Mn^{2+}-activated core-shell Ln-doped UCNPs giving a bright spot of emission with a green-coloured tail from a specific pattern under dynamic scanning [175]. Figure reproduced with permission from: (a), [53], Springer Nature; (b), [165], Wiley; (c), Top - [166], American Chemical Society, Bottom - [167], Springer Nature; (d), [168], RSC; (e), Top - [174], Wiley, Bottom - [175], Springer Nature.

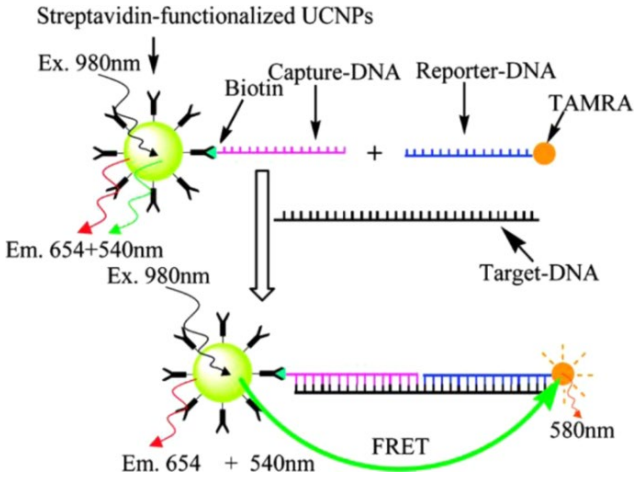

Figure 19. (a) Schematic illustration of the concept of Ruthenium-based complex N719-modified Ln-doped UCNPs and the upconversion luminescence (UCL) response to Hg^{2+} ions followed by addition of KI, which results in a color change in green UCL. (b) UC emission figures and their corresponding merged with bright-field photos of cancerous Hela cells incubated with 0.2mg/ml N719-UCNPs for 3hrs and, (b) Followed by incubation with Hg^{2+} ions for 15 min. Figure reproduced with permission from [177], American Chemical Society.

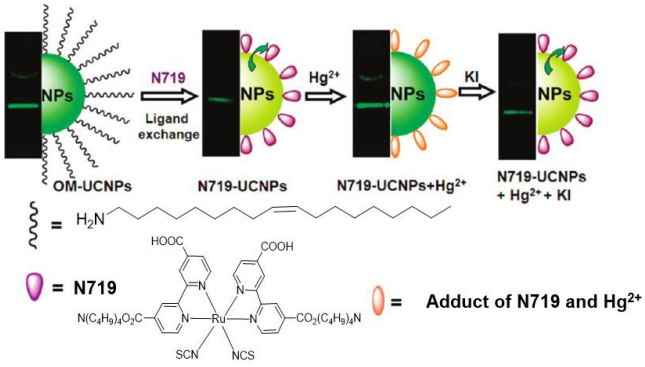

Figure 20. Schematic illustration of the lanthanide-doped UCNPs for mercury Hg^{2+} ion detection. Figure reproduced with permission from [178], American Chemical Society.

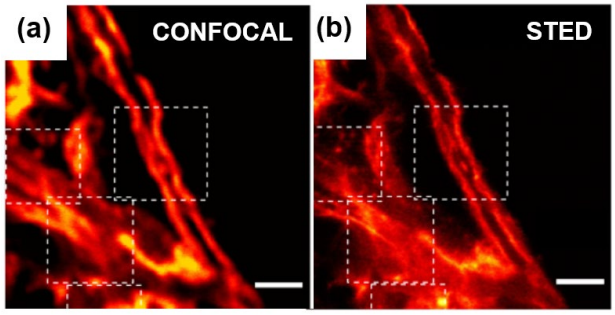

Figure 21. (a) Confocal (b) STED super-resolution images of cellular cytoskeleton labelled with antibody-conjugated 11.8 nm $NaGdF_4$:18%Yb^{3+},10%Tm^{3+} nanocrystals, scale bar represents 1 μm. Figure reproduced with permission from [97], Springer Nature.

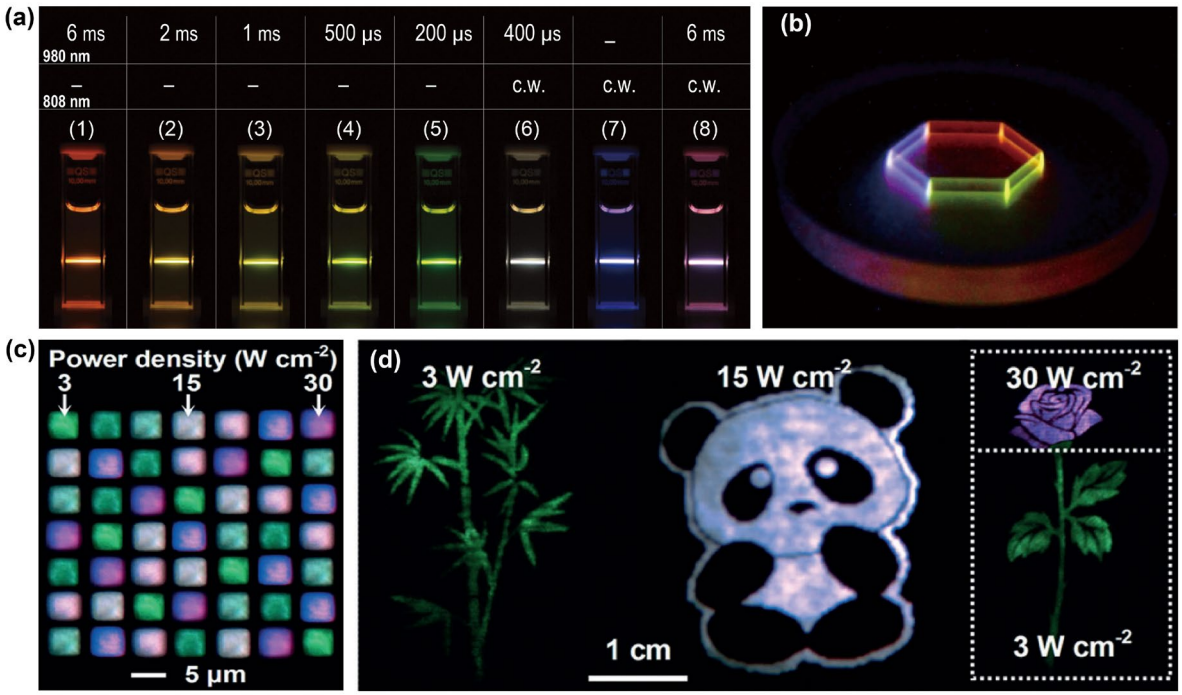

Figure 22. Various emerging display technological applications. (a) Luminescence photos illustrating multi-color tuning of the sample utilizing the combination of both NIR lasers. (b) Demonstration of volumetric full-color three-dimensional display generated via the use of the designed multi-layer upconversion nanoparticles. Scale bars, 1 cm. (c) A dot-array image on silicon wafer and Ln-doped UCNPs were loaded inside a 5 by 5 μm etched microwells on a silicon wafer. (d) Photos of bamboo, panda and rose printed on paper with an inkjet printer using the synthesized nanoparticles as colourless ink. Figure reproduced with permission from: (a-b), [93], Springer Nature; (c-d), [94], John Wiley and Sons.

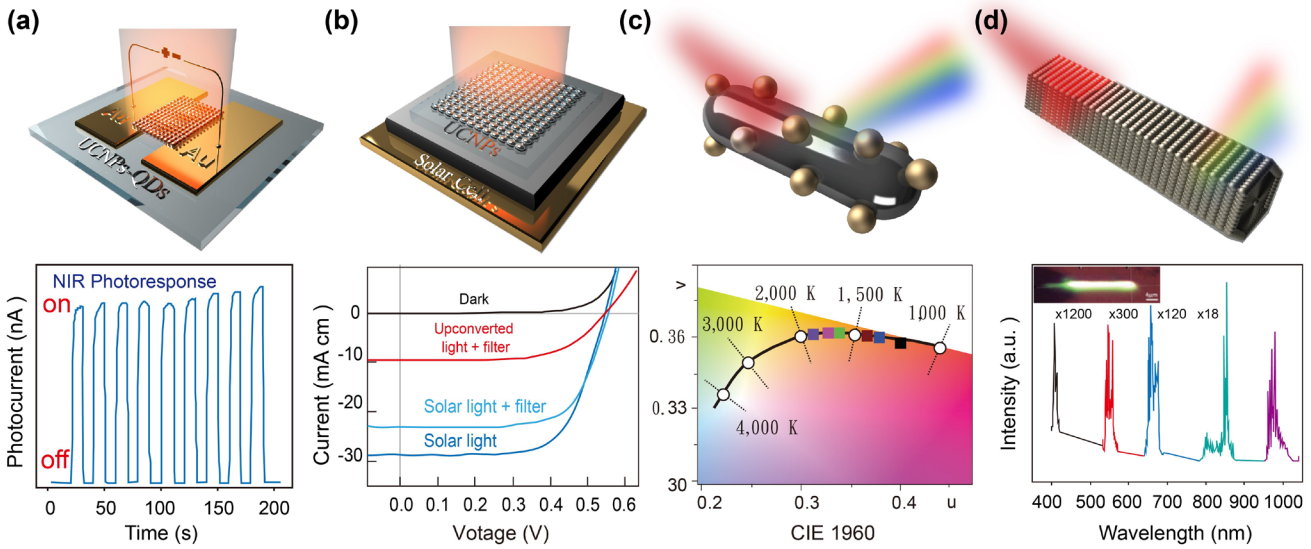

Figure 23. A variety of emerging optoelectronic devices and photovoltaic applications. (a) (Top) A novel nanoheterostructure consisting of lanthanide-doped upconversion nanoparticles with CdSe quantum dots (QDs) termed as CSNY. (Bottom) The reversible on-off switching characteristics profile upon 980-nm excitation. (b) (Top) An electronic device by assembling two contact devices via a spin-coating solution of CSNY particles in solution onto Si/SiO_2 substrate pre-patterned with gold electrodes. (Bottom) A graph depicting current density–voltage curves of the Si solar cell under AM1.5 solar light (blue) with the short-pass filter (cyan), under the upconverted white light with the short-pass filter (pink) and in dark (black). The upconverted white light came from 28 mol% Yb^{3+}-doped ZrO_2 under 976-nm laser excitation. (c) (Top) A unique nanoheterostructure nanorods consisting of lanthanide-doped upconversion nanoparticles $(Gd,Yb,Er)_2O_3$ with AuNPs. (Bottom) Temperature mapping in the form of a CIE 1960 (u,v) chromaticity diagram, generated by using Au particle-modified Gd_2O_3:Yb,Er nanorods. The similarity of emission location with the Planckian locus (curved line with circles) enables temperature mapping from 300–2,000 K. (d) (Top) A schematic diagram showing the designed NIR upconversion lasing using single-crystal Er-Y chloride silicate nanowires. (Bottom) The upconverted light emission spectra from 400-nm to 1000-nm of the Er-Y chloride silicate nanowires upon excitation at 1480-nm. Insert: Optical image of the pumped nanowire. Figure reproduced with permission from: (a), [86], American Chemical Society; (b), [151], Springer Nature; (c), [189], Wiley; (d), [190], Springer Nature.

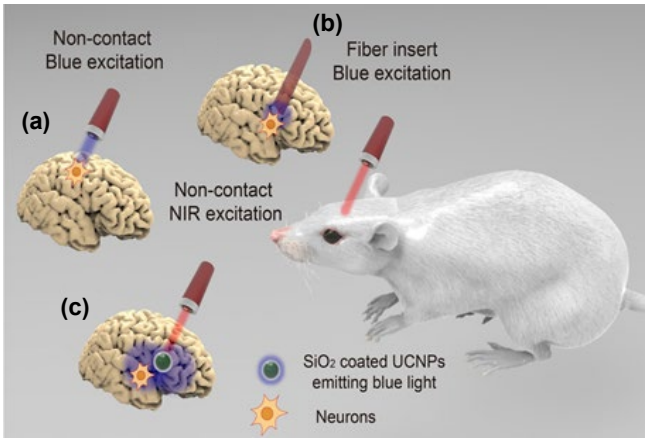

Figure 24. Various approaches to deliver and irradiate blue excitation light to the neurons that are found deep-lying in the mouse brain. (a) Low efficiency of blue light excitation via the non-contact blue excitation due to light scattering. (b) A surgical invasive implanted optical fiber to generate blue light excitation to modulate the neurons but restricts the movements of the mouse's movements and can result in surrounding brain tissue damage. (c) An optimal non-contact NIR-to-Blue visible light excitation via the use of upconversion nanoparticles to modulate the neurons.

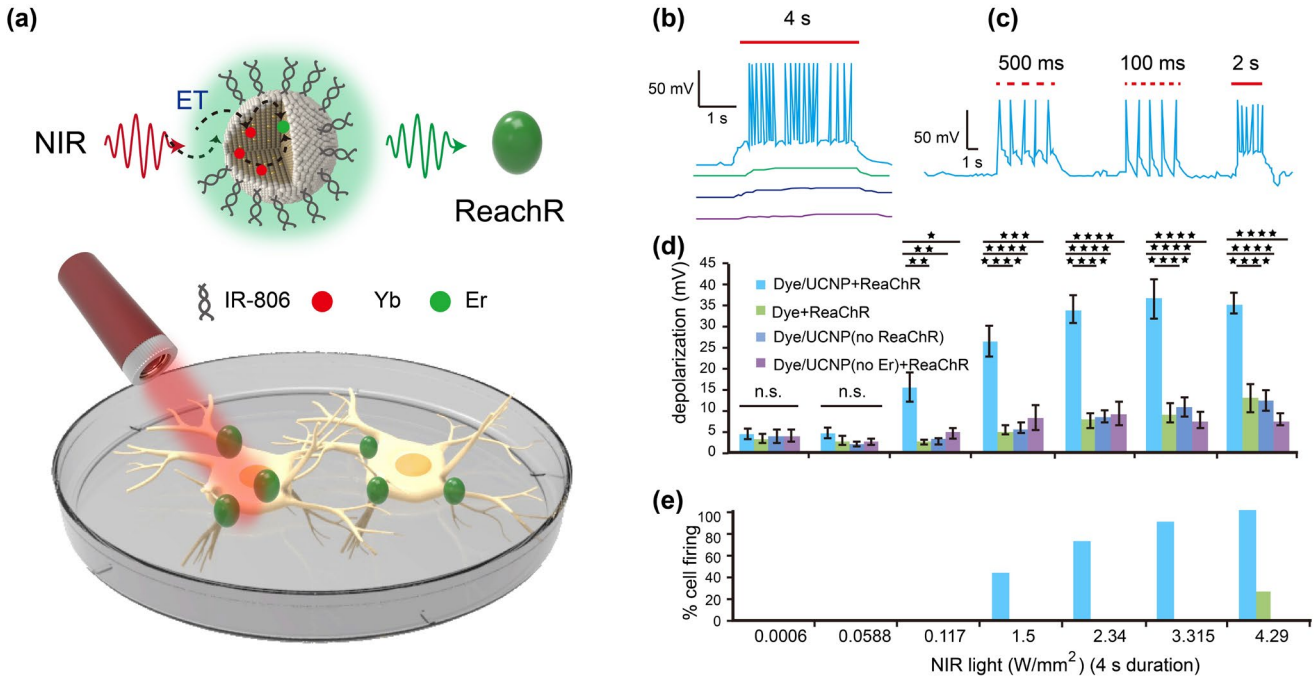

Figure 25. The design and crucial experimental results of the Ln-doped UCNPs in [193]. (a) Schematic illustration of the rationally designed novel IR-806 dye-sensitized core/shell lanthanide-doped upconversion nanoparticles (β-$NaYF_4$:20%Yb^{3+}/2%Er^{3+}@β-$NaYF_4$:10%Yb^{3+}) for NIR-activated optogenetic application to control the red-activatable channelrhodopsins (ReaChR) via 800-nm laser excitation. 800-nm activation of ReaChR in the designed cultured hippocampal neurons. Electrophysiology graphs demonstrating the potential firing in response to (b) Prolonged – 4s, (c) Pulsed (100ms, 500ms and 2s) delivery at (2.34 W/mm^2) (d) Neuronal depolarization and (e) Action potential firing triggered by 800-nm NIR laser excitation at various intensities for 4s. There can be neuronal activation and depolarization in some control cases. Figure reproduced with permission from [193], American Chemical

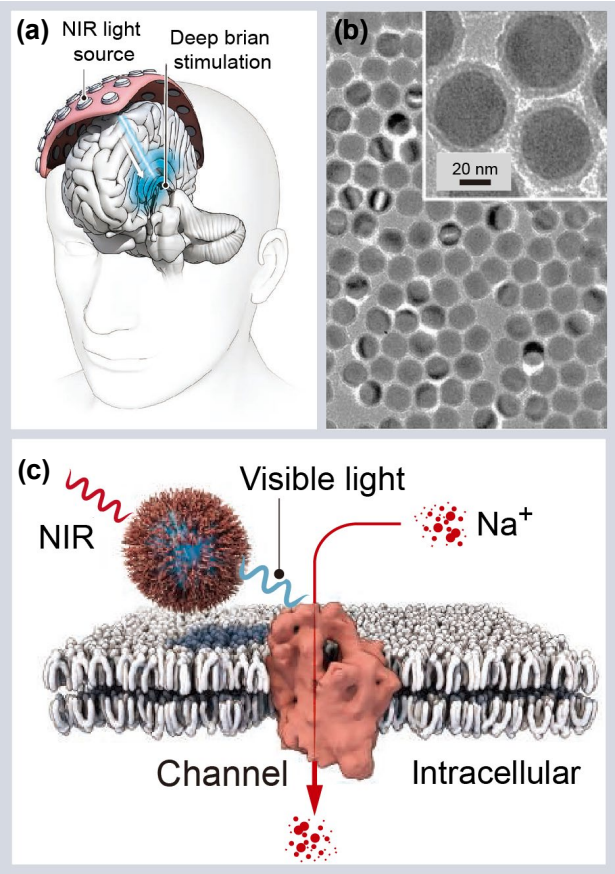

Figure 26. (a) Schematic figure of a typical light source array for deep-seated brain stimulation optogenetic applications. (b) TEM diagram of surface-modified lanthanide-doped nanoparticles. Insert: A close-up magnification of the corresponding as-synthesized silica coated lanthanide-doped nanoparticles. (c) Schematic illustration of the rationally designed surface-modified lanthanide-doped UCNPs for UCNP-assisted NIR upconversion optogenetics application. Figure reproduced with permission from [192], The American Association for the Advancement of Science (AAAS).

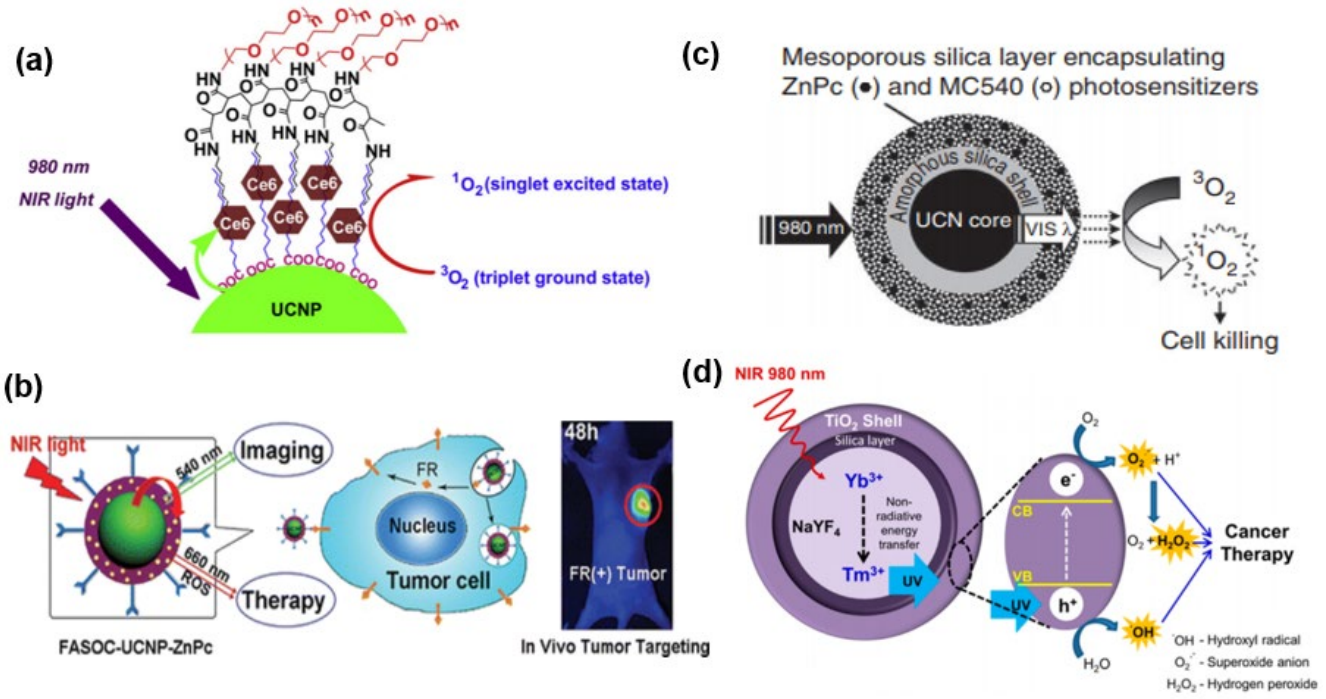

Figure 27. Various emerging NIR excitable Ln-doped UCNPs for Photodynamic Therapy (PDT) (a) A diagram showing NIR-induced PDT which has Ce6 functionalized onto the Ln-doped UCNP. (b) A figure illustrating the tumor-targeted Ln-doped UCNP using ZnPc and applied for *in-vivo* tumor PDT. (c) Figure showing the as-synthesized mesoporous-silica coated Ln-doped UCNPs doped with Er^{3+} and co-loaded with MC540 and ZnPc photosensitizers. Upon 980-nm irradiation, red and green visible upconverted light were generated and activated the photosensitizers to generate ROS. (d) A novel NIR-to-UV TiO_2 coated-Ln-doped UCNP for uniform and effective ROS generation in which UV light photoexcites the electrons from the valence band to the conduction band in TiO_2 shell. This results in photoinduced electron-hole pairs and the interaction of native triplet molecular oxygen and water molecules would lead to generation of various ROS and cause cancer cell death. Figure reproduced with permission from: (a), [204], Elsevier; (b), [205], American Chemical Society; (c), [206], Springer Nature; (d), [207], American Chemical Society.

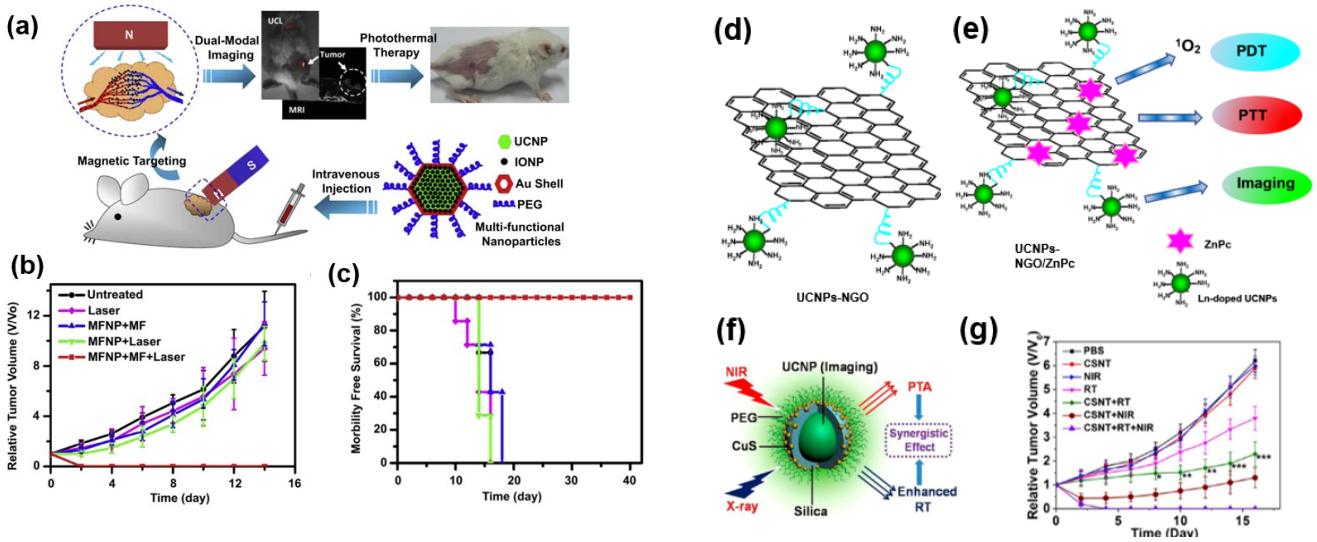

Figure 28. A variety of emerging photothermal therapy (PTT) applications integrating NIR excitable Ln-doped UCNPs (a) A diagram showing the composition of the as-synthesized MFNPs and the conceptual workflow for the in vivo image-guided magnetic targeting PTT application in a tumor mouse model. (b) *In vivo* magnetic targeted PTT profile and the growth of 4T1 tumors in various groups of the mice upon treatment with various control groups. (c) The representative survival curves of mice bearing 4T1 tumors after various therapeutic control groups [209]. (d) Schematic figure showing the Ln-doped UCNP-Nanographene oxide (NGO) nanocomposite in which the NGO was grafted with the UCNPs through bifunctional polyethylene glycol (PEG). (e) The intrinsic multifunctional theranostic features of the designed Ln-doped UCNPs-NGO/ZnPc nanocomposites [213]. (f) Schematic figure showing the Ln-doped UCNP-CuS-PEG nanocomposite and possess trimodal imaging with dual synergistic photothermal and radiation therapies [214]. Figure reproduced with permission from: (a-c), [209], Elsevier; (d-e), [213], Elsevier; (f-g), [214], American Chemical Society.